Aus dem
Walther-Straub Institut für Pharmakologie und Toxikologie
der Ludwig-Maximilians-Universität München
Direktor: Prof. Dr. med. Thomas Gudermann

Cytosolic and mitochondrial Ca^{2+} handling in pulmonary arterial smooth muscle and endothelial cells

Dissertation zum Erwerb des Doktorgrades der Naturwissenschaften
an der Medizinischen Fakultät der Ludwig-Maximilians-Universität
München

vorgelegt von

Diana Angela Stickel (geb. Koch)

aus Engen

2016

Gedruckt mit Genehmigung der Medizinischen Fakultät der Ludwig-Maximilians-Universität München

Betreuer: Prof. Dr. rer. nat. Alexander Dietrich

Zweitgutachter: Priv. Doz. Dr. Kai Hell

Dekan: Prof. Dr. med. dent. Reinhard Hickel

Tag der mündlichen Prüfung: 09.02.2017

Cytosolic and mitochondrial Ca²⁺ handling in pulmonary arterial smooth muscle and endothelial cells

by

Diana Angela Stickel (geb. Koch)

Abstract

Cytosolic Ca²⁺ elevated by receptor-operated (ROCE) or store operated Ca²⁺ entry (SOCE) and buffered by mitochondrial Ca²⁺ uptake plays an essential role in physiological processes of lung cells. Disturbed Ca²⁺ homeostasis in precapillary pulmonary arterial smooth muscle cells (PPASMC) induces pulmonary arterial hypertension (PAH) or disrupts barrier function of murine pulmonary microvascular endothelial cells (MPMVEC) resulting in vascular leakage and lung edema.

While SOCE is mediated by stromal interaction molecule (STIM1 and 2) dimers sensing Ca²⁺ in Ca²⁺ stores and plasma membrane Orai channels, ROCE is mediated by classical transient receptor potential (TRPC) channels via diacylglycerol (DAG) and receptor-activated phospholipase C (PLC). To investigate if TRPCs are also involved in SOCE, Ca²⁺ entry was analyzed in PPASMCs isolated from STIM1/2$^{\text{flox/flox}}$/TRPC1/3/6$^{\text{-/-}}$ mice as well as control mice and infected with Cre-recombinase expressing lentiviruses to delete STIM1/2 protein expression. Deficiency of STIM1/2 did only impair the long-lasting receptor-operated Ca²⁺ entry (ROCE), but TRPC1, TRPC3 and TRPC6 channels may be activated indirectly by store-operated Ca²⁺ entry (SOCE).

Lack of STIM1/2 or Orai1 in MPMVECs did not impair acetylcholine-induced vasodilatation of isolated aortic rings but pulmonary microvascular endothelial cells (MPMVECS) isolated from endothelial cell-specific STIM1/2 or Orai1 knockout mice (STIM1/2$^{\Delta\text{EC}}$ and Orai1$^{\Delta\text{EC}}$) were protected from Ca²⁺-dependent nuclear factor of activated T-cells c3 (NFATc3) nuclear translocation which is involved in expression of proinflammatory mediators highlighting their important role in inflammation processes. Migration and proliferation of MPMVECs was reduced in STIM1/2$^{\Delta\text{EC}}$ and Orai1$^{\Delta\text{EC}}$.

Disturbed mitochondrial Ca²⁺ uptake results in endothelial dysfunction and may affect energy production. The influence of mitochondrial Ca²⁺ uniporter (MCU) and mitochondrial Ca²⁺ uniporter regulator 1 (MCUR1) on mitochondrial bioenerget-

ics was investigated in MPMVECs from respective endothelial cell-specific knockout mice. Mitochondrial membrane potential and oxygen consumption rate was not impaired in MCUR1$^{\Delta EC}$ or MCU$^{\Delta EC}$. ATP production was reduced in MCUR1$^{\Delta EC}$ and MCU$^{\Delta EC}$. Probably resulting from reduced ATP levels, uncoupling protein2 (UCP2) was upregulated in MCUR1$^{\Delta EC}$. The upregulated UCP2 might flux protons to prevent mitochondrial membrane potential ($\Delta\Psi_m$) hyperpolarization, induce a metabolic shift from oxidative phosphorylation to glycolysis or stimulate compensatory mechanisms to rescue $[\text{Ca}^{2+}]_m$-uptake. In accordance with lower superoxide production in MCUR1$^{\Delta EC}$ and MCU$^{\Delta EC}$, we observed a reduced proliferation and migration in these cells. Low mitochondrial Ca^{2+} uptake and low cellular ATP levels in MCUR1$^{\Delta EC}$ and MCU$^{\Delta EC}$ activated AMPK and turned on autophagy. Therefore, cytosolic and mitochondrial Ca^{2+} handling is of foremost importance for lung cell function and proteins involved in these processes may serve as pharmacological targets for therapeutic approaches in patients with pulmonary hypertension or lung edema.

Zusammenfassung

Ca^{2+} gelangt durch einen Rezeptor-operierten (*receptor-operated Ca^{2+} entry (ROCE)*) oder Speicher-operierten Einstrom (*store-operated Ca^{2+} entry (SOCE)*) ins Zytosol und wird dort durch die mitochondriale Ca^{2+} Aufnahme abgepuffert. Gestörte Ca^{2+} Homöostase in prekapillären, pulmonalen, arteriellen glatten Muskelzellen (PPASMC) kann pulmonale arterielle Hypertonie (PAH) induzieren oder die Barrierefunktion muriner, pulmonaler, mikrovaskulärer Endothelzellen (MPMVEC) vermindern und die Bildung eines Lungenödems induzieren.

Während der Speicher-operierte Ca^{2+} Einstrom durch *stromal interaction molecules* (STIM1 und 2) als Sensoren in den Ca^{2+} Speichern und plasmamembranären Orai-Kanälen bewältigt wird, kann der Rezeptor-operierte Ca^{2+} Einstrom (*receptor-operated Ca^{2+} entry (ROCE)*) durch *classical transient receptor potential* (TRPC) Kanäle über Diacylglycerol (DAG) durch Rezeptor-aktivierte Phospholipasen C (PLC) erfolgen. Um zu analysieren ob TRPCs am SOCE beteiligt sind, haben wir den Ca^{2+} Einstrom in TRPC1/3/6$^{-/-}$ und STIM1/2-defizienten Zellen, die durch Infektion von STIM1/2$^{flox/flox}$ Zellen mit Cre Rekombinase exprimierenden Lentiviren erzeugt wird, untersucht. Die Abwesenheit von STIM1/2 Protein hatte nur einen Einfluss auf den lang-anhaltenden Rezeptor-operierten Ca^{2+} Einstrom, aber TRPC1-, TRPC3- und TRPC6-Kanäle könnten durch den Speicher-operierten Ca^{2+} Einstrom indirekt aktiviert werden.

Eine Acetylcholin-induzierte Vasodilatation in isolierten Aortenringen aus endothelzell-spezifischen STIM1/2 und Orai1 defizienten Mäusen (STIM1/2$^{\Delta EC}$ and Orai1$^{\Delta EC}$) war im Vergleich zu Kontroll-Aortenringen unverändert. Jedoch zeigten MPMVECs aus diesen Mäusen eine verringerte Translokation von nuclear factor of activated T-cells c3 (NFATc3) in den Zellkern, die für eine Expression von proinflammatorischen Mediatoren wichtig ist. Die Migration und Proliferation von MPMVECs war in STIM1/2$^{\Delta EC}$ and Orai1$^{\Delta EC}$ verringert.

Eine gestörte mitochondriale Ca^{2+} Aufnahme resultiert in einer endothelialen Dysfunktion und könnte die Energieproduktion beeinträchtigen. Deshalb wurde der Einfluss des mitochondrialen Ca^{2+} Uniporters (MCU) und des mitochondrialen Ca^{2+} Uniporter Regulators1 (MCUR1) auf die mitochondriale Energieproduktion in MPMVECs aus endothelzell-spezifischen MCU- und MCUR1-defizienten Mäusen (MCUR1$^{\Delta EC}$ und MCU$^{\Delta EC}$) untersucht. Das mitochondriale Membranpotential und die Sauerstoff Verbrauchsrate war in MCUR1$^{\Delta EC}$ or MCU$^{\Delta EC}$ nicht beeinträchtigt, aber die ATP Produktion war vermindert. Wahrscheinlich resultierte aus der verminderten ATP Produktion die vermehrte Produktion des Entkopplungproteins UCP2 in MCUR1$^{\Delta EC}$. Die Hochregulation von UCP2 könnte einen Protonentransport in die mitochondriale Matrix ermöglichen und damit eine Hyperpolarisation des mitochondrialen Membranpotentials der der inneren mitochondrialen Membran verhindern. Alternativ könnte die vermehrte UCP2-Expression zu metabolischen Veränderungen führen oder kompensatorische Mechanismen zur mitochondrialen Ca^{2+}-Aufnahme stimulieren. Niedrige Superoxid Level in MCUR1$^{\Delta EC}$ or MCU$^{\Delta EC}$ bedingten eine

verringerte Proliferation und Migration. Außerdem aktivierte die niedrige mitochondriale Ca^{2+} und die niedrigen ATP Spiegel in $MCUR1^{\Delta EC}$ or $MCU^{\Delta EC}$ die AMPK und Autophagie. Aus diesem Grund kommt der zytosolischen und mitochondrialen Aufnahme von Ca^{2+} Ionen eine elementare Rolle für die Funktion von pulmonalen glatten Muskelzellen und Endothelzellen zu. In Zukunft könnten an diesen Prozessen beteiligte Proteine als pharmakologische Zielsubstanzen zur Entwicklung von Medikamenten gegen pulmonale Hypertonie und Lungenödemen dienen.

Contents

List of Figures

List of Tables

Chapter 1

Introduction

1.1 Ca^{2+} as a cellular effector molecule

Intracellular Ca^{2+} regulates various cell functions. It is involved in exocytosis, cell growth, proliferation, apoptosis, contraction of muscle cells and energy homoeostasis. Ca^{2+} either originates from the extracellular space or from the intracellular pools, most importantly from the endoplasmatic reticulum (ER) and the mitochondria. The extracellular space contains approximately $1\,mM$ calcium, the cytosol 100-200 nM and the internal stores up to $100\,\mu M$ calcium. The Ca^{2+} concentration of the internal stores can vary tremendously during cell function. In particular, mitochondria are able to buffer high cytosolic Ca^{2+} levels [106].

Ca^{2+} influx into the cell is regulated by various Ca^{2+} channels. The type of Ca^{2+} channel mainly expressed depends on the cell type. In excitable cells, such as muscle and nerve cells, voltage-dependent Ca^{2+} channels and receptor operated Ca^{2+} (ROC) channels dominate but also store-operated Ca^{2+} (SOC) channels are expressed. In none-excitable cells, such as endothelial cells, the most important Ca^{2+} entry pathway is via SOC channels (see figure 1.1) [102] [94].

15

1.2 Ca²⁺ influx pathways

1.2.1 The store-operated Ca²⁺ influx pathway

Store-operated Ca^{2+} entry (SOCE) was first proposed by Putney et al. in 1986 who investigated the Ca^{2+} entry of parotid acinar cells depending on the Ca^{2+} release from internal stores [103]. His concept was further evidenced by Hoth and Penner in 1992 providing a store activated Ca^{2+} current in mast cells which they called Ca^{2+} release-activated Ca^{2+} current (CRAC) current [56]. I_{CRAC} is non-voltage activated, inwardly rectifying, selective for Ca^{2+} and has a low conductance[95].

The stromal interaction molecule (STIM) is an ER transmembrane protein that was finally identified in an RNAi screen in S2 cells in Drosophila melanogaster [107] and in HeLa cells in 2005 [74]- long after Putney had suggested the ER-plasma membrane coupling model. Both STIM isoforms, STIM1 and STIM2 are ubiquitously expressed. STIM1 expression is higher in most cell types and is assumed to be the main operator in SOCE. STIM2 is more sensitive to sense luminal ER Ca^{2+} and is therefore discussed to prevent uncontrolled activation of SOCE. STIM proteins have an N-terminal EF-hand domain which binds Ca^{2+}. Upon depletion of the ER Ca^{2+} store, Ca^{2+} dissociates from the EF-hand which triggers the translocation of STIM into close ER– plasma membrane junctions [78]. Eight STIM molecules form a cluster and interact electrostatically by their polybasic C-terminal STIM-Orai activating region (SOAR) region with the acidic C-terminal cytoplasmic domain of one tetrameric Orai channel [122].

Similar to the STIM proteins, the Orai1 protein was identified in an RNAi screen in Drosophila S2 cells in 2006 [37]. Ca^{2+} entry via CRAC channels is the main calcium entry pathway in T cells. T cells isolated from patients with severe combined immunodeficiency (SCID) have shown a functional deficiency in thapsigargin induced SOCE [36], an impaired T cell activation, resulting into reduced T cell proliferation, cytokine production and global gene expression, but normal T cell development [35]. As a result, patients are susceptible to fungal and viral infections and have a reduced life expectancy [37]. In 2006, sequencing of genomic DNA of SCID patients revealed
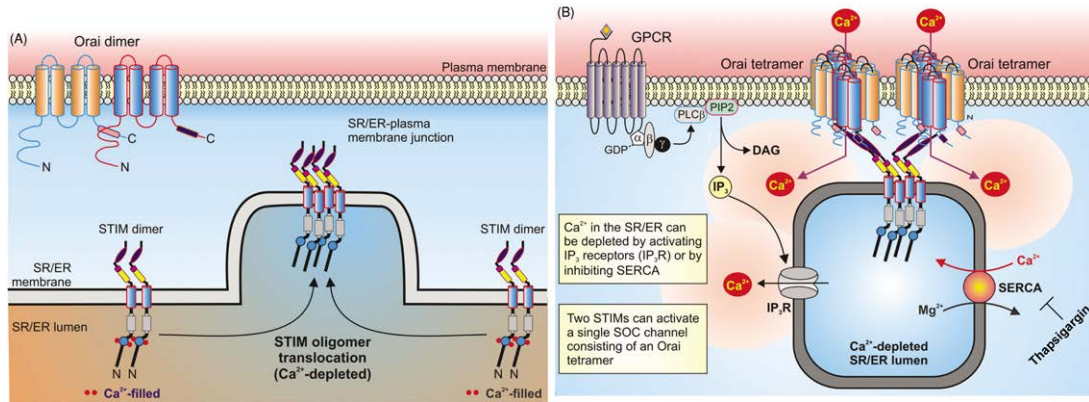
Figure 1.1: **Store-operated Ca²⁺ entry (SOCE).** A)The stromal interaction molecule (STIM) dimers senses Ca^{2+} with its N-terminal EF-hand domain. Upon Ca^{2+} depletion of the endoplasmic reticulum (ER), STIM oligomerizes and translocates to ER– plasma membrane junctions where it interacts electrostatically with Orai. B) Carbachol binds to its G_q protein coupled receptor (G_qPCR) in the plasma membrane which activates phospholipase C. Phospholipase C splits phosphatidylinositol 4,5-bisphosphate (PIP_2) into inositoltriphosphate (IP_3) and diacylglycerol (DAG). IP_3 depletes the ER from Ca^{2+} which induces STIM/Orai interaction and subsequently SOCE. Thapsigargin induces SOCE experimentally by inhibiting the sarcoplasmic/endoplasmic reticulum ATPase (SERCA) pump [122] (modified from [78]).

a C→T missense mutation in exon 1 of human Orai1. Thus, arginine is replaced by tryptophan at position 91 of the protein (R91W). Restoration of wildtype Orai1 in mutated T cells from SCID patients rescued SOCE and I_{CRAC} [37].

The name 'Orai' originates from the Greek mythology, where the Orai are the keepers of the heaven's gate. The Orai proteins are plasma membrane proteins, with four predicted transmembrane domains and intracellular C- and N-termini. Orai1 exists mainly as a dimer under resting conditions and forms tetramers containing the Ca^{2+}-selective pore after store depletion [97]. The three Orai isoforms, Orai1, 2 and 3 differ in their activation and inactivation kinetics, monovalent permeation, and response to 2-APB (2-aminoethoxydiphenyl borate). Orai3, but not Orai2 was reported to be able to restore SOCE in cells lacking Orai1 [35].

SOCE is initiated by binding of an agonist to a tyrosine kinase receptor or a G_qPCR in the plasma membrane, e.g. carbachol binds to its muscarinic acetylcholine receptor and activates phospholipase C, which cleaves PIP_2 into IP_3 and DAG. The second

messenger IP_3 releases Ca^{2+} from the internal stores of the ER via its receptor in the ER plasma membrane. As a result of the depletion of the ER store, the stromal interaction molecule (STIM) molecules oligomerize and activate Ca^{2+} channels in the plasma membrane [122][35][25]. Ca^{2+} enters from the extracellular space and increases the intracellular Ca^{2+} level. The Ca^{2+} pump of the ER, sarcoplasmic/endoplasmic reticulum ATPase (SERCA), pumps intracellular Ca^{2+} into the ER, to refill its internal stores (see figure 1.1). To induce SOCE experimentally, the SERCA inhibitor thapsigargin is used. Thapsigargin blocks the SERCA pump thereby blocking refilling of the ER with cytosolic Ca^{2+}. Because Ca^{2+} leaks through the ER membrane, the ER is gradually depleted by Ca^{2+} after application of thapsigargin. Depletion of the ER from Ca^{2+} triggers activation of SOC channels.

It is widely accepted that Orai channels are strictly store-activated. However there are various reports about SOC channels which are less selective for Ca^{2+} than Orai-induced CRAC channels [94]. It is suggested that TRPC channels could be involved although they are nonselective for Na^+ as well as Ca^{2+} and are activated downstream of phospholipase C.

1.2.2   The receptor-operated Ca^{2+} influx pathway

Receptor-operated Ca^{2+} entry (ROCE) occurs when the second messenger diacyl-glycerol directly activates plasma membrane Ca^{2+} channels. An example for ROCE is the TRPC3/6/7 subfamily which can be activated by G_qPCR agonists, such as carbachol. As a consequence phospholipase C is activated which cleaves PIP_2 into DAG and IP_3. DAG directly activates classical transient receptor potential 3, 6 and 7 (TRPC 3, 6 and 7) channels in the plasma membrane [25]. The influx of cations through classical transient receptor potential (TRPC) channels depolarizes the membrane, activates voltage-dependent calcium channels and increases the intracellular calcium concentration (see figure 1.2).

The TRPC channels are the first TRP channels which were cloned and characterized in mammals, share the closest homology to the Drosophila TRP channels and are therefore termed as 'classical' or 'canonical' TRP channels. However, it is still a mat-
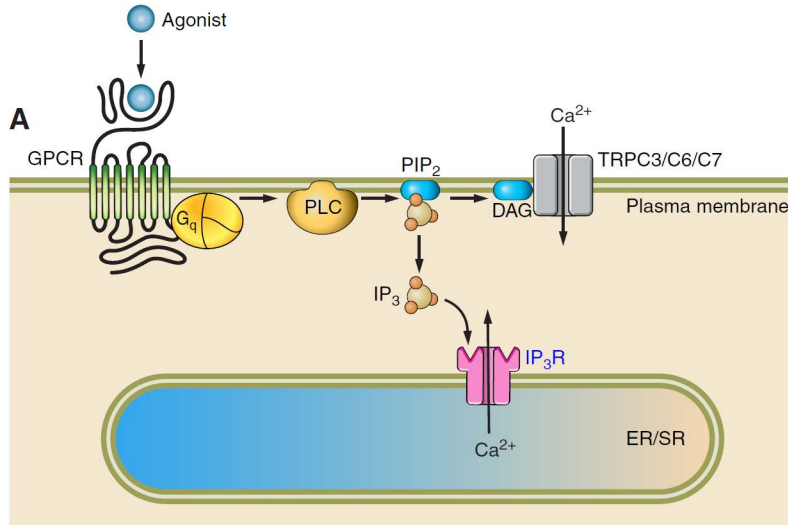
Figure 1.2: **Receptor-operated Ca^{2+} entry (ROCE).** A G$_q$PCR agonist activates phospholipase C (PLC) which cleaves PIP$_2$ into DAG and IP$_3$. DAG activates TRPC3/6/7 channels. PIP$_2$: phosphatidylinositol 4,5-bisphosphate, DAG: diacylglycerol, IP$_3$: phosphatidylinositoltriphosphate (from [32]).

ter of debate, if TRPC channels are also store-operated. The transient receptor potential (TRP) genes were discovered in the fruit fly Drosophila melanogaster by Cosens and Manning over 40 years ago. They recorded a transient response to steady light in a visually impaired TRP mutant fly instead of a sustained response in a wild type fly. According to this observation they named the mutant 'transient receptor potential' [18]. 20 years later, Montell and Rubin identified the trp gene [87]. The superfamily of TRP channels can be divided into seven families depending on the protein homology: TRPC (canonical), TRPV (vanilloid), TRPM (melastatin), TRPA (ankyrin), TRPML (mucolipin), TRPP (polycystin) and TRPN (NO-mechano-potential C). All TRP channels are characterized by intracellular amino and carboxyl tails which vary from subfamily to subfamily, six transmembrane domains (S1 to S6) and a pore-forming loop between S5 and S6 (see figure 1.3) [91].

The TRPC family is also characterized by four amino-terminal ankyrin repeats and can be further divided into four subfamilies: TRPC1, TRPC2, TRPC3/6/7 and TRPC4/5. TRPC1 is structurally and functionally unique but TRPC 4/5 share 65% amino acid sequence homology and the TRPC 3/6/7 subfamily shares 70%-80% amino sequence homology [26].
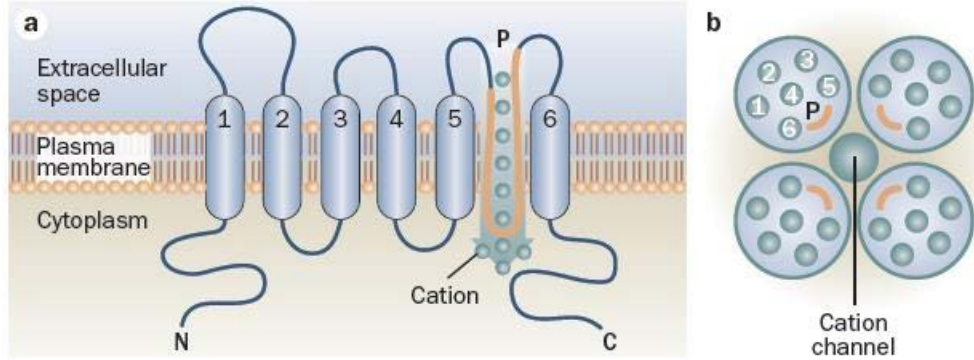
Figure 1.3: **Structure of transient receptor potential (TRP) channels.** a) TRP channels consist of six transmembrane domains (1–6), a pore forming-loop (P) between S5 and S6 and intracellular carboxyl (C) and amino (N) termini. b) Four TRP channels form a functional cation channel [91] (from [148])

The first subfamily consists only of the TRPC1 channel. It was the the first human TRP channel which was cloned in 1995 [145] and characterized in 1996 [155]. The human TRPC1 gene is localized on chromosome 3, while the murine TRPC1 is localized on chromosome 9 [16]. The molecular structure of the TRPC1 channels is similar to the other TRP channels. The physiological role TRPC1 is still a matter of debate. TRPC1 is expressed in most human and murine tissue [145]. TRPC1 can build heterotetramers with TRPC4 and TRPC5 or with TRPC3, TRPC6 and TRPC7 but may not function as homotetramer [52] [125].

The second subfamily consists only of TRPC2, a human pseudogene which does not code for a functional protein in humans. The third subfamily consist of TRPC 4 and 5. Different from other TRPC channels, they own a postsynaptic density protein 95-binding motif. TRPC4 is expressed in most tissue, TRPC5 mainly in the central nervous system [91].

The fourth subfamily consists of TRPC3, TRPC6 and TRPC7. They are activated by diacylglycerol [53]. TRPC7 is mainly expressed in the pituitary glands, kidney, central nervous system, heart and lung [91].

The first murine TRPC6 cDNA was isolated from brain [8] and the respective murine TRPC6 gene is localized on chromosome 9. Human TRPC6 was cloned from placenta [53] and its gene is localized on chromosome 11q21-q22 and has 13 exons [24]. TRPC6

is ubiquitously expressed and shows higher expression levels in lung, placenta, ovary and spleen [51]. The molecular structure of the TRPC6 channel is similar to that of other TRP channels (see figure 1.3). Four TRPC6 monomers build a tetramer with a functional pore domain in the center. The two glycosylation sites at the first and second extracellular loops (Asn473, Asn561) determine that TRPC6 acts as a receptor-operated calcium channel [28]. A mutation of Asn651 to Gln prevented glycosylation and increased the basal activity of TRPC6 [28].

The dual glycosylation is responsible for the lower basal activity of the TRPC6 compared to the single glycosylated TRPC3 channel [28]. The TRPC3 channel further distinguishes from the TRPC6 channel by its lower Ca^{2+} selectivity and higher single channel conductance [53] [28]. TRPC3 is mainly expressed in the central nervous system, smooth and cardiac muscle cells. It has been described to be involved in brain-derived neurotrophic factor mediated growth and glutamate receptor signaling and as postsynaptic cation channel essential for metabotropic glutamate receptor1 (mGluR1)-dependent synaptic transmission in cerebellar Purkinje neurons [91].

1.2.3 The role of Ca^{2+} signaling during pulmonary arterial hypertension (PAH)

Several research groups have studied the function of TRPCs, STIM and Orai in cells of the lung and lung associated diseases, such as pulmonary arterial hypertension (PAH). PAH is a progressive disease which is characterized by vascular remodeling, vascular arterial wall stiffness, vasoconstriction and thrombosis [58]. Risk factors to develop a PAH are hypoxia in parts of the lung, induced by COPD [144], idiopathic pulmonary fibrosis [114], appetite suppressant drugs (such as aminorex, fenfluramine derivatives and benfluorex) [117], a genetic predisposition (most of them mutations of the bone morphogenetic protein receptor 2) [58], or changes in endothelin expression [34].

Endothelin is the strongest vasoconstrictor known. It is synthesized from big endothelin1 by the endothelin converting enzyme. Two different G-protein coupled endothelin

receptors mediate the effect of endothelin1: the endothelin A and endothelin B receptors [86]. Endothelin A receptors are mainly expressed in pulmonary vascular smooth muscle cells where they mediate vasoconstriction and proliferation, while endothelin B receptors are mainly expressed in endothelial cells where they promote vasodilatation. There are regional differences in endothelin receptor localization and distribution in the pulmonary vasculature. Due to these differences in distribution, endothelin induces dilatation of the pulmonary circulation and at the same time vasoconstriction of the systemic circulation [128] [33].

Takahashi et al. demonstrated that the mRNA levels of endothelin1 and the endothelin A receptor were upregulated in lung of rats which had been exposed to hypoxia. Immunostaining with anti-big endothelin1 antibody revealed that endothelin1, the endothelin converting enzyme and endothelin A receptors were significantly increased in distal segments. The shift of endothelin A receptor expression from proximal arteries during normoxia to distal arteries after hypoxia might play a role during vascular remodeling [128] [33]. Polymorphisms of the endothelin receptor might affect endothelin signaling and the therapy with endothelin receptor antagonists [54].

Up to date PAH is treated with phosphodiesterase 5 inhibitors (e.g. sildenafil), cGMP (cyclic guanosine monophosphate) activator (e.g. riociguat, cinaciguat), NO-releasing substances, prostanoids (e.g. epoprostenol) or endothelin-receptor antagonists (e.g. bosentan) (see figure 1.4) [58]. The reduced production and bioavailability of NO in endothelial cells is targeted by the phosphodiesterase 5 inhibitor, the cGMP activator and NO-releasing substances. The NO-synthase releases NO when catalyzing the reaction of L-arginine to L-citrulline. NO activates the soluble guanylate cyclase (sGC) which in turn induces the formation of cyclic guanine monophosphate (cGMP) and cGMP relaxes smooth muscle cells. Phosphodiesterase 5 degrades cGMP and its inhibition enhances the bioavailability of cGMP as well as increases vasodilatation. Prostanoids are prostacyclin analogues. Prostacyclin is produced endogenously from arachidonic acid by the cyclooxygenase and prostacyclin synthase. It has vasodilatatory, anti-inflammatory and antiproliferative effects on the blood vessel. Endothelin receptor antagonists prevent the binding of endogenous endothelin on its receptor and

therefore prevent vasoconstriction [58].

Even though this symptomatic treatment can slow down the progression and the subsequent right heart failure, it does not interfere with the development of PAH. Ca^{2+} signaling in precapillary pulmonary arterial smooth muscle cells (PPASMC) and mouse pulmonary microvascular endothelial cells (MPMVEC) plays an essential role in the development and progression of PAH but is not affected by currently available therapeutic drugs. A combination of the previously used therapeutic drugs with new Ca^{2+} channel blockers may have the potential to improve the therapy for PAH patients.

PPASMC are located in the small, arterial vessels ($<500\,\mu m$ in diameter [142]) which regulate the vascular tone [29]. This fact and because remodeling of these smooth muscle cells is an essential step during PAH formation [58], prompted us to isolate smooth muscle cells from precapillary arteries for our experiments. PPASMC appear in two different phenotypes: the quiescent contractile vascular phenotype and the proliferative and migratory phenotype. While the beneficial contractile phenotype regulates the vascular tone, the pathophysiological proliferative phenotype is involved in remodeling. A switch to this phenotype can be induced by inflammatory mediators or mechanical stress [115]. Many Ca^{2+} channels have an altered gene expression and are dysregulated during PAH inducing high cytosolic Ca^{2+} concentrations. This rise in intracellular Ca^{2+} concentration triggers proliferation, migration and vasoconstriction in PPASMCs. Proliferation is regulated by Ca^{2+}-dependent kinases, such as CaMK, and Ca^{2+}-dependent transcription factors, such as nuclear factor of activated T-cells (NFAT). Moreover, Ca^{2+} affects gene expression by protein kinase C and calmodulin activation [65] [26].

Quantitative RT-PCR-analysis revealed that TRPC1 and TRPC6 are the main isoforms expressed in non-passaged PPASMC cultivated for 5 days. The other TRPC channels play only a minor role in PPASMC [143]. Quantitative RT-PCR-analysis of thoraic aortas and cerebral aortas from TRPC6$^{-/-}$ mice demonstrated a compensatory upregulation of TRPC3 [29]. Resulting from the compensatory upregulation of TRPC3, TRPC6$^{-/-}$ mice show a higher smooth muscle contractility in isolated aortic

rings [29]. To circumvent this upregulation, we used TRPC 1/3/6 deficient mice for investigating functional SOCE in PPASMC.
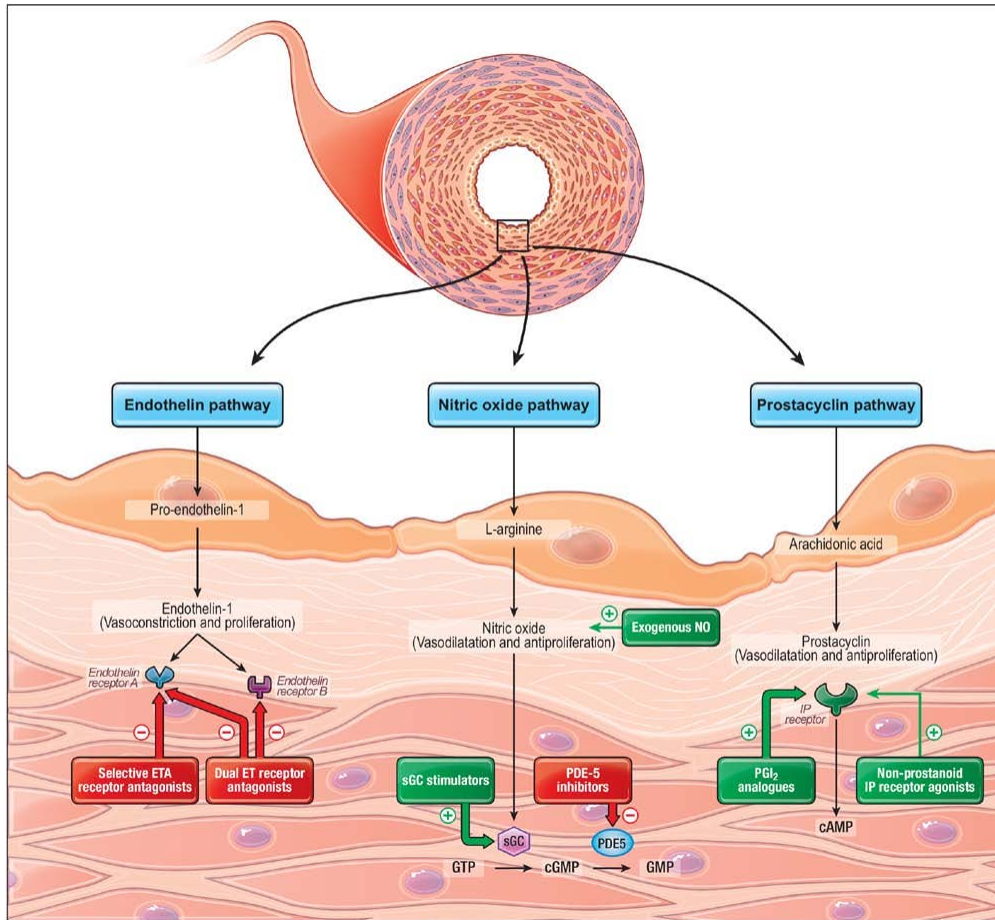
Figure 1.4: **Treatment of pulmonary arterial hypertension (PAH).** PDE: phosphodiesterase, sGC: soluble guanylate cyclase, GTP: guanosine-5'-triphosphate, cGMP: cyclic guanine monophosphate, GMP: guanine monophosphate, NO: nitric oxide, PGI$_2$: prostacyclin, cAMP: cyclic adenosine monophosphate, IP receptor: prostacyclin receptor. For more details see text (from [58])

TRPC6 and TRPC3 have been shown to be upregulated in smooth muscle cells of idiopathic pulmonary arterial hypertension (IPAH) patients and in a rat model of pulmonary hypertension. TRPC6 siRNA downregulated the TRPC6 expression in smooth muscle cells of IPAH patients and decreased proliferation. Genomic DNA analysis of IPAH patients identified a single nucleotide polymorphism in the promotor of the TRPC6 gene in patients inducing enhanced nuclear factor kappa B-mediated promoter activity and increased TRPC6 expression [150].

TRPC6 and TRPC1 have been demonstrated to be involved in hypoxic pulmonary vasoconstriction. Isolated, buffer-perfused, and ventilated mouse lungs of TRPC6^{-/-} mice did not show an acute response to hypoxia which was observed in Wt lungs. But similar to Wt lungs, an increase in pulmonary arterial pressure during sustained response was observed in TRPC6^{-/-} lungs [143]. When TRPC6^{-/-} mice were exposed to chronic hypoxia, they developed similarly a pulmonary hypertension compared to Wt mice [143]. In contrast to TRPC6^{-/-} mice, TRPC1^{-/-} mice showed an unchanged acute and sustained response to hypoxia. When mice were kept under hypoxic conditions for 21 days, wildtype mice developed a pulmonary hypertension but TRPC1^{-/-} mice were protected [79]. PPASMC from mice chronically treated with hypoxia, displayed upregulated TRPC1, but unchanged TRPC3 and TRPC6 mRNA levels. Proliferation of PPASMC exposed to hypoxia for 24h was reduced significantly in PPASMC isolated from TRPC1^{-/-} or TRPC1/6[-/-] mice but unchanged in PPASMC isolated from TRPC6^{-/-} mice [79].

STIM2 and Orai2, but not STIM1, have been shown to be upregulated in PPASMC from IPAH patients and enhanced SOCE in PPASMC from IPAH patients was reduced after transfection with STIM2 specific siRNAs [123]. PPASMC from IPAH patients treated with STIM2 siRNA showed similar proliferation levels after 72hrs as cells from non-pulmonary hypertension donors [123]. Overexpression of STIM2 in control PPASMC did neither enhance SOCE nor proliferation and PPASMCs treated with hypoxia for 48hrs showed enhanced STIM2 and Orai2 protein expression levels [123].

1.2.4 Do TRPCs interact with STIM and induce SOCE?

It is widely accepted that SOCE resulting from STIM-Orai interaction is the molecular correlate of the I_{CRAC} in immune cells [56] [11]. However, in recent years the question arose if STIM may also interact with other plasma membrane Ca^{2+} channels besides Orai in other cells forming a SOCE current clearly different from I_{CRAC}. There are two main hypotheses describing the involvement of TRPCs in SOCE reported by the research groups from Shmuel Muallem and Lutz Birnbaumer.

The Muallem group claims that STIM can activate both Orai and TRPCs directly (see figure 1.5A).The STIM protein contains a positive charged lysine domain. Zeng et al. analyzed the TRPC protein for negatively charged complement domain which could interact electrostatically with the STIM protein. Mutation analysis revealed that negatively charged aspartates in TRPC1(^{639}DD^{640}) interact electrostatically with the positively charged STIM1(^{684}KK^{685}). Similar gating was observed with TRPC3(^{697}DD^{698}) [152]. However, Lee et al. have shown that the STIM1 lysine domain is not required for binding, but close contacts between the SOAR region of STIM and the coiled coil domains of TRPC [68]. While the SOAR region of STIM seems to activate both Orai and TRPC, the electrostatic interaction only occurs between STIM and TRPC [68].
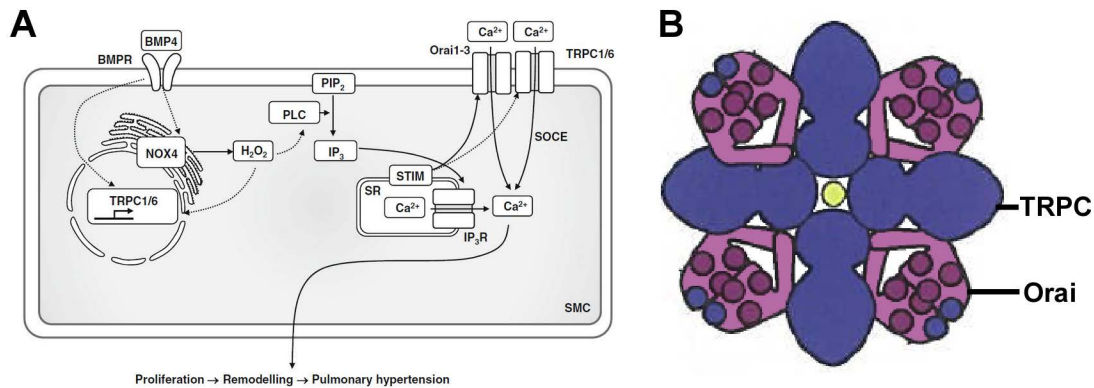
Figure 1.5: **Schematic presentation of two hypotheses for TRPC-Orai interaction.** A)The research group of Shmuel Muallem claims that STIM can activate both Orai and TRPCs directly. SOCE mediated by Orai and SOCE by TRPCs could interact but fulfill different cellular functions e.g. in precapillary pulmonary arterial smooth muscle cells (PPASMC) (from [80]). B)The research group of Luz Birnbaumer is presenting data in favor for a TRPC-Orai octamer (from [70]). TRPCs in these heteromeric channels could contribute to SOCE. Are less then four Orai dimers part of the channel, the channel acts as receptor-operated channel (ROC). BMP: bone morphogenetic protein, NOX: NADPH oxidase, SR: sarcoplasmic reticulum, PIP$_2$: phosphatidylinositol 4,5-bisphosphate, PLC: phospholipase C, IP$_3$: inositol 1,4,5-trisphosphate, IP$_3$R: inositol 1,4,5-trisphosphate receptor,

The research group of Lutz Birnbaumer claims that TRPCs and Orai form heteromers. Orai could act as regulatory subunits of TRPC channels in these heteromeric SOC channels. Are less then four Orai dimers part of the octameric channel, the TRPC channels act as ROC. The Birnbaumer group bases their hypothesis on the data pre-

sented in two manuscripts [71] [73]. Liao et al. observed a functional interaction between TRPCs and Orai e.g. Orai1 interacted with the N- and C-termini of TRPC3 and TRPC6 in co-immunoprecipitation experiments. HEK293 cells stably overexpressing TRPC3 and TRPC6 and transfected with Orai1, 2 or 3 showed increased SOCE as compared with control cells not expressing TRPC3 and TRPC6. HEK293 cells stably overexpressing TRPC3 or TRPC6 showed reduced single-channel cation currents after Orai1 overexpression [71]. Moreover, $1\,\mu M$ Gd^{3+} blocks SOCE but not ROCE mediated by TRPC channels. The dominant negative Orai1 mutant G91W prevented Gd^{3+} induced ROCE in HEK 293 cells. The same mutant reduced OAG-mediated Ca^{2+} entry in stably or transiently expressing TRPC3 HEK 293 cells. These results suggest that TRPC and Orai form a complex which could be involved in both SOCE and ROCE [73] (see figure 1.5B).

It is suggested that TRPC1 is only functional with other TRPC channels [52]. TR-PCs haven been shown to form homo- or heterotetramers within the TRPC1/4/5 and TRPC3/6/7 subfamilies by Foerster resonance energy transfer (FRET) and co-immunoprecipitation [52]. TRPC1 channels were detected in heterodimers with TRPC3 and TRPC4 with TRPC6 [151]. Recently it was demonstrated that TRPC1 reduces Ca^{2+} permeability in heteromeric channels with TRPC3, TRPC4, TRPC5, TRPC6 and TRPC7. Interestingly, these heteromeric channels displayed a significantly reduced Ca^{2+} influx compared to homomeric channels [125].

It was also reported that TRPC1 is colocalized with STIM1 in lipid rafts and its expression is controlled by Orai [14]. The same research group described that blocking of SOCE by gadolinium, extracellular Ca^{2+} free medium, Orai1 knockdown or expression of dominant- negative mutant Orai1 lacking a functional pore (E106Q) prevented TRPC1 expression in the plasma membrane. STIM1 was able to interact by its polybasic tail with PIP_2 in the plasma membrane lipid domains and deletion of the polybasic tail resulted in abrogation of SOCE and inhibition of STIM1 punctae formation in the ER membrane [14].

TRPC6, Orai1 and STIM1 were also analyzed in human platelets. Double deficient Orai1$^{-/-}$/Trpc6$^{-/-}$ platelets showed a stronger reduction in thapsigargin-induced SOCE

than Orai1-/- platelets. TRPC6 channels are activated by DAG and DAG can be produced by two different ways in platelets: hydrolysis of PIP_2 by phospholipase C (PLC) as well as hydrolysis of phosphatidic acid (PA) by phospholipase D (PLD) and phosphatidic acid phosphohydrolase (PAP) (see figure 1.6). A radioactive PLD assay revealed a strong reduction in PLD activity in Orai1^{-/-} platelets. An IP-ELISA identified a reduced PLC activity in Orai1-/- compared to wild-type platelets in the presence of thapsigargin and extracellular calcium. Stimulation of different GPCRs by platelet agonists demonstrated that Orai is not necessary for PLC and PLD activation by platelet GPCRs under physiologic conditions. However, Orai1-mediated activation of phospholipase C and D might play a role during pathophysiological platelet hyperreactivity [13] (see figure 1.6). The STIM1/Orai1/TRPC6 interaction was further analyzed in human platelets by Jardin et al. [59]. They reported an interaction of hTRPC6 and STIM1 and Orai1 in co-immunoprecipitation experiments after inducing SOCE by thapsigargin. Stimulation by the diacylglycerol analogue OAG (1-oleoyl-2-acetyl-glycerol) or dimethyl-BAPTA (1,2-bis-(o-aminophenoxy)ethane-N,N,N',N'-tetra-acetic acid) loading abolished the interaction and enhanced the association of hTRPC6 with hTRPC3 [59].

The physiological role of the proposed STIM/TRPC/Orai interaction is not yet known. Isolated platelets from TRPC1 knockout mice showed an intact SOCE [137]. This contradicted previous results of other authors who had claimed a TRPC1 involvement in SOCE after using TRPC1 antibodies of questionable quality [108]. However, in salivary gland acinar cells isolated from TRPC1^{-/-} mice no SOCE was detectable after thapsigargin stimulation, while the expression of STIM1 and other TRPC channel was unchanged in these cells [75]. Along these line, pancreatic acinar cells from TRPC1^{-/-} mice showed decreased SOCE and Ca^{2+}-activated Cl- channel activity [55]. However in thoracic smooth muscle cells from TRPC1-deficient mice, no changes in thapsigargin-induced Ba^{2+} influx was detected, and there was no significant difference in the membrane capacitance and current densities of wildtype and TRPC1^{-/-} cells [27].
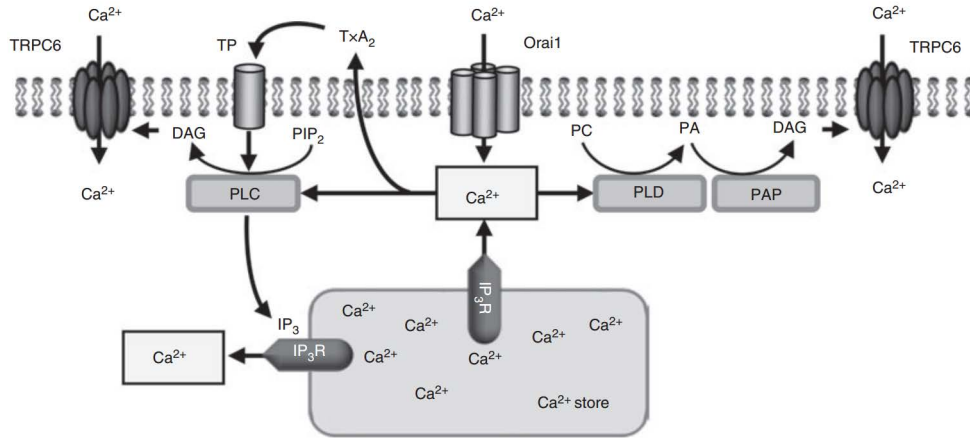
Figure 1.6: **Orai-induced Ca^{2+} entry activates PLC and PLD which produces DAG and activates TRPC3 and TRPC6.** DAG: diacylglycerol, IP_3: inositol 1,4,5-trisphosphate, IP_3R: inositol 1,4,5-trisphosphate receptor, PC: phosphatidylcholine, PLD: phospholipase D, PA: phosphatidic acid, PAP: phosphatidic acid phosphohydrolase, PIP_2: phosphatidylinositol 4,5-bisphosphate, PLC: phospholipase C, TP: thromboxane A_2 receptor, TxA_2: thromboxane A_2. For more details see text (from [13])

1.3 The role of SOCE in vascular endothelial and smooth muscle cells during physiology and pathophysiology

1.3.1 SOCE in vaso- and bronchoconstriction

Ca^{2+} signaling in PPASMC and MPMVEC plays an essential role in the development and progression of PAH. Under hypoxic conditions vasoconstriction in PPASMC at the low ventilated areas redirect the blood flow to the still oxygen rich regions to supply the body with sufficient O_2 even if parts of the lung are destroyed. The contraction of PPASMCs has therefore some characteristic features which distinguishes it from the contraction of skeletal or cardiac muscle cells. PPASMC undergo slow, sustained and tonic contractions. The contraction can be either initiated by changes in membrane potential or by pharmacomechanical coupling. Regardless of the mechanism of initiation, a rise in cytosolic Ca^{2+} induces PPASMC contraction and pulmonary vasoconstriction. Intracellular Ca^{2+} binds to calmodulin which activates the myosin

light chain kinase to phosphorylate the myosin light chain. This phosphorylation induces hydrolyzation of ATP (adenosine triphosphate) by ATPases and the myosin head crossbridges to the actin filament which causes contraction. Dephosphorylation of the myosin light chain, which does not require Ca^{2+}, induce smooth muscle cell relaxation[78].

A model widely used to investigate the capacity of smooth muscle constriction or relaxation is the myograph. Intact rings from different vessels can be isolated from a mouse model and mounted in a physiological organ bath. Upon receptor stimulation, the mechanical force is transduced into an electrical signal which is recorded. Tracheal ring and thoracic aorta segments have been used in numerous studies. Tracheal smooth muscle cells mainly express the muscarinic acetylcholine receptor subtypes M_2 ($G\alpha_i$) and M_3 ($G\alpha_q$) which can be stimulated with carbachol. At the M_3 receptor, Carbachol induces a G_q-coupled signaling cascade by activating phospholipase C leading to increased intracellular Ca^{2+} levels [118]. Different from smooth muscle cells of the trachea, stimulation of the muscarinic acetylcholine receptor in vascular endothelial cells induces relaxation. High intracellular Ca^{2+} in PPASMCs can be passed to MPMVECs via gap junctions and induce Ca^{2+}-dependent NO production [78]. This apparently opposing mechanism is highly beneficial because it limits the smooth muscle contraction and therefore fine tunes vasoconstriction. Similar to the pathway in PPASMCs, carbachol binds to its M_3 receptor in endothelial cells and induces a G_q-mediated signaling pathway which elevates the cytosolic Ca^{2+}. Ca^{2+} enables the endothelial NO-synthase to produce NO. NO diffuses into smooth muscle cells of the tunica media and activates guanylate cyclases which convert GTP into cGMP activating protein kinase G. Stimulation of protein kinase G induces dephosphorylation of myosin light chains by its phosphatases which results into smooth muscle relaxation and vasodilatation [45].

The role of SOCE in vasoconstriction and vasodilatation has already been investigated by several research groups. Aortic rings from mice with a STIM1-deficiency in smooth muscle cells (STIM1$^{\Delta SMC}$) displayed a reduced phenylephrine-induced aortic vasoconstriction [83]. This result was reproduced by Kassan et al. in aortic rings [61].

After depleting internal Ca^{2+} stores by phenylephrine and thapsigargin, aortic rings from STIM1$^{\Delta SMC}$ mice showed a reduced SOCE-mediated contraction. The research group of Donald Gill further performed Ca^{2+} refilling experiments after store depletion to elucidate the molecular background of the myograph contraction experiments. They demonstrated that the Ca^{2+} refilling rates after store depletion are reduced in STIM1$^{\Delta SMC}$ after repetitive treatment with cyclopiazonic acid in the presence of extracellular Ca^{2+} in comparison to wild-type (WT) SMCs. [83]. Moreover, Kassan et al. demonstrated that STIM1$^{\Delta EC}$ aortic rings treated with acetylcholine dilatated significantly less than heterozygous STIM1$^{\Delta EC}$ and wildtype aortic rings [61].

1.3.2   SOCE during inflammation and edema formation

STIM1 and Orai1 are involved in inflammatory processes. Loss of function mutations in STIM1 and Orai1 in human patients causes a severe combined immunodeficiency which is characterized by an impaired T-cell function [35]. The role of STIM1 and Orai1 in T-cells has already been extensively studied by other authors. However, not only circulating immune cells are involved in inflammation but also endothelial cells play an important role. Endothelial cells are specialized epithelial cells which line the interior of all blood vessels. Intact endothelial cells form a tight barrier between blood and interstitium. If endothelial cells are dysfunctional, barrier permeability is decreased and fluid can pass and induce edema [99]. Bacterial products like lipopolysaccharide (LPS) and endogenous cytokines stimulate the endothelium and increase the endothelial barrier permeability. This response enables neutrophils and monocytes to penetrate infected tissue and kill the pathogens during infection. But at the same time it allows protein-rich edema fluid to leak into the alveoli causing impaired gas exchange and hypoxemia [116].

LPS (lipopolysaccharide) is the main component of the outer gram negative bacterial membrane, for example in *Klebsiella pneumoniae*, a bacterium which can induce pneumoniae, an inflammation of the alveoli, in human and mice. In experimental pneumoniae models, bacteria are applied intratracheally or intranasally. When LPS binds to the toll-like receptor 4, this initiates a signaling cascade via the two adaptor

proteins TRIF and myD88 and results in nuclear translocation of AP-1, NF-κB, and IRF3. As a consequence, several inflammatory cytokines, such as TNF-α, IL-6 and IFN-β are expressed. TNF-α binds to its respective receptor at the endothelial plasma membrane and induce a signaling cascade which results in gene expression of inflammatory genes, such as E-selectin, intercellular adhesion molecule 1 (ICAM1), vascular cell-adhesion molecule 1 (VCAM1) and COX2 [99]. Finally, the inflamed endothelial cells become dysfunctional, allow fluid to leak through tight junctions and form a lung edema.
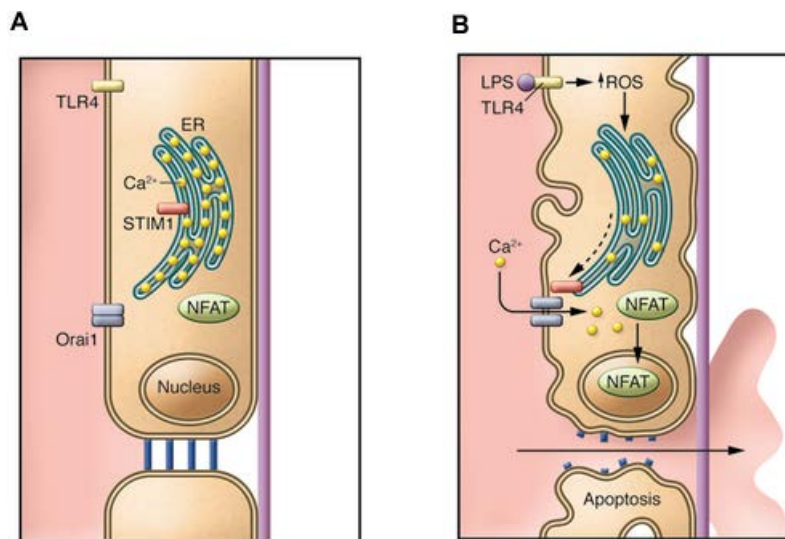
Figure 1.7: **STIM1 is essential for LPS-mediated NFAT activation.** A) Intact pulmonary endothelial cells form a barrier between blood vessels, interstitium and alveoli, B) Lipopolysaccharide (LPS)-induced reactive oxygen species (ROS) accumulation, Ca^{2+} oscillations and nuclear factor of activated T-cells (NFAT) accumulation makes the endothelial barrier leaky. TLR4: Toll-like receptor4 (from [116]).

LPS can not only be used experimentally to induce pneumoniae, but also to induce acute lung injury by intraperitoneal application. In this model, LPS binds to its Toll-like receptor4 (TLR4) in endothelial cells and thereby elevates intracellular ROS levels. According to Gandhirajan et al., STIM senses the increase of ROS by S-glutathionylation of its cysteine residues. This induces high-frequency Ca^{2+} oscillations through Ca^{2+} originating from the ER and the extracellular space via membrane Ca^{2+} channels and results into nuclear NFAT translocation (see figure 1.7) [39]. The NFATs are Ca^{2+}-sensitive transcription factors which are involved in transcription of

proinflammatory mediators. Inactive, phosphorylated NFAT is located in the cytoplasm. Upon intracellular Ca^{2+} elevation, the calmodulin-dependent serin/theronine phosphatase calcineurin dephosphorylates NFAT and triggers translocation into the nucleus. The NFAT isoforms c1 and c3 control vascular development, angiogenesis and are involved in inflammation of the vasculature [105].

Gandhirajan et al. investigated how a STIM1-deficiency in endothelial cells (STIM1$^{\Delta EC}$) affects NFAT translocation and endothelial barrier function. They demonstrated that STIM1$^{\Delta EC}$ cells heterologously expressing GFP-tagged NFATc3 (NFATc3-GFP) translocated a significant lower amount of NFATc3 to the nucleus compared to wild-type MPMVECs. The constitutively active STIM1 mutant C56A showed SOCE and NFATc3-GFP nuclear translocation in MPMVECs which were lacking a subunit of the ROS producing NADPH oxidase. To investigate endothelial barrier function, Gandhirajan et al. induced a vascular inflammation in STIM1$^{\Delta EC}$ mice by injecting LPS (1mg/kg body weight) intraperitoneally. 24hs after LPS treatment, the mice were injected with 5% FITC-dextran via the facial vein and vascular permeability was assessed based on the fluorescence intensity in the extravascular space. STIM1$^{\Delta EC}$ mice showed significantly less extravascular FITC-dextran leakage than STIM1 floxed control mice. The reduced vascular leakage in the LPS-treated STIM1$^{\Delta EC}$ mice resulted in less lung edema formation indicated by a reduced lung wet-to-dry weight ratio. Delivery of the unspecific SOCE blocker 3,5-bis(trifluoromethyl)pyrazole reduced vascular leakage and lung wet-to-dry weight ratios in LPS-treated wildtype mice [39].

Vascular permeability of endothelial cells can be investigated on cellular levels using the coagulation protease thrombin. Thrombin induces formation of stress fibers and an opening of the cellular tight junctions. When MPMVECs are stimulated with the PAR1 receptor agonist thrombin, G_q, $G_{12/13}$ and G_i coupled signaling cascades are induced resulting in elevated intracellular Ca^{2+} levels and RhoA activation. G_q-mediated phospholipase C signaling induces ROCE and SOCE through TRPC, STIM and Orai and the resulting elevated intracellular Ca^{2+} establishes a Ca^{2+}-calmodulin complex. Ca^{2+}-calmodulin activates the myosin light chain kinase (MLCK) which
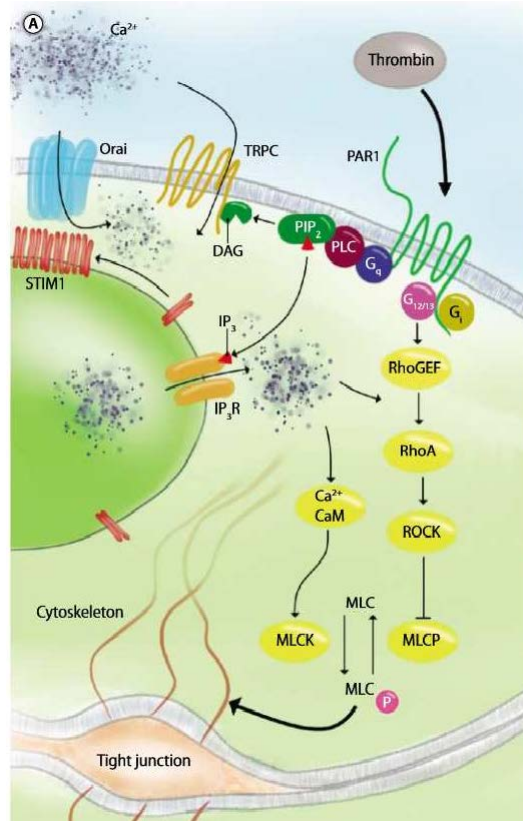
Figure 1.8: **Thrombin-induced disruption of the endothelial barrier.** Thrombin induces induces elevated intracellular Ca^{2+} levels and RhoA activation which results into stress fiber formation and opening of tight junctions. PAR1: protease-activated receptor1, CaM: Ca^{2+}-calmodulin, MLCK: myosin light chain kinase, MLCP: myosin light chain phosphatase (from [42]).

phosphorylates the myosin light chain (MLC). Simultaneously, thrombin induces the $G_{12/13}$-mediates RhoA signaling cascade. Specifically, the free G-protein $\beta\gamma$ subunits activate guanine nucleotide exchange factor (Rho–GEF) which converts inactive RhoA-GDP to active RhoA-GTP. RhoA-GTP induces Rho-dependent kinase (ROCK) phosphorylation which results in inactivation of MLC phosphatase. Phosphorylated MLC contracts actin filaments which are bound to tight junctions and adherens junction complexes thereby opening junctions between endothelial cells and inducing leakage of plasma proteins. Under resting conditions, MLC phosphatase dephosphorylates MLC and consequently prevents opening of tight junctions. After G_q-protein-coupled-receptor stimulation, MLC is phosphorylated and induces an opening of the tight junctions (see figure 1.8) [121]. F-actin filaments can be stained

with phalloidin to quantify their intensities. The opened tight junctions allow either FITC-dextran or an electrical current to pass. Therefore, the fluorescence of FITC-dextran which has passed the barrier can be quantified in a transwell permeability assay or the resistance of a small alternating current which is applied to the endothelial layer can be analyzed using the Electrical Cell-Substrate Impedance Sensing (ECIS). The influence of STIM and Orai in the endothelial barrier function has been investigated by Shinde et al. in siRNA transfected human umbilical vein endothelial cells (HUVECs) and human dermal microvascular endothelial cells (HDMECs). They demonstrated that thrombin-induced reduction of endothelial resistance is attenuated in HUVECs transfected with STIM1 specific siRNAs. Transfection of HUVECs with Orai1 specific siRNAs did not show any differences in thrombin-induced transendothelial resistance in comparison to untreated control cells. Thrombin-induced SOCE was also absent in HDMECs transfected with STIM1 and Orai1 specific siRNA. These results indicate that SOCE via Orai1 is not essential for endothelial barrier disruption. Thrombin-induced stress fiber and VE-cadherin cell junction formation was reduced in HUVECs after application of STIM1 specific siRNAs while RhoA activity was enhanced. The thrombin-induced enhanced RhoA activity of HUVECs transfected with STIM1 specific siRNA was attenuated, but not in HUVECs transfected Orai1 specific siRNA. Thus, it is assumed that STIM1 could also be an upstream effector of of RhoA [121].

1.3.3 SOCE induced endothelial migration and proliferation

Endothelial cell migration and proliferation is an essential process during formation of new blood vessels (angiogenesis)and vascular repair. Moreover, both play an important role in pathophysiological processes such as atherosclerosis. The characteristics of endothelial cells vary according to the tissue they originate from. The process of endothelial migration can be divided into several steps. Before an endothelial cell moves, it senses the chemotaxical gradient, mostly driven by vascular endothelial growth factor (VEGF), via its filopodia. Afterwards, protruding lamellipodia attach to the focal adhesion sites. The following stress fiber-mediated contraction of

the cell induces a forward movement. Finally, the rear is released by focal adhesion disassembly and adhesive and signaling components are recycled [67].

Endothelial migration is induced by several stimuli, such as shear stress, chemotaxis and binding of integrins [67]. Even though one major stimulus for migration is the expression of VEGF, other stimuli also contribute, such as intracellular Ca^{2+}, ROS or NO. Endothelial migration is often investigated experimentally by the scratch assay. Scratching of an endothelial monolayer disrupts contact inhibition and induces Ca^{2+} entry from the extracellular space [15]. High intracellular Ca^{2+} activate protein kinase C and calmodulin-dependent protein kinases. As a result, the immediate early genes c-fos and c-jun are transcribed and induce expression of secondary genes, such as VEGF [133]. The basal Ca^{2+} concentration of the leading edge of the endothelial cell is reduced compared to the trailing edge. This Ca^{2+} gradient within the cell allows a fine-tuned regulation of endothelial migration [15]. Both the Ca^{2+} originating from the internal stores and from the extracellular space is assumed to contribute to migration. The intracellular Ca^{2+} affects the cytoskeletal remodeling, the focal adhesion turnover, the matrix degradation and formation of lamellipodia - all functions which affect the endothelial migration [90].

The endothelial migration has shown to be affected by SOCE. Kimura et al. demonstrated that inhibition of SOCE reduced wound healing after scratch formation. They treated bovine aortic endothelial cells with thapsigargin or cyclopiazonic acid for 6h or 24h and quantified the number of cells which migrated. When cyclopiazonic acid was removed after 6h the destructed migration was rescued. Comparing intracellular Ca^{2+} levels of non-migrating and migrating cells demonstrated that basal $[Ca^{2+}]_i$ was lower but the total amount of stored Ca^{2+} was higher in migrating cells. These results indicate that a functional SERCA pump is essential endothelial migration. In which way cytosolic Ca^{2+}-binding proteins or the mitochondrial Ca^{2+} uptake/release affects endothelial migration after thapsigargin or cyclopiazonic acid stimulation needs further investigation [15]. The importance of STIM and Orai during migration has been confirmed in smooth muscle cells. Aortic smooth muscle cells transfected with STIM1 or Orai1 specific siRNAs showed a reduced PDGF-induced migration in a

Boyden chamber [124]. SiRNA-mediated knockdown of STIM1 and Orai1 in vascular smooth muscle cells reduced wound healing 12h or 24h after scratch formation [6] [101] while knockdown of STIM2, Orai2 and Orai3 was not effective [6].

ROS is produced in vascular endothelial cells by NADPH oxidase (NOX). NOX are proteins which mediate a redox reaction during which oxygen is reduced to superoxide and electrons are transferred across a biological membrane. The NOX isoforms (NOX1, NOX2, NOX3, NOX4, NOX5, DUOX1, and DUOX2) fulfill different functions according to the cells they are expressed. NOX1, NOX2, NOX4 and NOX5 are expressed in endothelial cells [5] and regulate cell differentiation, proliferation, migration, angiogenesis and vascular tone [111]. NOX2 is the prototypical NOX which was first described in neutrophils and macrophages. NOX2 in endothelial cells plays an important role during ROS production and bioavailability of endothelium derived NO [5] and it suggested to play an important role during angiogenesis [136] NOX1 and NOX4 have been reported to be involved in cell growth and growth suppression. The function of NOX5 in endothelial cells is still poorly understood [111].

NOX constantly releases low levels of superoxide but upon stimulation can increase superoxide production [136]. MPMVECs derived from STIM1$^{\Delta EC}$ mice showed similar NOX2 protein levels and cytosolic superoxide production by DHE fluorescent staining as MPMVECs from wiltype mice. NOX2 can be stimulated experimentally to produce ROS by application of LPS which binds to the cellular TLR4 receptor, interacts with NOX2 and elevates intracellular ROS levels.

Gandhirajan et al. showed that LPS/TLR4 and NOX2 mediated increased ROS levels induced Ca^{2+} oscillations in MPMVECs. Inhibition of NOX2 abrogated these Ca^{2+} oscillations. Moreover, they demonstrated that ROS can induce STIM1-mediated SOCE by ROS sensing of STIM1 through S-glutathionylation of its cysteine residues [39][116]. The NOX-mediated superoxide production stimulates migration in vascular endothelial cells [136]. In accordance with the unaltered NOX2 and and cytosolic superoxide production, STIM1$^{\Delta EC}$ migrated similarly to wildtype MPMVECs 24h after scratch formation [39].

NO is produced by the nitrite oxide synthase (NOS) and is a major player in the

induction of vasodilatation. In the inactive, unphosphorylated, state, NOS exists as a monomer which transfers electrons from reduced nicotinamide adenine dinucleotide phosphate (NADPH) to flavin adenine dinucleotide (FAD) and flavin mononucleotide (FMN) but with a low capacity. It can bind calmodulin but neither the cofactor tetrahydrobiopterin (BH_4), nor the substrate L-arginine and subsequently does not catalyze NO production. In the active, phosphorylated, state, NOS exists as a dimer. It has several phosphorylation sites which enhance the sensitivity of NOS for Ca^{2+} which is required for calmodulin binding. The phosphorylation site, serine (Ser)1177, is activated by AMP-activated protein kinase (AMPK), Ca^{2+}/calmodulin dependent protein kinase II or protein kinase A which is mainly induced by fluid shear stress. Active NOS transfers electrons from NADPH to hem where L-arginine is oxidized to L-citruline and NO. NO stimulates the soluble guanylyl cyclase, generates cyclic guanosine monophosphate (cGMP) and induces vasodilatation. Under oxidative stress, NOS produces superoxide and peroxynitrite instead of NO which is described by the term uncoupling. In detail, radicals of NO and oxygen react to peroxynitrite instead of NO which can oxidize BH_4 to the inactive trihydrobiopterin (tBH_3). The lack of the cofactor BH_4 and the substrate L-arginine are discussed as causes for the uncoupling from oxygen reduction of NO [127]. As a consequence of uncoupling NO availability is reduced and the existing oxidative stress enhanced, depolarisation of Ψ_m increased and respiratory control ratio is decreased [38]. Similar to the superoxide produced by NOX, the superoxide produced by endothelial NOS (eNOS) can stimulate endothelial migration.

Endothelial proliferation after vascular injury occurs much slower than migration. Scientists are discordant if the proliferating cells originate either from resident vascular endothelial cells or endothelial progenitor cells. Hagensen et al. demonstrated that endothelial cells of the neoendothelium originated from the transplanted artery segment formed after wire-injury [46]. Other authors suggested that endothelial derived microparticles promote proliferation of resident endothelial cells [154] [62]. Similar to endothelial migration, Ca^{2+} affects endothelial proliferation.

Abdullaev et al. has shown that downregulation of STIM1 and Orai1 reduced prolif-

eration in HUVECs. HUVECs transfected with siRNAs specific for STIM1, Orai1 or STIM1 plus Orai1 were counted 96h later by trypan blue exclusion. Downregulation of Orai1 and both STIM1 plus Orai1 induced significant reduced cell numbers as compared to STIM1 knockdown. Combined transfection of STIM1 and STIM2 specific siRNAs reduced cell numbers significantly but to a minor extent than Orai1 knockdown. These results could indicate that Orai1 proliferation is partly independent of STIM. Propidium iodide staining revealed that transfection with Orai1 specific siRNAs and a mixture of STIM1 and Orai1 specific siRNAs increased the proportion of cells in the S and G2/M phases of the cell cycle compared to control cells. Transfection by siRNA specific for STIM1 alone had a much smaller effect[1]. Furthermore, the role of STIM1 was demonstrated in a rat carotid artery balloon injury model by Guo et al. Knockdown of STIM1 by adenovirus delivery of specific siRNAs suppressed neointima hyperplasia 14 days after injury. The re-expression of human STIM1 reversed this effect. In vitro, proliferation and migration of STIM1 deficient vascular SMCs was reduced [44]. In summary, other groups have demonstrated that a SOCE defect in smooth muscle cells or endothelial cells reduces endothelial migration and proliferation. Because in most experiments immortalized cells transfected with siRNA were used, theses results need further investigation in primary cells isolated from knockout mice.

1.4   Mitochondrial Ca^{2+} homeostasis

1.4.1   The role of MCUR1 in mitochondrial Ca^{2+} influx pathways

Mitochondrial calcium uptake is mediated by an inner mitochondrial membrane protein, the mitochondrial Ca^{2+} uniporter (MCU). Integrative bioinformatics and RNAi screening approaches, discovered three components of the MCU complex (mitochondrial calcium uptake 1 (MICU1) [98], MCU [4] [21] and mitochondrial Ca^{2+} uniporter regulator 1 (MCUR1) [81] [82] [49]). The MCU complex is further regulated by:

MICU2, MCUb, EMRE and SLC25A23. Even though some of the MCU complex components have been investigated, the precise structure and regulation of the MCU complex is still unknown [21].

MCU is a 40 kDa protein with low affinity but high capacity and high selectivity to Ca^{2+}(dissociation constant $\leq$ 2 nM). Due to these properties, MCU can induce mitochondrial Ca^{2+} rises above 100 µM despite of relative low cytoplasmic Ca^{2+} concentrations [21]. The MCU-mediated Ca^{2+} uptake is dependent upon the negative (-160 mV) mitochondrial membrane potential $\Delta\Psi_m$ and pH [43] [82] [19] [112] and can be blocked by ruthenium red. The I_{MCU} is produced by an inward rectifying channel with a high half-saturation of 20 mM $[Ca^{2+}]_c$ [64]. Physiologically, the rapid mitochondrial Ca^{2+} uptake by MCU is essential for mitochondrial functions such as ATP production and cell signaling processes [31] [41] [106] and for buffering pathophysiological high cytosolic Ca^{2+} concentrations [106].

MICU1 prevents Ca^{2+} uptake via MCU at low cytosolic Ca^{2+} concentrations and enables uptake at high concentrations. When extramitochondrial Ca^{2+} increases, the gatekeeper MICU2 is inhibited and the stimulator MICU1 is activated. MICU1 interacts via its polybasic region and a Ca^{2+} sensing EF-hand with the coiled-coil domain of MCU [49]. This enables MCU-dependent Ca^{2+} uptake. EMRE (essential MCU regulator) is a single pass transmembrane inner mitochondrial membrane protein which is essential for MCU complex formation but its exact role is not known yet [21] [50] [81] [110].

MCUR1 was identified as a positive regulator of the MCU complex through its interaction with MCU and enhances the MCU-mediated Ca^{2+} uptake. It has been demonstrated that the N-terminal domain of MCU interacts with MCUR1 and regulates ruthenium-red-sensitive MCU-dependent Ca^{2+} uptake. Stable shRNA mediated knockdown of MCUR1 in HeLa cells disrupted oxidative phosphorylation, lowered cellular ATP levels and activated AMPK-dependent autophagy. Thus MCUR1 is an essential component for MCU complex formation, and maintenance of normal cellular bioenergetics [81]. Knockdown of MCUR1 in immortalized human fibroblasts resulted in a cytochrome c oxidase assembly defect, decreased $\Delta\Psi_m$ and reduced

mitochondrial Ca^{2+} uptake [96].
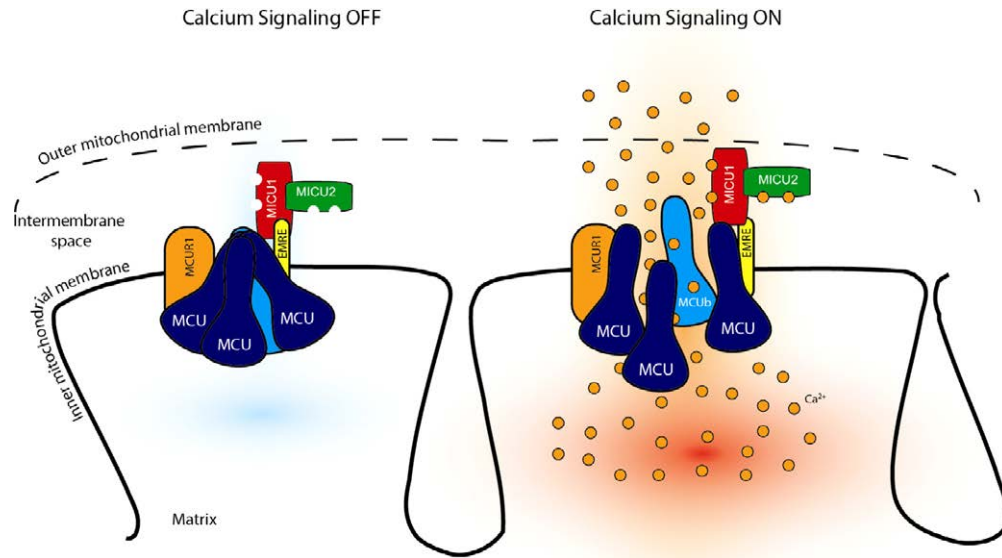
Figure 1.9: **The MCU-mediated Ca^{2+} uptake.** Mitochondrial Ca^{2+} uniporter (MCU)-mediated Ca^{2+} uptake is regulated by several proteins which form a complex with MCU: MICU1, MICU2, MCUb, MCUR1, EMRE and SLC25A23 (omitted for simplicity). When extramitochondrial Ca^{2+} increases, the gatekeeper MICU2 is inhibited and the stimulator MICU1 activated. This enables MCU-dependent Ca^{2+} uptake. EMRE: essential MCU regulator, MICU: mitochondrial Ca^{2+} uptake, MCUR1: mitochondrial Ca^{2+} uniporter regulator1 (from [21]).

1.4.2 Coupled oxidative phosphorylation, uncoupling and ATP production in mitochondria

Mitochondria are the major energy production units of the cell. ATP as the carrier of cellular energy is mainly produced in mammalian cells by either glycolysis or oxidative phosphorylation in the respiratory electron chain [154]. The respiratory electron chain consists of five complexes which generate a proton gradient over the inner mitochondrial membrane that drives ATP synthesis. The process of ATP synthesis in the mitochondrial respiratory chain is called oxidative phosphorylation. NADH and FADH$_2$ provided by glycolysis, fatty acid oxidation or the citric cycle feed the respiratory chain with electrons. These electrons are transported to O$_2$ which is reduced to H$_2$O in complex IV. NADH and FADH$_2$ are oxidized at complex I and II which releases electrons and produces H$^+$. H$^+$ is pumped out of the mitochondrial

matrix by complex I, III and IV. The uneven distribution of H^+ generates a proton gradient. Because the intermembrane space is charged positive relative to the matrix side, a transmembrane electrical potential -the mitochondrial membrane potential, Ψ_m -is created. The membrane potential has a large negative potential of -180mV. The process of electron donation by NADH in complex I is depending on substrate oxidation of pyruvate/malate in the citric cycle. Complex II oxidizes succinate and reduces FAD^+ to $FADH_2$. In the same way as NADH, $FADH_2$ feeds its electrons to the respiratory chain. H^+ produced during these reactions which generates the proton gradient is therefore tightly coupled to electron donation. Because the electrons are finally used to reduce O_2 to H_2O, the oxygen reduction rate is an accurate measure for the proton gradient. The rate by which O_2 is reduced is defined as oxygen consumption rate (OCR). Addition of complex I and II substrate consequently results into an enhanced electron flow, proton gradient and OCR. The energy of substrate oxidation that is conserved in this proton gradient is used to synthesize ATP from ADP and inorganic phosphate when H^+ flows back to the matrix through complex V. The term 'coupled' in this context describes the dependance of ATP synthesis on the proton gradient. Accordingly, addition of substrates enhances the proton gradient and thereby drives H^+ reentry through complex V which results into higher ATP synthesis. However, how much oxygen is required to produce one molecule of ATP is dependent on factors such as the complex substrate. For example, consumption of succinate and pyruvate/maleate requires both one unit of oxygen but succinate pumps in turn 6 H^+ while pyruvate/maleate pumps 10 H^+. [109] [9] [129] [17] [10]. H^+ does not only flow back to the mitochondrial matrix through the ATP synthase but also through the uncoupling proteins (UCP) and adenine nucleotide transporters (ANT). This process separates the electron transport and proton gradient from the ATP synthesis and is therefore described with the term 'uncoupling'. The energy conserved in the proton gradient which is used for ATP production during 'coupling' is released as heat during 'uncoupling' if H^+ flows back via UCP [119]. Among the five UCP isoforms UCP1 is involved in uncoupling during thermogenesis in brown adipose tissue [127]. Based on the sequence homology of UCP2 and UCP1 a similar function
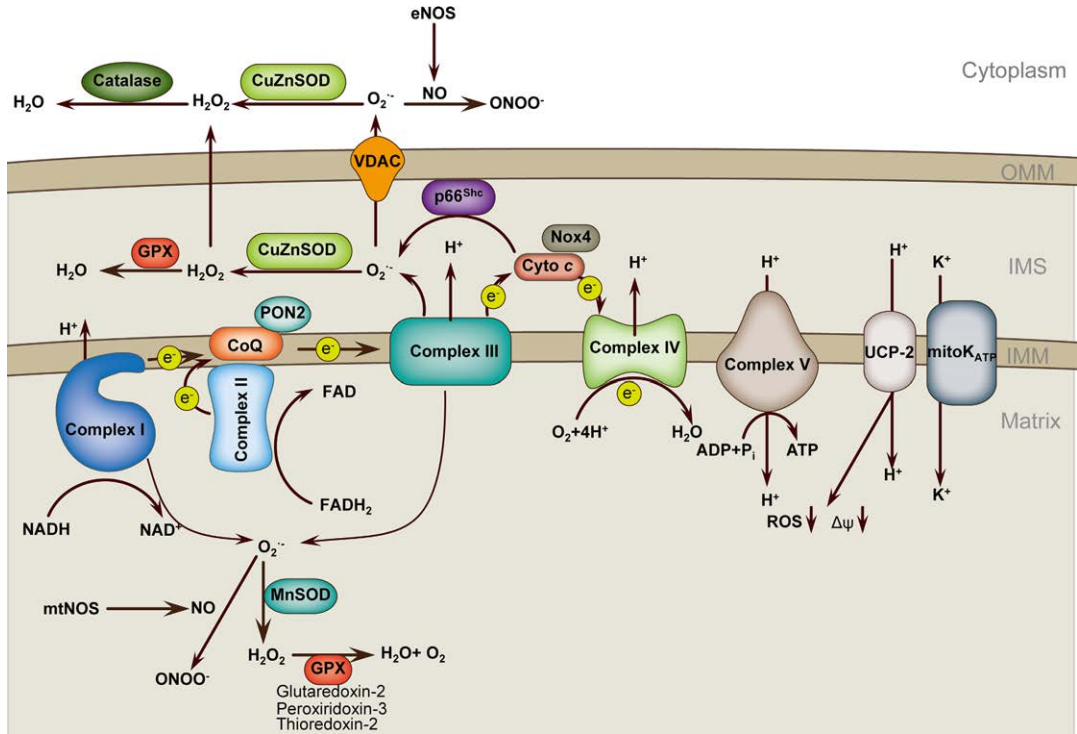
Figure 1.10: **Oxidative phosphorylation.** The respiratory electron chain consists of five complexes which generate a proton gradient over the inner mitochondrial membrane that drives adenosine triphosphate (ATP) synthesis. The process of ATP synthesis in the mitochondrial respiratory chain is called oxidative phosphorylation. OMM: outer mitochondrial membrane, IMS: intermembrane space, IMM: inner mitochondrial membrane, CoQ: co-enzyme ubiquinol, PON2: paraoxonase2, cyto c: cytochrome c, NOX4: nicotinamide adenine dinucleotide phosphate oxidase4, UCP2: uncoupling protein2, mitoK$_{ATP}$, mitochondrial ATP-sensitive potassium channel, eNOS: endothelial NO synthase, NO: nitric oxide GPX: glutathione peroxidase, MnSOD: manganese superoxide dismutase, CuZnSOD: Copper-zinc superoxide dismutase, VDAC: voltage-dependent anion channel (from [10]).

was assumed for UCP2 [139]. UCP2 and UCP3 are the main isoforms expressed in endothelial cells. But the involvement of UCP2 in uncoupling is questioned by many scientists. One argument against the role of UCP2 and UCP3 in uncoupling is the low amount of UCP2 and UCP3 in the mitochondrial membrane. Therefore UCP2 and UCP3 probably do not have the capacity to induce a proton leak by uncoupling which is high enough to lower the $\Delta\Psi_m$. Moreover, unlike UCP1-deficient mice, UCP2$^{-/-}$ mice are not susceptible to obesity even when they are fed with a high fat diet and depletion of UCP2 in spleen or lung which express endogenously high levels of UCP2, did not change the uncoupling state [66]. It has also been postulated that the

'mild uncoupling' of UCPs would protect from oxidative damage of reactive oxygen species (ROS) produced during high $\Delta\Psi_m$. However, only succinate-mediated ROS production seems to be sensitive to high $\Delta\Psi_m$. During conditions of reversed electron flow, it is questionable if the succinate level of 0.5mM is reached physiologically because succinate is only an intermediate product in the citric acid cycle. The citric acid substrates which fuel complex I 2-oxoglutarate, pyruvate, glutamate and malate produce only minor amounts of ROS. This ROS production is not influenced by changes of the proton gradient and therefore addition of the uncoupler FCCP does not have an effect on ROS production [119].

More and more evidence has accumulated suggesting that the main role of UCP2 is in the reprogramming of metabolic pathways [139]. Endothelial cells cover their main energy demand by glucose, fatty acids and glutamine. They preferentially use glucose for glycolysis and not for oxidative phosphorylation even when oxygen is present. As long as glucose and NAD^+ are available, glycolysis produces as much ATP as oxidative phosphorylation. Glutamine can fuel oxidative phosphorylation instead. This feature allows endothelial cells to ensure energy supply even during conditions of low oxygen which is required in particular during the formation of new blood vessels. Glucose is oxidized to pyruvate and glutamine is metabolized to α-ketoglutarate. Pyruvate and α-ketoglutarate fuel the tricarboxylic acid cycle (TCA) cycle. The TCA cycle intermediates feed oxidative phosphorylation [100].

One study evidencing that UCP2 plays a role in metabolic pathways was conducted by Vozza et al. They showed that UCP2 operates as a metabolite transporter which determines substrate oxidation in mitochondria. More specifically, they demonstrated that UCP2 exchanges intramitochondrial C4 intermediates against H^+ and P_i under high glucose supply. $UCP2^{KD}$ HepG2 cells (liver hepatocellular cells with stable knockdown of UCP2) grown in high glucose DMEM showed an increased $\Delta\Psi_m$ and ATP/ADP ratio. Moreover, $UCP2^{KD}$ HepG2 revealed elevated TCA intermediates (citrate, 2-oxoglutarate, succinate, fumarate, L-malate)and reduced lactate levels by mass spectrometry [139]. The elevated TCA intermediates level suggested that the higher ATP/ADP ratio is due to an impaired TCA function. The low amount of

44

lactate indicates that most of the ATP produced does not originate from glycolysis. Based on these findings Vozza et al. hypothesized that UCP2 could transport C4 metabolites, such as pyruvate which regulates the oxidation of pyruvate- derived acetyl-CoA in mitochondria. Accordingly, UCP2 but not UCP1 catalyzed the substrate uptake of radioactive phosphate, L-malate and L-aspartate into liposomes containing the same substrate. Cell swelling experiments with isosmotic ammonium phosphate solution applied to isolated yeast mitochondria further demonstrated that the inward H^+-coupled P_i transport depends on the endogenous Mir1P or UCP2 protein. Addition of FCCP increased the exchange between external P_i and internal malate. It can be concluded from these experiments that the substrates malate, oxaloacetate and aspartate are exchanged for P_i and H^+ across the mitochondrial inner membrane suggesting that UCP2 negatively regulates the oxidation of acetyl-CoA-producing substrates such as glucose by removing substrates of the Krebs cycle from the mitochondrial matrix. As a consequence the redox pressure of the mitochondrial chain, the ATP/ADP ratio and the ROS production is reduced. In contrast to the effect of UCP2 on glucose oxidation, UCP2 promotes the use of glutamine, feeding the Krebs cycle, enhancing the redox pressure and therefore ATP/ADP ratio. Thus increased UCP2 expression limits the contribution of glucose on mitochondrial oxidative phosphorylation and promotes oxidation of substitute substrates such as glutamine and fatty acids [139]. Kukat et al. further confirmed that high UCP2 levels inhibit glucose oxidation and promote fatty acid oxidization in an in-vivo model. They demonstrated that UCP2$^{-/-}$ mice had reduced lactate levels and normal circulating free fatty acid levels under normal chow diet at 25 weeks. The maximal OCR in mitochondria isolated from the heart of UCP2-deficient mice was significantly reduced after addition of CCCP. The maximal OCR upon addition of octanoyl-carnitine+glutamate was unchanged in UCP2 KO mitochondria but significantly reduced after addition of palmitoyl-carnitine+glutamate. This result indicates that UCP2 upregulation might allow better fatty acid oxidation in the heart [66].

Dysfunction of the mitochondrial respiratory chain can be investigated experimentally by measuring the OCR. This is achieved by monitoring the OCR in response to

addition of substrates, uncouplers or inhibitors. The physiological background will be discussed here, for technical information refer to the methods section. During basal respiration, the OCR is mainly dominated by the ATP turnover and partly by proton leakage. To determine to which extend ATP synthesis influences the basal state, the ATP synthase can be blocked with oligomycin. The remaining OCR is due to the proton leakage and therefore caused by uncoupling. Because oligomycin blocks the ATP synthesis during oxidative phosphorylation, the cell shifts its ATP production to glycolysis. To maintain the ATP production, glycolysis accelerates approximately 10-fold. This increase of glycolysis can be measured by the extracellular acidification rate (ECAR). Pyruvate is converted to lactic acid during anaerobic glycolysis. When lactic acid is released it acidifies the extracellular space and can be measured as an increase in ECAR.

The maximum respiration rate can be induced by addition of the uncoupler FCCP (Carbonyl cyanide-p- trifluoromethoxyphenylhydrazone). An uncoupler is a lipid soluble compound that allows H^+ to diffuse back to the matrix while bypassing the ATP synthase. As a results the $\Delta\Psi_m$ collapses. In an attempt to rescue the $\Delta\Psi_m$ the OCR accelerates and the cell switches its metabolism from oxidative phosphorylation to glycolysis which increases ECAR. As a result, any substrate available in the medium is oxidized and contributes to the maximal respiration rate [113] [10].

If mitochondrial electron transport chain is inhibited only the OCR caused by non-mitochondrial respiration remains. The non-mitochondrial respiration is caused by desaturation and detoxification enzymes and is only responsible for approximately 10% of total cellular oxygen consumption. Inhibitors such as rotenone in combination with antimycin A completely block the mitochondrial electron transport chain. Rotenone inhibits the electron transfer from complex I to ubiquinone and thereby prevents usage of the potential energy of NADPH. Antimycin A blocks the cytochrome c reductase and therefore disrupts the proton gradient across the inner mitochondrial membrane resulting in a decreased OCR and an increased ECAR to maintain energy homeostasis. Cyanide inhibits complex IV and also some haem-containing enzymes responsible for non-mitochondrial oxygen consumption[113] [10].

1.4.3 How does Ca^{2+} influence bioenergetics?

Rapid mitochondrial Ca^{2+} uptake is import for various mitochondrial functions, such as maintenance of the $\Delta\Psi_m$, ATP production and various cellular signaling processes [31] [106] [41]. Consequently, the disruption of mitochondrial Ca^{2+} uptake results into reduced oxygen consumption, reduced ATP levels and activation of the AMPK which activates cell death pathways. The outer mitochondrial membrane is permeable to Ca^{2+} but through the inner mitochondrial membrane (IMM) which is impermeable to ion flux, Ca^{2+} passes via MCU. Ca^{2+} acts as an energy production messenger for various transport mechanisms while minimizing electron leak and subsequent damage. Important Ca^{2+} regulated mitochondrial functions are ATP production and enzyme activity depending on MCU-mediated Ca^{2+} uptake which is regulated by the $\Delta\Psi_m$ and the mitochondrial respiratory electron chain [12] [146].

Mitochondrial Ca^{2+} stimulates ATP production directly and indirectly. It stimulates indirectly ATP production by enhancing the activity of the mitochondrial complexes I, III and IV during conditions of elevated Ca^{2+}. Increased activity of these complexes stimulates mitochondrial respiration and leads to an increase in Ψ_m. Ψ_m, NADH but also Ca^{2+} itself regulates the activity of the ATP synthase (complex V). NADH is reduced Ca^{2+}-dependently from NAD^+ during the tricarboxylic acid cycle (TCA) cycle. The pyruvate dehydrogenase which fuels the TCA cycle is also Ca^{2+} dependent. Pyruvate dehydrogenase phosphatase activates the dehydrogenase by dephosphorylation. The dephosphorylated pyruvate dehydrogenase feeds acetyl coenzyme A (acetyl-CoA) to the cycle and isocitrate dehydrogenase and α-ketoglutarate dehydrogenase break down metabolites of the cycle. During these reactions NAD^+ is reduced to NADH. NADH feeds complex I and thus enhances electron flow and ATP production. The increased autofluorescence of NADPH after Ca^{2+} stimulation of the Ca^{2+}-dependent enzymes can be measured experimentally [106] [130] [146] [93].

Mitochondrial Ca^{2+} influx is driven by the electrochemical potential gradient for Ca^{2+}. If $\Delta\Psi_m$ is in the physiological range, mitochondrial influx and efflux mechanisms operate uni-directionally to allow the recycling of Ca^{2+} across the inner mitochondrial

membrane. This mechanism is controlled kinetically by the maximal Ca^{2+} uptake rate through MCU (e.g. 5.5 nmol Ca^{2+} per min^{-1} and mg^{-1} in liver mitochondria). The kinetic control allows Ca^{2+} distribution without disrupting $\Delta\Psi_m$ and δpH and therefore without disturbing ATP synthesis. In detail, the $\Delta\Psi_m$ is maintained by the following mechanism: If Ca^{2+} enters the mitochondrium via MCU the positive ion charge depolarizes the $\Delta\Psi_m$. To equilibrate the ion charge of extra- and intramitochondrial space, Ca^{2+} effluxes by Na^+-Ca^{2+} and Na^+-H^+ exchanger and H^+ enters the mitochondrium instead. The exchanger thereby transports Ca^{2+} out of the mitochondrium against its electrochemical potential gradient. Because the netto ion charge inside the mitochondrium remains unaltered the $\Delta\Psi_m$ and δpH are not affected. If the $\Delta\Psi_m$ collapses, the electrochemical potential does not drive Ca^{2+} influx anymore which results into a lack of mitochondrial Ca^{2+} uptake [31] [89].

UCP2 has been shown to be involved in the mitochondrial uptake of intracellular Ca^{2+} [140]. Deak et al. further investigated the role of UCP2 in mitochondrial Ca^{2+} uptake. Knockdown of UCP2 (UCP2^{KD}) in HeLa cells stimulated with histamine in Ca^{2+}-free medium showed an impaired mitochondrial Ca^{2+} uptake. In contrast, thapsigargin stimulated UCP2^{KD} cells did not show an impaired mitochondrial Ca^{2+} uptake after restoration of Ca^{2+}. These results indicate that a UCP2 knockdown impairs mitochondrial uptake only if the Ca^{2+} originates from the cytosol or ER but not after SOCE stimulation [22]. Large currents in mitochondrial mitoplast (mitochondria without their outer membranes) have been investigated by Bondarenko et al. in HeLa cells overexpressing UCP2 or UCP2 knockdown HeLa cells. SiRNA mediated UCP2 knockdown reduced the open probability of the large mitoplast currents by approximately 38%. Overexpression of UCP2 enhanced the current approximately 3-fold. However, it has to be taken into account that these results were obtained in mitoplast and can therefore not directly extrapolated on intact cells [7]. It is assumed that UCP2 indirectly mediates MCU activity because Sancak et al. demonstrated the absence of a direct interaction between UCP2 and MCU in a proteomic assay. They analyzed MCU-Flag expressing HEK293T cells containing heavy or light amino acid isotopes during quantitative mass spectrometry. Mass spectrometry iden-

tified five proteins to form a complex with MCU which were detected by protein immunoblotting as EMRE, MICU1, MICU2 and MCU. The mitochondrial Ca^{2+} handling proteins LETM1, NCLX,UCP2 and 3, MCUR1, and TRPC3 did not form a complex with MCU [110].

1.4.4 Formation of reactive oxygen species (ROS) during respiration and autophagy

ROS is mainly generated in the cell by cytosolic enzymes such as NADPH oxidases or cyclooxygenases and during oxidative phosphorylation. However, it is also assumed that approximately 90% of the cellular ROS is related to mitochondrial activity. Between 0.15% and 2% of the cellular oxygen may be used to produce superoxide instead of being reduced to H_2O by complex IV. The premature utilization of oxygen can occur at complex I, II and III. ROS formed at complex I and II is released into the matrix, ROS produced at complex III can be released to both the matrix and mitochondrial inner membrane and could therefore act as a signaling molecule in the cytosol [47]. The reactive superoxide can be formed because the oxygen molecule is capable of accepting an additional electron. Superoxide can be converted by superoxide dismutase to hydrogen peroxide which reacts with NO and forms peroxynitrite. Peroxynitrite can irreversibly damage proteins of the electron transport chain [20]. The antioxidant scavenging enzymes catalase, glutathione peroxidase and peroxiredoxin catalyze the reaction of the toxic H_2O_2 to H_2O [3]. Superoxide production can occur for example if the supply of oxygen, ADP or FADH is not sufficient. As a result the electron flow through the respiratory chain is disturbed and can reverse. For example in complex I, nicotinamide adenine dinucleotide (NADH) is not oxidized to NAD^+ anymore but NAD^+ is reduced to NADH. Consequently, NADH reduces molecular oxygen to superoxide [127].

UCPs and ANTs limit the ROS production by lowering the $\Delta\Psi_m$. The ANT exchanges ATP against ADP across the inner mitochondrial membrane and therefore supplies the ATP synthase constantly with ADP. H^+ which enters the matrix does not couple

directly to ATP synthesis and therefore reduces $\Delta\Psi_m$. Thus, activation of UCP or ANT reduces ROS production by lowering the $\Delta\Psi_m$. If ROS accumulates, it activates UCP or ANT which dissipate the proton gradient, decreases $\Delta\Psi_m$ and as a consequence lowers ROS production. If the function of ANT is impaired, ANT can contribute to apoptosis [63].

While moderate levels of ROS are essential for cell signaling, cell growth, proliferation and inflammatory responses, excessive ROS levels are associated with cell death and autophagy [3] [47] [127]. Autophagy is a protective mechanism in response to stress but excessive or insufficient autophagy can contribute to cell death. During autophagy, moderate levels of ROS degrade misfolded proteins or defective organelles clearing the cell from dysfunctional proteins and providing an alternative energy source by self-digestion during starvation. By inducing autophagy the cell might prolong its own survival. If a cytosolic dysfunctional organelle is detected, it is engulfed in the autophagosome, a double- or multimembrane vesicle. The autophagosome is fused with lysosomes which degrade its content and recycle the amino and fatty acids to generate ATP. Decreased cellular ATP levels can not only be enhanced by autophagy but also by activation of the AMPK. The AMPK phosphorylates substrates to limit anabolic pathways, that consume ATP and activates catabolic pathways to generate substrates to support oxidative phosphorylation. AMPK is regulated by the calmodulin-dependent protein kinase kinases (CaMKK) which is depending on cytosolic Ca^{2+}. High ATP levels inactivate the AMPK or accelerate ATP consumption [12] [48].

The role of mitochondrial Ca^{2+} ($[Ca^{2+}]_m$)in the formation of ROS and induction of autophagy and cell death has been investigated by several research groups. Excessive Ca^{2+}_m is associated with increased ROS production. If ROS levels exceed the antioxidant capacity of the scavenging enzymes, ROS in turn might disrupt Ca^{2+} handling pathways [20]. An overload of mitochondrial Ca^{2+} reduces the $\Delta\Psi_m$ and can result into loss of the inner membrane impermeability. This allows molecules which can not pass without a transporter under physiological conditions to enter the matrix and induce apoptotic cell death. This phenomenon is called the 'opening of the mem-

brane permeability transition pore (PTP)' [57]. The effect of several MCU complex-associated components on ROS production and induction of autophagy and cell death has been explored. Rasmussen et al. investigated the effect of MCU overexpression on ROS in an ischemia-reperfusion model. They perfused hearts isolated from cardiac specific MCU overexpressing mice, loaded with the $\Delta\Psi_m$ indicator TMRE and the cytosolic ROS indicator DCF (2',7'-dichlorofluorescein) during an injury-reperfusion model. 10, 20 and 30min after reperfusion, they did not observe a significant change in TMRE but reduced DCF levels in the MCU overexpressing hearts. Furthermore, they showed that reduced ROS levels resulted from reduced manganese sodium dismutase levels [104]. Their result suggests that manganese sodium dismutase is upregulated compensatory in MCU overexpressing hearts and reduced the superoxide levels that only moderate levels were measurable.

The expression of the negative MCU regulator MICU1 has been reported to limit superoxide production, to ensure the expression of antioxidant enzymes, to promote proliferation and migration and to limit cell death. MICU1, MCU and MCUR1 are tightly linked to each other in the MCU complex [49] [82] but proteomic analysis demonstrated that MCUR1 can bind to MCU and EMRE independent of MICU1 [132]. Human cardiovascular derived endothelial cells have higher $Ca^{2+}{}_m$levels and increased basal superoxide levels after knockdown of the negative MCU regulator MICU1. MICU1^{KD} EA.hy926 cells (human endothelial cell line ATCC^{R}CRL-2922^{Tm}) showed significantly elevated superoxide levels which were downregulated by the rescue of MICU1. Furthermore, the MCUI1 knockdown reduced the glutathione content in MICU1^{KD} EA.hy926 cells and reconstitution of MICU1 rescued the glutathione levels. The proliferation rate was reduced in MICU1^{KD} endothelial cells but rescued after reconstitution with shRNA (short hairpin RNA)-insensitive MICU1 cDNA. The human cardiovascular derived endothelial cells migrated less than control cells and migration was rescued by stable expression of MICU1 [49]. Basal superoxide levels were elevated in a MICU1^{KD} endothelial cell line. Double knockdown of MCU and MICU1 or rescue of MICU1 abrogated the elevation in superoxide levels. Thus it can be concluded that the lack of MICU1 inhibiting MCU-mediated Ca^{2+} influx gives

rise to superoxide production. Heterologous expression of mitochondrial manganese superoxide dismutase and the cytosolic glutathione peroxidase in MICU1^{KD} endothelial cells decreased AMP/ATP ratio and elevated basal OCR. From this result it can be concluded that chronically enhanced mitochondrial Ca^{2+} promotes the generation of excessive ROS which inhibits the Ca^{2+}-activated oxidative phosphorylation. LPS and cyclohexamide induced cell death was enhanced in MICU1 ^{KD} endothelial cells, and revoked by MICU1 rescue while overexpression of the mitochondrial manganese superoxide dismutase and the cytosolic glutathione peroxidase protected MICU1^{KD} endothelial cells from cell death [82].

The soluble carrier SLC25A23 transports ATP-dependently Ca^{2+} into the matrix. Hoffman et al. demonstrated that the direct interaction between SLC25A23 and MCU is essential for MCU-mediated Ca^{2+} uptake. Knockdown of SLC25A23 in Hela cells did not alter the $\Delta\Psi_m$ and resulted into preserved ATP production. Interestingly, SLC25A23 knockdown cells decreased basal superoxide levels indicated by MitoSox red fluorescence. They were further protected from oxidative stress (applied via t-butyl hydroperoxide) induced cell death which was demonstrated by annexinV and propidium iodide staining. Rescue of SLC25A23 elevated MitoSox red levels and cell death markers. T-butyl hydroperoxide mediated cell death requires Ca^{2+} [50] and MCU expression protected from oxidative stress induced cell death. Liao et al. demonstrated that short hairpin RNA-mediated down-regulation of MCU expression in HeLa cells(shMCU HeLa cells) showed reduced H_2O_2 induced apoptosis after 24h detected by FITC-labeled annexin-V staining during flow cytometry. Overexpression of Flag-MCU (flag is a polypeptide protein tag used to label poorly immunogenic proteins when protein specific antibodies are not available) in HeLa cells significantly enhanced the H_2O_2 induced apoptosis rate [72].

Knockdown of the mitochondrial Ca^{2+}-H^+ exchanger LETM1 reduced ATP production, basal OCR, complex IV activity and proliferation in HeLa cells, but NADPH levels were not changed. These results indicate that reduced complex IV activity lowers respiration and therefore basal OCR. As a result of the decreased OCR, ATP production was decreased which was rescued by shRNA insensitive LETM1. The decreased

proliferation in siRNA-mediated down-regulation of LETM1 expression (LETM1^{KD}) in HeLa cells was rescued by shRNA insensitive LETM1 as well. LETM1^{KD} significantly elevated superoxide production which was abrogated by the expression of the mitochondrial-targeted manganese superoxide dismutase and glutathione peroxidase. Overexpression of antioxidant superoxide dismutase and glutathione peroxidase further restored complex IV activity and ATP levels. Disabled complex IV activity can not retain partially reduced oxygen anymore. Consequently this oxygen contributes to basal ROS production. Based on the low ATP levels Doonan et al. hypothesized that the AMP/ATP ratio could be high which induces the phosphorylation of AMPK. According to their expectation, they detected high phosphorylated AMPK levels in LETM1^{KD} HeLa cells which were rescued by reconstitution of LETM1.

Activation of AMPK results into autophagosome formation which can be monitored by expression of the microtubule-associated protein light chain (LC)3 protein. LC3-I and LC3-II were elevated in LETM1^{KD} HeLa cells which showed a disrupted cell cycle progression [30]. In summary, these results demonstrate that several components of the MCU complex are involved in mitochondrial superoxide production and apoptosis. While knockdown of MCU and SLC25A23 has protective effects, knockdown of LETM1 or MICU1 elevates oxidative stress.

1.5   Aims of my thesis

As outlined in the introduction, cytosolic Ca^{2+} elevated by receptor-operated (ROCE) or store operated Ca^{2+} entry (SOCE) and buffered by mitochondrial Ca^{2+} uptake, plays an essential role in physiological processes of lung cells. An abnormal high intracellular Ca^{2+} concentration induces excessive contraction in precapillary pulmonary arterial smooth muscle cells (PPASMC) inducing pulmonary arterial hypertension (PAH), while Ca^{2+} overload in endothelial cells (MPMVEC) decreases vasculoprotective NO-production and increases vascular leakage and formation of lung edema. Moreover mitochondrial Ca^{2+} uptake may affect energy production and life time of these cells. Therefore, we believe that identification of signaling components in intra-

cellular Ca^{2+} handling at the plasma membrane, in the cytosol, and in mitochondria which can be targeted by drugs might be beneficial in future therapeutic approaches of PAH and lung edema.

Three hypotheses need to be investigated:

1. STIM and Orai proteins are not the only molecular correlates of SOCE in PPASMC and MPMVEC, because TRPC proteins which regulate ROCE are also involved.

2. Deficiency of SOCE or ROCE in PPASMCs and MPMVECs protects from vasoconstriction and lung edema formation.

3. Mitochondrial Ca^{2+} uptake by mitochondrial Ca^{2+} uniporter (MCU) complexes affects cellular bioenergetics and dysfunction of lung cells.

Investigation of the first hypothesis requires creation of quintuple TRPC1/3/6/STIM1/2- deficient mice by mating STIM1/2 floxed mice with TRPC1/3/6$^{-/-}$ mice. A STIM1/2 deficiency is induced by infecting cells with Cre-recombinase expressing lentiviruses or by mating the mice with tissue specific Cre lines for smooth muscle (Myh11-Cre) or endothelial cells (Cdh5-Cre).

To verify the second hypothesis, we aim to establish store-operated and receptor-operated Ca^{2+} channel deficient mouse strains and validate SOCE protocols for live cell-imaging as well as for quantification of vasoconstriction and endothelial barrier function. Assessment of cell migration and proliferation, morphological examination by histology, immunofluorescence as well as gene and protein expression also need to be analyzed..

The third hypothesis aimed to elucidate the effects of reduced mitochondrial Ca^{2+}-uptake on mitochondrial membrane potential, energy homeostasis, mitochondrial stress, proliferation and autophagy. Characterization of mouse samples should involve simultaneous live-cell measurement of mitochondrial Ca^{2+}-uptake and mitochondrial membrane potential in permeabilized cells, mitochondrial respiration rate, confocal live-cell imaging and protein expression analysis.

Chapter 2

Material

Product	Manufacturer	Product number
Acetylcholine chloride	Sigma Aldrich, Deisenhofen, Germany	A6625
Agarose	Carl Roth, Karlsruhe, Germany	2267.4
Antibiotic-antimycotic solution	Thermo Fisher Scientific, Pittsburgh, PA, US	15240-062
Antimycin A	Sigma Aldrich, Milwaukee, US	A8674
BCA (bicinchoninic acid) Protein assay kit	Pierce, Thermo Fi. Sci., Schwerte, Germany	23225
Bradford assay	Thermo Fisher Scientific, Pittsburgh, PA, US	23200
BSA (bovine serum albumin)	Sigma-Aldrich, Deisenhofen, Germany	9418
Ca^{2+}-free HBSS (Hank's Buffered Salt Solution)	PAA, Cölbe, Germany	15-009
Camco Quick Stain^R II	Thermo Fisher Scientific, Pittsburgh, PA, US	04-330-1
Carbamoylcholine chloride	Sigma Aldrich, Deisenhofen, Germany	C4382
Carbonyl cyanide m-chorophenylhydrazone (CCCP)	Sigma Aldrich, Milwaukee, US	C2759
Cell Trace CFSE (carboxyfluorescein succinimidyl ester) cell proliferation kit	Thermo Fisher Scientific, Pittsburgh, PA, US	C34554
CellTiter-Glo luminescent assay kit	Promega Corporation, Madison, US	G7570
CGP-37157 (7-Chloro-5-(2-chlorophenyl) -1,5-dihydro-4,1-benzothiazepin-2(3H)-one	Sigma Aldrich, Milwaukee, US	C8874 Sigma
Collagenase/dispase	Sigma Aldrich, Deisenhofen, Germany	11097113001
Collagenase	Sigma Aldrich, Deisenhofen, Germany	C5138
Cyclopiazonic acid	Sigma Aldrich, Deisenhofen, Germany	C1530
Digitonin	Sigma Aldrich, Milwaukee, US	D141
Dil-Ac-LDL	Harbor Bio products, Norwood, MA, US	J65597
DMEM (Dulbecco's Modified Eagle's Medium)	Thermo Fisher Scientific, Pittsburgh, PA, US	HyClone SH30022.01
Dynabeads protein G	Thermo Fisher Scientific, Pittsburgh, PA, US	1004D
ECGS (endothelial cell growth supplement-heparin)	Merck Millipore, Billerica, MA, US	02-102
EconoTaq polymerase	Lucigen, Middleton, US	F93481-1

EGTA (ethylene glycol-bis(β-aminoethyl ether)-N,N,N',N'-tetraacetic acid)	Sigma Aldrich, Milwaukee, US	34596
Eosin	Thermo Fisher Scientific, Pittsburgh, PA, US	s176
FCCP (carbonyl cyanide-4-(trifluoromethoxy)phenylhydrazone	Sigma Aldrich, Milwaukee, US	C2920
Formaldehyde	Sigma Aldrich, Deisenhofen, Germany	252549
Fe_3O_4	Sigma-Aldrich,Deisenhofen, Germany	310050
FITC (fluorescein isothiocyanate) dextran 70 kDa	Molecular Probes, Invitrogen	46945
Fluo-4^{Tm}	Thermo Fisher Scientific, Pittsburgh, PA, US	F14201
Fura-2-AM (acetoxymethyl-ester)	Fluka, Sigma-Aldrich, Deisenhofen, Germany	47989
GenElute^{Tm}	Sigma Aldrich, Deisenhofen, Germany	G1N70-1KT
Goat serum	Bio-West, Nuaille, France	S2000-100
Hematoxylin	Thermo Fisher Scientific, Pittsburgh, PA, US	s212A
Heparin	Sigma Aldrich, Milwaukee, US	H3393
Hoechst	Sigma Aldrich, Deisenhofen, Germany	33342
InviTrap^{Tm}	STRATEC Molecular GmbH, Berlin, Germany	1060100300
JC-1^{Tm}	Thermo Fisher Scientific, Pittsburgh, PA, US	T3168
Krebs-Henseleit-Buffer	Sigma Aldrich, Deisenhofen, Germany	K3753
Low-melting-point agarose	Sigma Aldrich, Deisenhofen, Germany	A9045
MacConkey Agar	BD Biosciences, Franklin Lakes, NJ, US	BD 212123
Mammalian Genomic DNA Miniprepkit	Sigma Aldrich, Deisenhofen, Germany	G1N70-1KT
MitoSOX Red^{Tm}	Invitrogen, Eugene, OR, US	M36008
Mounting media	Dako, Hamburg, Germany	53023
Mygliol	Caelo, Hilden, Germany	3274
Oligomycin	Sigma Aldrich, Milwaukee, US	75351
Phosphate-buffered saline (PBS)	Thermo Fisher Scientific, Pittsburgh, PA, US	10010056
Permount^{Tm}	Thermo Fi.Sci, Schwerte, Germany	SP15-100
Phalloidin-TRITC (tetramethylrhodamine)	Sigma Aldrich, Deisenhofen, Germany	P1951
Phenylephrine	Sigma Aldrich, Deisenhofen, Germany	P1250000
Pluronic^{R} F-127	Thermo Fisher Scientific, Pittsburgh, PA, US	P6867
Polyethylene glycol precipitation solution	BioCat, Heidelberg, Germany	LV825A
Protease inhibitor	Roche, Sigma Aldrich, Milwaukee, US	04693116001
Restore^{TM} Western Blot Stripping Buffer	Thermo Fisher Scientific, Pittsburgh, PA, US	21059
Reverse transcriptase	Thermo Fi.Sci, Schwerte, Germany	K1632
Rhod-2 AM^{Tm}	Thermo Fisher Scientific, Pittsburgh, PA, US	R1245MP
Rhodamin 123^{Tm}	Thermo Fisher Scientific, Pittsburgh, PA, US	R302
RIPA buffer	Merck Millipore, Billerica, MA, US	20-188
Rotenone	Sigma Aldrich, Milwaukee, US	R8875
Ru360	Santa Cruz Biotechnology Inc., Dallas, TX, US	sc-222265
Smooth Muscle Cell Growth Medium 2	PromoCell, Heidelberg, Germany	C-22062

Sodium nitroprusside dihydrate	Sigma Aldrich, Milwaukee, US	71778
Sodium pyruvate	Sigma Aldrich, Milwaukee, US	P2256
Spin Universal RNA MiniKit	Stratec Molecular, Berlin, Germany	1060100300
Succinate	Sigma Aldrich, Milwaukee, US	14160
Sulphinpyrazone	Sigma Aldrich, Milwaukee, US	S9509
SuperSignal^{TM} West Femto Maximum Sensitivity Substrate	Pierce,Thermo Fi.Sci, Schwerte, Germany	34096
SuperSignal^{TM} West Pico Chemiluminescent Substrate	Pierce,Thermo Fi.Sci, Schwerte, Germany	34080
SYBR Green I	Pierce,Thermo Fi.Sci, Schwerte, Germany	AB 1159B
Tamoxifen	Sigma Aldrich, Deisenhofen, Germany	T5648
Thapsigargin	Calbiochem, Darmstadt, Germany	586005
TMRM (tetramethylrhodamine methyl ester)	Thermo Fisher Scientific, Pittsburgh, PA, US	T668
Triton X-100	Carl Roth, Karlsruhe, Germany	3051.2 Carl Roth
Thrombin	Calbiochem, Merck, Darmstadt, Germany	605157
XF Cell Mito Stress Test Kit^{Tm}	Seahorse Bioscience, North Billerica, MA, US	103015-100

Table 2.1: **List of chemicals and reagents**

Antibody specific for	Product number	Manufacturer	Dilution
α-Drp1	sc-32898	Santa Cruz Biotechnology Inc., Dallas, TX, US	1:500
α-Mfn2	sc-100560	Santa Cruz Biotechnology Inc., Dallas, TX, US	1:500
α-SMA	A5228	Sigma Aldrich, Milwaukee, US	1:1000
α-TOM20	sc11415	Santa Cruz Biotechnology Inc., Dallas, TX, US	1:1000
β-actin	sc-4778	Santa Cruz Biotechnology Inc., Dallas, TX, US	1:10000
AMPK	2532	Cell Signaling Technology, Beverly, MA,US	1:1000
anti-cycF	ab110324	Abcam,Cambridge, MA, US	1:1000
anti-goat IgG-HRP	sc-2056	Santa Cruz Biotechnology Inc., Dallas, TX, US	1:5000
anti-mouse IgG-HRP	7076S	Cell Signaling Technology, Beverly, MA,US	1:5000
anti-mouse IgG-FITC	F9006	Sigma Aldrich, Milwaukee, US	1:50
anti-rabbit FITC-labelled antibody	A11008	Thermo Scientific	1:200
anti-rabbit IgG-HRP	7074S	Cell Signaling Technology, Beverly, MA,US	1:5000
CD-144 (VE-Cadherin5)	BD 55528	clone 11D4.1 BD biosciences, Heidelberg, Germany	
eNOS	9572S	Cell Signaling Technology, Beverly, MA,US	1:500
LC3	L8918	Sigma Aldrich, Milwaukee, US	1:5000
MCU		custom-made antibody	1:500
MCUR1	ARP44777_P050	Aviva Systems Biology, San Diego, CA, US	1:1000
Mitocomplex	ab110411	Abcam,Cambridge, MA, US	1:500
mTFA	ab138351	Abcam,Cambridge, MA, US	1:5000
Orai1	sc-68895	Santa Cruz Biotechnology Inc., Dallas, TX, US	1:500
OXPHOS	ab110413	Abcam,Cambridge, MA, US	1:250
p62	5114S	Cell Signaling Technology, Beverly, MA,US	1:1000
PGCI-α	ab54481	Abcam,Cambridge, MA, US	1:500

phospho-AMPK	40H9	Cell Signaling Technology, Beverly, MA,US	1:1000
phospho-eNOS (Ser1177)	9571	Cell Signaling Technology, Beverly, MA,US	1:500
STIM1	4917S	Cell Signaling Technology, Beverly, MA,US	1:500
STIM1	sc-66173	Santa Cruz Biotechnology Inc., Dallas, TX, US	1:500
UCP2	sc-6525	Santa Cruz Biotechnology Inc., Dallas, TX, US	1:500
ZO-1	40220	Life Technologies, Darmstadt, Germany	1:100

Table 2.2: **List of antibodies**

Buffer	Composition
PBS	1.06mM KH_2PO_4, 1.55NaCl
	2.97mM Na_2HPO_4-$7H_2O$)
ECM (extracellular medium)	121 mM NaCl, 5 mM NaHCO3, 10 mM Na-HEPES, 4.7 mM KCl
	1.2 mM KH_2PO_4, 1.2 mM $MgSO_4$
	2 mM $CaCl_2$, 10 mM glucose, and 2.0% BSA
Running buffer	250mM tris base, 1,920M glycin, 35mM SDS
Transfer buffer	250mM tris base, 1,920M glycin, 7mM SDS

Table 2.3: **List of buffers**

Chapter 3

Methods

3.1 Breeding and genotyping of gene deficient mice

The heterozygous STIM1$^{+/-}$ Orai1$^{+/-}$ were provided by Dr. Attila Braun, Rudolf-Virchow- Center Würzburg, Germany. Mutated embryonic stem (ES) cell lines originally established by BayGenomics using the gene-trap technology [126] were used to generate heterozygous mice for STIM1 [137] (MGI Symbol: STIM1$^{Gt(RRS558)Byg}$) and Orai1 [138] (MGI Symbol: Orai1$^{Gt(XL922)Byg}$). A double STIM1$^{+/-}$ Orai1$^{+/-}$ mouse line was established by breeding both strains in our animal facility. We needed to design new specific primers to genotype the offspring. The forward primers bind to the sequence of intron 7 (STIM1) or intron 1 (Orai1) and the reverse primers to the beta-geo cassette (see figure 3.1 and table 3.1). Details of the used PCR program and expected PCR products are summarized in (see table 3.2).

	Primer
STIM1 Wt	5'-GTC ATA GCC TGT AAA CTA GA-3'
	5'-GTA GCT GCA GGT AGC ACT AG-3'
STIM1$^{+/-}$	5'-TGT ATG CTT GGG CTA CAG GTG-3'
	5'-TGT GCT GCA AGG CGA TTA AG-3'
Orai1 Wt	5'-CTC TTG AGA GGT AAG AAC TT-3'
	5'-GAT CCC TAG GAC CCA TGT GG-3
Orai1$^{+/-}$	5'-TTG AGC GAG CCG TTC ACT TT-3
	5'-AGG GGT CTT GGG TTA GAG GG-3

Table 3.1: **Primer for genotyping of STIM1$^{+/-}$ Orai1$^{+/-}$ mice**

	STIM1 Wt	STIM1$^{+/-}$	Orai1 Wt	Orai1$^{+/-}$
	5 min 96°C	5 min 96°C	3 min 96°C	5 min 96°C
	45 cycles of:	45 cycles of:	45 cycles of:	45 cycles of:
	(1 min 94°C	(1 min 94°C	(1 min 94°C	(1 min 94°C
	1 min 51.5°C	1 min 60.0°C	1 min 51.5°C	1 min 53.0°C
	1 min 72°C)	1 min 72°C)	1 min 72°C)	1 min 72°C)
	5 min 72°C	10 min 72°C	5 min 72°C	10 min 72°C
	store at 14°C	store at 14°C	store at 14°C	store at 14°C
Expected fragments	750 bp	500 bp	900 bp	250 bp

Table 3.2: **Wt and STIM1$^{+/-}$Orai1$^{+/-}$ PCR program**

The LoxP/Cre technology was used for a tissue-specific deletion of STIM1 and STIM2 genes in smooth muscle cells. STIM1 and STIM2 floxed mice were provided by Dr. Stefan Feske , New York University, US (see figure 3.2) [92] and the Myh11-Cre/ERT2 line was purchased by Jackson Laboratory (B6.FVB-Tg(Myh11-Cre/ERT2)1Soff/J; #019079) [147].

In the Myh11-Cre/ERT2 mice, the Cre-recombinase is expressed under the control of the smooth muscle cell specific promotor of the myosin heavy chain 11 (Myh11) gene. Therefore, the Cre-recombinase only deletes the STIM1/2 exons in smooth muscle cells. In the used Cre line however the Cre recombinase is fused to the estrogen receptor 2 (ERT2) which is only activated by tamoxifen injected in the mouse model. The mutated ligand binding domain of ERT2 prevents binding of its natural ligand estradiol. Cre-ERT2 is bound to the heatshock protein 90 which inhibits
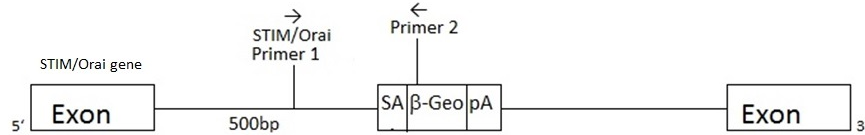
Figure 3.1: **Gene trapping method to generate heterozygote STIM1$^{+/-}$ Orai1$^{+/-}$ C57BL/6 mice.** A trap vector is randomly integrated in transcriptional active genes of ES cells [126]. The ES cell line carrying the gene trap cassette in the gene of interest can be selected from the database of the International Gene Trap Consortium.The trap vector consists of the splice acceptor site (SA), a selection construct (e.g. β-geo) and a polyadenylation tail (pA). The endogenous transcription continues at the splice acceptor site but is interrupted by the polyadenylation signal and results in a truncated mRNA. Primers binding to the trap cassette were used for sequencing the mRNA product in 3' to 5' direction to identify the trapped gene. To generate gene deficient mice which only produce truncated mRNAs and proteins from the gene of interest, a fusion protein containing LacZ is produced instead to detect transcriptional active tissues of the gene of interest in the corresponding gene trap mouse model [40].
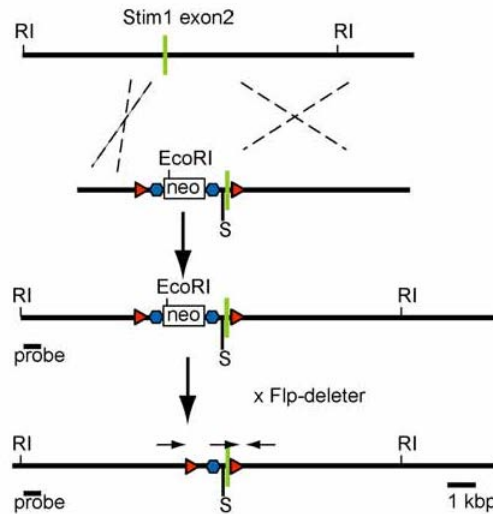
Figure 3.2: **Generation of STIM1/2 floxed mice [92].** Exon2 of the STIM1 gene and exon3 of the STIM2 gene were replaced by the neomycin resistance gene flanked by loxP and Frt recombination sites. Exon2 codes for the EF hand motif of the STIM1 gene and exon3 codes for sequences c-terminal to the EF-hand of the STIM2 gene. The modified embryonic stem cells were injected into blastocyts to generate chimeric mice. Mating of the STIM1$^{neo/+}$ or STIM2$^{neo/+}$ mice with the 'Flp deleter' transgenic mice removed the neomycin cassette but not the loxP site [92]. The exon2 or exon3 flanked by the loxP sites are deleted after mating the mouse model with a line expressing Cre recombinase under the control of a promoter from a protein (myosin heavy chain 11) specifically expressed in smooth muscle cells.

the Cre-recombinase activity. Upon tamoxifen application, the heatshock protein is dissociated and the Cre-recombinase is activated. The Cre-recombinase removes the floxed DNA segments resulting in STIM1/2 gene deficient 'knock-out' only in smooth muscle cells (see figure 3.3). A STIM1/2 mediated interaction with store-operated Ca^{2+} channels (e.g. Orai) is not possible anymore.
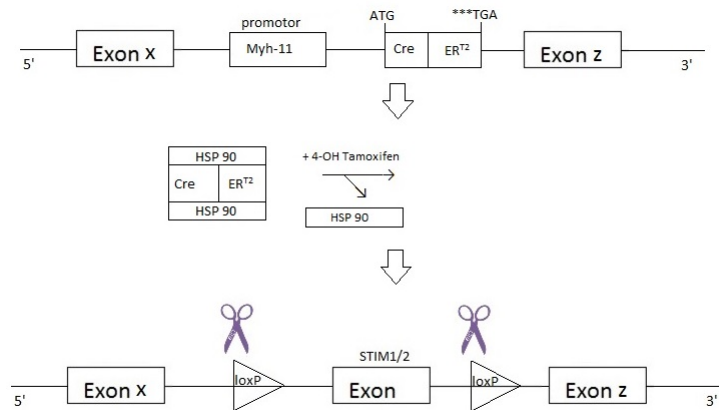
Figure 3.3: **Inducible smooth muscle cell specific knockout using tamoxifen.** The Cre-recombinase is expressed under the control of the Mhy11 promotor only in smooth muscle cells. Upon tamoxifen application, the Cre-recombinase is activated and deletes the floxed STIM1/2 exon. See text for a more detailed description

The transgene coding for Cre/ERT2 sequence under the control of the Myh11 promoter is inserted in the Y chromosome (B6.FVB-Tg(Myh11-Cre/ERT2)1Soff/J; #019079) [147]. Therefore only males express Cre/ERT2 fusion protein in their smooth muscle cells and can be used for tamoxifen induced recombination. Male Myh11-Cre/ERT2 STIM1/2 flox mice were injected intraperitoneal with corn oil only (controls) or with tamoxifen dissolved in corn oil (100 µl, 20 mg/ml tamoxifen) every second day three times. As additional controls, wildtype mice were injected with tamoxifen. After a period of 14 days, PPASMC were isolated from all mice. PCRs from the genomic DNA and reverse transcribed cDNA from the isolated mRNA (see figure 3.2) of different smooth muscle tissues and PPASMCs was performed to identify a successful deletion of STIM1/2 exons (see table 3.3 and 3.4). Animal experiments with these mice were approved by the federal government of Oberbayern and implemented at the Walther-Straub-Institute for Pharmacology and Toxicology, Munich, Germany.

	Primer
STIM1 Wt	5'-CGA TGG TCT CAC GGT CTC TAG TTT-3'
STIM1 AS	5'-GGC TCT GCT GAC CTG GAA CTA TAG TG-3'
STIM1 KO	5'-AAC GTC TTG CAG TTG CTG TAG GC-3'
STIM2 Wt	5'-CAT CAG AAG GTA AAA CTG TGC AGT GCT C-3'
STIM2 AS	5'-GGA TGT CCT GGA CTC ACT CTG TAG ACC A-3'
STIM2 KO	5'-GCT GAA CTG TGT GCT TGA CTG TAG C-3'

Table 3.3: **Primer for genotyping of STIM1 flox and STIM2 flox mice**

	STIM1 flox	STIM1 KO	STIM2 flox	STIM2 KO
	2 min 96°C	2 min 96°C	2 min 96°C	2 min 96°C
	30 cycles of:	30 cycles of:	30 cycles of:	30 cycles of:
	(20sec 96°C	(20sec 96°C	(20 sec 97°C	(20 sec 97°C
	30 sec 60°C	30 sec 60°C	30 sec 61°C	30 sec 68°C
	25 sec 72°C)	25 sec 72°C)	25 sec 72°C)	40 sec 72°C)
	5 min 72°C	5 min 72°C	5 min 72°C	5 min 72°C
	store at 14°C	store at 14°C	store at 14°C	store at 14°C
Expected fragments	399 bp STIM1 flox 348 bp Wt	580 bp STIM1 KO	335 bp STIM2 flox 262 bp Wt	683 bp STIM2 KO

Table 3.4: **Wt and STIM1 flox and KO and STIM2 flox and KO PCR program**

STIM1/2ΔEC, Orai1ΔEC, MCUΔEC [76] and MCUR1ΔEC [132] mice were generated by breeding the respective flox/flox mice with B6.Cg-Tg(Cdh5- Cre)7Mlia/J;(VE-Cre) mice (stock 006137, The Jackson Laboratory) which express a constitutively active Cre-recombinase under the control of the cadherin 5 (Cdh5) promoter only in endothelial cells. STIM1/2ΔEC, Orai1ΔEC, MCUΔEC and MCUR1ΔEC knockout mice did neither show any developmental defects nor any changed behavior to wild-type mice was observed. The presence of the floxed gene sequence was confirmed by genotyping from ear clips. The endothelial specific knockout was confirmed by mRNA and protein detection in freshly isolated MPMVEC from lungs. Animal experiments with these mice were approved by Temple University's IACUC, followed AAALAC guidelines and implemented at Temple University, Philadelphia, US.

3.2 RNA isolation and analysis by quantitative reverse transcription (RT)-PCR

RNA was isolated using the InviTrap^{Tm}Spin Universal RNA MiniKit (1060100300, Stratec) according to the manufacturer's instruction. In brief, tissue or cells were lysed. The lysate was first passed through a column to remove genomic DNA and through a second column which binds RNA. After washing, the purified total RNA was eluted and stored at -80 °C for further analysis.

Single-stranded RNA was transcribed into complementary DNA (cDNA) by the reverse transcriptase (K1632, ThermoScientific) in a Thermocycler (Peqstar 96 Universal Gradient, Peqlab). The resulting cDNA was used for quantitative (reverse transcription) polymerase chain reaction (PCR). During quantitative PCR, the cDNA is amplified using specific primers (see table 3.5). SYBR Green I (AB 1159B, Thermo-Scientific) binds double stranded DNA during amplification resulting in an emission of light of 521 nm after excitation at 494 nm. The signal is proportional to the cDNA content and therefore potentiates after each cycle. The relative expression of the 'gene of interest' is expressed in ratio to a 'housekeeping gene', such as β-actin.

	Primer
STIM1 forward	5'-AAG CTT ATC AGC GTG GAG GA-3'
STIM1 reverse	5'-CCT CAT CCA CAG TCC AGT TGT-3'
STIM2 forward	5'-GAG GGC GCA GAG TGT GAG-3'
STIM2 reverse	5'-TTT AGA GCC ATG CGG ACCT-3

Table 3.5: **Quantitative, reverse, transcription (RT)-PCR primer**

3.3 DNA extraction and purification

Genomic DNA was isolated from tail clips, intestine, aorta or PPASMCs using the GenElute^{Tm} Mammalian Genomic DNA Miniprepkit (G1N70-1KT, Sigma Aldrich) according to the manufacturer's instruction. In brief, tissue or cells were lysed with proteinase K and purified on a anion exchange column. PCR products were ampli-

	Primer
STIM1 Cre forward	5'-ACG ATG CCA ATG GTG ATG TG-3'
STIM1 Cre reverse	5'-TCT GAT GAC TTC CAC GCC TT-3'
STIM2 Cre forward	5'-AGT CAC CTG CAC AGA GAA GA-3'
STIM2 Cre reverse	5'-GGA GTG TTG TTC CCT TCA CA-3

Table 3.6: **Quantitative, reverse, transcription (RT)-PCR primer in tissue specific gene deficient mice** To detect deleted mRNA transcripts in tissue specific gene deficient mice primer were used which anneal to the deleted exon sequences (exon 2 for STIM1 and exon 3 for STIM2).

fied from purified genomic DNA by EconoTaq polymerase (Lucigen, F93481-1) using specific primers (see table 3.3 and 3.4. The resulting DNA fragments were separated by gel electrophoresis and visualized under UV-light using ethidiumbromide.

3.4 Production of lentiviruses

The production of recombinant lentiviruses which are derived from the human immunodeficiency virus (HIV-1) requires additional lab biosafety procedures and was done in the S2 tissue culture lab of the Walther-Straub-Institute. Lentiviral vectors can deliver, integrate and control the expression of transgenes in dividing cells.

Three vectors were transfected by calcium phosphate transfection into HEK293T cells to produce lentiviruses: the lentiviral coding plasmid (pLM-CMV-R-Cre, plasmid #27546 from addgene), the packaging plasmid (psPAX2, plasmid #27546 from addgene) and a plasmid coding for the envelope protein (PMD2.G, plasmid #12259 from addgene) (see figure 3.5). After transfection, they recombine, integrate and the cellular machinery produces recombinant virus particles which are released into the cell supernatant. When the virus from this supernatant infects STIM1/2 floxed cells, the viral RNA is reverse-transcribed into DNA, enters the nucleus and is stably integrated into the chromosomal DNA of the target cell (see figure 3.4). We used a second generation lentivirus system, which is designed in a way that it is less probable that replication competent viruses are formed from the lentiviral infected cells. This is achieved by separate expression of the transfer, envelope and packaging components
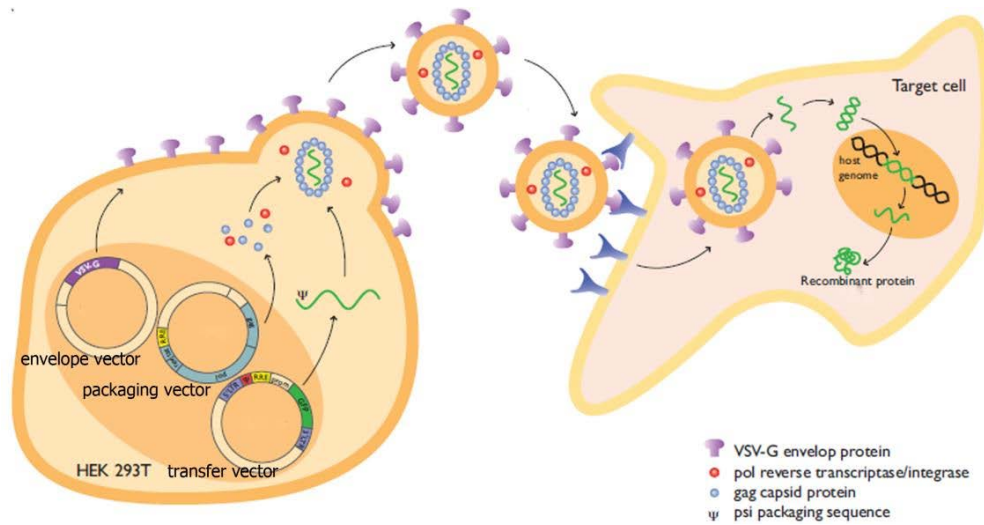
Figure 3.4: **Production of recombinant lentiviruses and cell infection.** Recombinant lentiviruses are produced in HEK 293T cells transfected with three plasmids expressing essential lentiviral genes. The produced recombinant lentiviruses can be used to infect target cells, where they are stably integrated in the host genome (modified from [2]).

Figure 3.5: **Map of plasmids used for lentivirus production.** For more details see text [2]

on different vectors. The lentiviral transfer vector contains the Cre-recombinase gene sequence that is incorporated into the host genome. Therefore, it stably induces the expression of the Cre-recombinase but it does not express envelope proteins and genes required for packaging which are essential to produce replication competent virus particles. To obtain a 1 to 2 log higher viral titer we concentrated the lentivirus with a polyethylene glycol precipitation solution (product number #LV825A from Bio-Cat). PPASMCs were infected at 70-80% confluence with naked or mCherry-tagged lentivirus which produced a red fluorescence in infected cells (plasmid #27546 from addgene) or control lentivirus (G5A, eGFP-5-Aequorin). After 7days, the recombination efficiency was checked by PCR or detection of fluorescent cells [2]. Our protocol was adapted from the lentivirus production protocol of the Tronolab [135] [2].

3.5 Isolation of cells and cell culture

3.5.1 Precapillary pulmonary arterial smooth muscle cells (PPASMC)

Mouse precapillary PPASMC were isolated from small pulmonary arterial vessels ($30\,\mu$m to $150\,\mu$m in diameter). In detail, the lung of a heparinized (500U) and euthanized ($125\,$mg/ml xylazine and $100\,$mg/ml ketamine) mouse was flushed with PBS and instilled with 0.5% low-melting-point agarose (A9045, Sigma-Aldrich) containing 0.5% Fe_3O_4 particles (310050, Sigma-Aldrich) via a catheter in the right ventricle. The lungs were removed, chopped and digested with 0.1 mg/ml collagenase (C5138, Sigma Aldrich) at 37 °C for 1 hour. Afterwards, the digestion was stopped, the solution was sheared with a 18G (4665120, Sterican, Braun) needle and placed into a magnetic holder. As a result, only the iron particles which are stuck in the precapillary arterial vessels are drawn to the magnet and are separated from other cell types released during digestion. The vessels were plated on coverslips in Smooth Muscle Cell Growth Medium 2 (C-22062, PromoCell) and cells were grown for 5 or 6 days before passaging and staining with α-smooth muscle actin antibody (A5228 Sigma

Aldrich) to identify them as smooth muscle cells according to the method described in [143].

3.5.2 Tracheal smooth muscle cells (TSMC)

The trachea of a heparinized (500U) and euthanized (125 mg/ml xylazine and 100 mg/ml ketamine) mouse was dissected and cleaned mechanically from surrounding tissue and endothelium. It was cut into small pieces, grown in Smooth Muscle Cell Growth Medium 2 (C-22062, PromoCell) and grown for 5 or 6 days before passaging.

3.5.3 Murine pulmonary microvascular endothelial cells (MPMVEC)

Primary murine MPMVECs were isolated from lungs of four mice. Briefly, freshly harvested mouse lungs were digested with 1 mg/ml collagenase/dispase (11097113001 Roche) and incubated with CD-144 (VE-Cadherin5 BD 55528 clone 11D4.1 BD biosciences) antibody labeled magnetic dynabeads (1004D protein G Thermo Scientific). Endothelial cells which adhered to the beads were washed and plated in MPMVEC media. MPMVECs were cultured in DMEM (HyClone SH30022.01 Thermo Fisher Scientific), containing 4.5 g/ml glucose, 4mM glutamine, 10% FBS, 1% antibiotic-antimycotic solution (15240-062 Thermo Fisher Scientific), 11 µg/ml ECGS (02-102 Merck Millipore) and 17 U/ml heparin (H3393 Sigma-Aldrich). MPMVECs were always plated at a minimum of 60% confluency on 0.2% gelatine coated flasks, split once or twice a week and used between passage 2 and 8.
To identify MPMVECs, Dil-Ac-LDL (10 µg/ml) was added to the growth media for 4h at 37 °C. After washing cells with PBS several times, fluorescence was visualized using a rhodamine excitation/emission filter.

3.5.4 Murine lung fibroblasts (MLF)

Cells which were not bound to the dynabeads during isolation of MPMVEC were plated separately and grown as murine lung fibroblasts (MLF). MLF contain the

68

loxP sites but not the Cre-recombinase which is under the promotor of VE-Cadherin and is only expressed in endothelial cells. Therefore, excision of the floxed exons was achieved by infection with house-made adenoviruses constitutively expressing the Cre recombinase (50-100MOI, different batches: $1x10^8$ IFU/ml or $3.1x10^{10}$ IFU/ml or $1.27x10^9$ IFU/ml) for 10days. Downregulation of STIM1/2 and Orai1 was confirmed by quantitative RT-PCR and Western Blot.

3.6 Protein analysis by Western Blotting

Western blots have been run in our lab in Munich according to the following method: In brief, proteins were lysed with 1x RIPA buffer (10x RIPA buffer: 1% Igepal CA 630, 0,5% Na-deoxycholat, 0,1% SDS in 1 X PBS) and the concentration of the lysate was measured with a BCA Protein assay kit (23225, Pierce). 4x Laemmli buffer was added to the lysate and boiled at $95\,°C$ to break the disulfide bonds and tertiary structure of the protein. Equal amounts of proteins were loaded on an acrylamide gel and run at constant $20\,mA$. After protein separation, proteins were transferred to a polyvinylidene difluoride membrane. The transfer was confirmed by Ponceau S which binds proteins unspecifically. Membranes were blocked with 5% milk powder in PBST, incubated with primary, HRP-conjugated secondary antibodies and developed with the SuperSignal^{TM} West Femto Maximum Sensitivity Substrate (34096, Thermo Scientific) or SuperSignal^{TM} West Pico Chemiluminescent Substrate (34080, Thermo Scientific) using the Chemismart analyzer.

Western blots have been run in the lab of Madesh Muniswamy in Philadelphia according to the following method:

Cells were lysed in 1x RIPA buffer (20-188 Millipore) and 1x protease inhibitor (04693116001 Complete, Roche). Equal amounts of protein were loaded per lane and separated on a 4 to 12% bis-tris polyacrylamide gel, transferred to a polyvinylidene difluoride membrane, blocked and probed with primary antibodies (see table 2.2). Secondary antibodies used were: anti-rabbit (7074S Cell signaling 1:5000), anti-goat (sc-2056 Santa Cruz Biotechnology Inc., 1:5000) and anti-mouse (7076S, Cell

signaling, 1:5000) conjugated to horse radish peroxidase. Western blots were developed using either SuperSignal$^{\text{TM}}$ West Femto Maximum Sensitivity Substrate (34096, Thermo Scientific) or SuperSignal$^{\text{TM}}$ West Pico Chemiluminescent Substrate (34080, Thermo Scientific). If membranes were reprobed with antibody, they were stripped with Restore$^{\text{TM}}$ Western Blot Stripping Buffer (21059, Thermo Scientific).

3.7 Analysis of bronchial reactivity

3.7.1 Myograph

The primary bronchus, trachea and thoracic aorta were dissected from STIM1$^{+/-}$ Orai1$^{+/-}$, STIM1/2$^{\Delta EC}$ or Orai1$^{\Delta EC}$ mice, cleaned from connective tissue, cut in rings and mounted in a myograph (610M, DMT) containing physiological (37 °C warm Krebs-Henseleit-Buffer (K3753, Sigma Aldrich) perfused with carbogen gas (95% O_2 /5% CO_2) (see figure 3.6.) Tissue was pre-streched to 4.5mN for aortic rings and to 2.5mN for tracheal rings from primary bronchi and equilibrated 1h while the buffer was changed every 20min. 120mM KCl was added which induces a membrane depolarisation and activates voltage-dependent calcium channels. Tissue which did not respond to KCl treatment was classified as non-functional and not used for further analysis.

Aortas of STIM1/2$^{\Delta EC}$ or Orai1$^{\Delta EC}$ mice mice were treated with 1 µM phenylephrine (PE). Phenylephrine, an α1-adrenoceptor agonist, activates G_q-coupled receptors and phospholipase C producing DAG which activates TRPC3/6/7 channels. Membrane depolarisation, activation of voltage-gated calcium channels and influx of extracellular calcium, subsequently contracted aortic rings. At the steady maximal contraction, cumulative concentrations of acetylcholine (ACh, 0.01 µM-30 µM) and finally sodium nitroprusside (SNP, 3 µM) were added. Cumulative concentrations of ACh induced endothelium-dependent relaxation, SNP induces an endothelium-independent relaxation. The relaxation was normalized to the PE contraction of the same aorta.

The primary bronchus of STIM1$^{+/-}$ Orai1$^{+/-}$ mice was dissected and mounted. After

confirming the vitality of the tracheal rings from primary bronchi, they were incubated with Ca^{2+}-free Krebs-Henseleit-Buffer. To deplete intracellular stores, tracheal rings were stimulated with cumulative concentrations of the muscarinic acetylcholine receptor agonist, carbachol (CCH, 500nM, 1 µM, 10 µM) before 2mM Ca^{2+} was restored. Restoration of Ca^{2+} resulted into a contraction of the tracheal rings. After washing and reaching baseline contraction levels, this protocol was repeated at least five times with the same tracheal rings. The contraction response was normalized to the first contraction of the same ring.
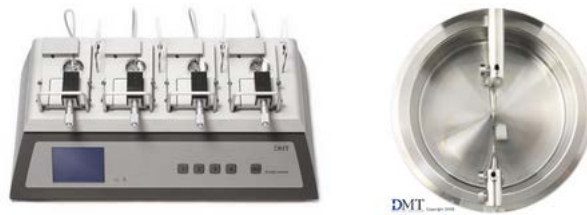
Figure 3.6: **Measurement of contraction and dilatation with a myograph.** Rings from blood vessels, trachea or bronchi are mounted in an organ bath of a myograph (610M, DMT) and stimulated by different pharmacological agonists. The resulting contraction or dilatation was recorded.

3.7.2   Precision cut lung slices (PCLS)

The lung of an euthanized mouse was filled with low-melting point agarose. After the agarose had solidified the lung was cut into 200 µM thick slices using a vibratome. Slices were cultivated in a cell culture incubator for several days. Their vitality was confirmed by their ciliary movement and intact bronchial smooth muscle layer under a microscope. Intact PCLS were mounted in an imaging chamber and hold in position with a metal ring. Additive concentrations of carbachol (500nM-2,3mM, over a period of 40min) were applied to the PCLS. Images were taken as a time lapse series using the bright field mode of a Zeiss LSM710 META microscope.

3.8 Scratch assay

MPMVECs were seeded at equal density in 6-well plates to form a confluent mono-layer. A 1.8 mm scratch was cut per well using a sterile 200 μl tip. The wells were washed with PBS and filled with DMEM, containing 2% FBS. Immediately after the scratch, after 24h and after 48h, cells were fixed with CAMCO Quick Stain[R] II and bright field images were taken with a 4x objective at multiple locations. Migration was quantified using the Image J software (NIH) and results are expressed as percent gap closure.

3.9 Proliferation assay

MPMVECs were stained with 5-(and-6)-carboxyfluorescein diacetate succinimidyl ester (CFSE) using a Cell Trace CFSE cell proliferation kit (C34554; Invitrogen). Cells were labeled with 5 μM CFSE for 15min at 37°C and 5% CO_2 and plated on T75 flasks for 72h. These cells were used as 'proliferated cells' after 72hs. 'Nonprolifer-ated cells' were stained in the same way but used directly for the experiment without plating and growing for 72hs. 15'000 events/sample were assessed using standard gating procedures with a BD FACSCalibur[Tm]. Relative fluorescence intensities were analyzed using FlowJo software.

3.10 Analysis of vascular permeability and edema formation

3.10.1 Immunohistochemistry and phalloidin staining

Cells were fixed with 3.7% formaldehyde (252549 Sigma-Aldrich), permeabilized and blocked with 0,3% Triton X-100 (3051.2 Carl Roth) and 5% goat serum (S2000-100 Bio-West). Primary antibody was diluted (in 1% BSA in PBS and 0,3% Triton X-100) and incubated overnight at 4°C. After washing (PBS 0.1% BSA, 9418 Sigma-Aldrich),

the secondary antibody was incubated at room temperature, in the dark, for 2 hours. Hoechst (33342 Sigma-Aldrich 1:5000 in PBS) was used to stain the nuclei. The coverslips were mounted on microscope slides using Dako Mounting media (53023, Dako Hamburg) and transparent nail polish.

To induce stress fiber formation, MPMVECs were stimulated with 5nM thrombin (605157, Calbiochem, Merck, Darmstadt) for 5min. After permeabilization and fixation, cells were stained with phalloidin-TRITC (tetramethylrhodamine) ($50\,\mu g$/ml, P1951 Sigma-Aldrich) in the dark, for 40min. Phalloidin stabilizes the F-actin filaments of the cytoskeleton which can be visualized under a fluorescence microscope.

3.10.2 Adenoviral Nuclear Factor of Activated T cells (NFATc3) translocation assay

On glass cover slip grown MPMVECs were infected with adenovirus expressing NFATc3-GFP (100 MOI) for 36 hours, treated with LPS ($1\,\mu g$/ml) and imaged after additional 16h with 488-nm excitation using a 40x oil objective (Zeiss LSM510 META). Images were analyzed and quantified using ZEN2 2010 software. Cells with nuclear NFATc3-GFP were manually counted and quantified as percentage of cells with nuclear translocation.

3.10.3 Infection of mice with *Klebsiella pneumoniae*

Klebsiella pneumoniae was isolated from the lung of a mouse which had been infected with the bacteria. The lung homogenate was plated on MacConkey Agar (BD 212123 BD Biosciences) and a single colony picked to grow bacteria which were used to infect other mice. When the bacterial culture reached an OD_{600} of 0.8, $100\,\mu l$ of the bacterial culture was pelleted, diluted with PBS 1:10 and solubilized in $50\,\mu l$ PBS. Mice were anesthetized with Avertin[Tm] (tribromoethanol/2-methyl-2-butanol) and instilled intranasally with 8×10^6 colony forming units (CFU) *Klebsiella pneumoniae* (OD_{600}=0.8). After 20h, broncho-alveolar lavage was collected and mice were either injected with FITC (fluorescein isothiocyanate) dextran (70 kDa, 5% in saline;

Molecular Probes, Invitrogen) or lungs were fixed in formalin (see figure 2.10.5).

3.10.4   FITC-dextran vascular leakage

Mice were anesthetized with Avertin^{Tm} (tribromoethanol/2-methyl-2-butanol), injected intraocularly with FITC-dextran (70 kDa, 5% w/v in saline; Molecular Probes, Invitrogen) and allowed to rest for 10min. After euthanasia, 0.5ml PBS ($+$ 0.5%EDTA) was instilled into the lung via a tracheal catheter, retrieved and frozen at $-80\,°C$ for further analysis. The lung was filled completely with PBS via the trachea, the trachea was tied with a cotton threat and the lung mounted in an imaging chamber. Images were collected at different regions of the lung using a 20x water immersion objective with Zeiss 710 META NLO 2-photon microscope equipped with a Chameleon Coherent^{Tm} IR laser. The alveolar area and the background fluorescence of the alveolar space which was defined as vascular leakage was quantified using the ZEN^{Tm} (Zeiss) program. Broncho alveolar lavage (BAL) fluid was used to quantify FITC-dextran leakage by excitation at 488nm with a Tecan plate reader (Infinite^{R} 200Pro. Protein content was measured using a commercially available Bradford assay (23200, Thermo Scientific).

3.11   Measurement of cytosolic and mitochondrial Ca^{2+} and the mitochondrial membrane potential ($\Delta\Psi_m$)

To investigate the store-operated Ca^{2+} entry (SOCE) in living cells, PPASMCs were analyzed in Alexander Dietrich's lab and MLFs in Madesh Muniswamy's lab.

PPASMC were grown on glass coverslips and loaded with $2\,\mu M$ fura-2-acetoxymethyl ester (47989, Sigma Aldrich) in Hepes Ringer solution (140 mM NaCl, 5mM KCl, 1mM MgCl$_2$, 10mM hepes, 5mM glucose, 2mM CaCl$_2$) at room temperature for 30min. Coverslips were mounted in Ca^{2+}-free HBSS (15-009, PAA, 5.33mM KCl, 0.44mM KH$_2$PO$_4$, 4.17mM NaHCO$_3$, 137.93mM NaCl, 0.34mM Na$_2$HPO$_4$, 5.56mM D-Glucose) supplemented with 0.005% EGTA in an imaging chamber. After base-

line recording, PPASMCs were stimulated with the SERCA inhibitor thapsigargin (586005, Calbiochem) or cyclopiazonic acid (CPA) (C1530, Sigma Aldrich). Either $2\,\mu$M thapsigargin or $10\,\mu$M CPA was used to empty the ER from Ca^{2+}. After the ER Ca^{2+} was released, $CaCl_2$ solution was added to reach a final extracellular Ca^{2+} concentration of 2mM to induce SOCE. The emitted fluorescence after excitation at 340 and 380 nm was recorded with a 14-bit EMCCD camera (iXON3 885, Andor, Belfast, UK) of a monochromator-equipped (Polychrome V, TILL-Photonics, Martinsried, Germany) inverted microscope (Olympus IX 71 with an UPlanSApo 20x/0.85 oil immersion objective). Intracellular Fura-2 AM bound to Ca^{2+} emits maximal fluorescence at an excitation wavelength of 340 nm, while Fura-2 AM without Ca^{2+} has its emission maximum at an excitation wavelength of 380nm. Accordingly, the ratio 340nm/380nm determines the intracellular Ca^{2+} concentration independent of variabilities in dye loading.

To investigate the mitochondrial function of MLFs and MPMVECs, cells were grown on glass cover slips and loaded with the mitochondrial calcium indicator $2\,\mu$M Rhod-2 AM for 50min and the cytosolic calcium indicator $5\,\mu$M Fluo-4 AM for 30min in extracellular medium (ECM), pH 7.4, in the presence of $100\,\mu$M sulphinpyrazone (Sigma Aldrich) and 0.003% pluronic acid (Thermo Fisher Scientific) which improved the dye loading. Coverslips were mounted on a stage of a Zeiss LSM510 META microscope. After 1 min of baseline recording, $1\,\mu$M ionomycin was added and Ca_{2+} influx in the cytosol and the mitochondria was quantified.

Alternatively, cells were loaded with 100nM tetramethyl rhodamine methyl ester (TMRM), a $\Delta\Psi_m$ indicator, and $2.5\,\mu$M Dihydrorhodamine 123, an mitochondrial dye labeling active mitochondria, in ECM at $37\,°$C for 30 min. Mitochondrial superoxide production was quantified using MitoSOX Red (Invitrogen; $10\,\mu$M) for 40 min in ECM at $37\,°$C and 5% CO2.

After dye loading cells were washed with mounting ECM containing 0.25% BSA and sulfinpyrazole, mounted in an open perfusion microincubator (PDMI-2; Harvard Apparatus) at $37\,°$C and imaged. Rhod-2 AM, TMRM and MitoSox Red were visualized at an excitation wavelength of 561nm, Fluo-4 AM at 488-nm every 3 seconds. TMRM

and Rhodamin1/2/3 were visualized using a a 63x oil objective, Rhod-2 AM, TMRM, MitoSox Red and Fluo-4 AM using a 40x oil objective of a confocal microscope (Zeiss LSM510 META, Inc.). Images were analyzed using ZEN2 2010 software (Zeiss).

3.12 Ca²⁺ uptake and membrane potential ($\Delta\Psi_m$) measurement in the permeabilized cell system

Equal numbers of MPMVECs were resuspended and permeabilized with $20\,\mu g/ml$ digitonin in 1.5 ml of intracellular medium composed of 120 mM KCl, 10mM NaCl, 1mM KH_2PO_4, 20mM Hepes-tris (pH 7.2) and $2\,\mu M$ thapsigargin to block the SERCA (sarcoplasmic/endoplasmic reticulum Ca^{2+} ATPase) pump. The mitochondrial substrate succinate (5mM) and the intracellular Ca^{2+} indicator Fura-2FF ($0.5\,\mu M$, Fura-FF pentapotassium salt), which is relatively insensitive to Mg^{2+}, were added and the cuvette was immediately mounted in a multiwavelength excitation, dual-wavelength emission fluorimeter (DeltaRAM, Photon Technology International). The sample was stirred constantly and temperature controlled at 37 °C. Extramitochondrial Ca^{2+} was monitored at an excitation ratio of 340 nm/380 nm of Fura-2FF fluorescence. After baseline recording, the $\Delta\Psi_m$ indicator JC-1 ($800\,nM$, Thermo Fisher Scientific) was added. The dye JC-1 accumulates potential dependent in mitochondria, which is indicated by the ratio fluorescence at an excitation wavelength of 490nm and 570nm. A mitochondrial membrane depolarization is consequently visualized by a reducing fluorescence ratio at 490/570nm. The intracellular, extramitochondrial Ca^{2+} concentration was analyzed simultaneously at an excitation wave length of 340nm and 380nm by Fura-2FF. Several $10\,\mu M$ Ca^{2+} pulses were added in 50 seconds intervals and intracellular Ca^{2+} fluorescence of Fura2-FF and $\Delta\Psi_m$ of JC-1were recorded simultaneously. Mitochondrial Ca^{2+} uptake was visualized by a decline in intracellular Ca^{2+} fluorescence. When the mitochondrial Ca^{2+} uptake was exhausted and $\Delta\Psi_m$ collapsed, the total mitochondrial Ca^{2+} content was verified by the mitochondrial uncoupler FCCP ($2\,\mu M$) which generates a nonspecific proton leak.

76

3.13 Cellular ATP measurement

Cellular ATP levels were measured using the commercially available CellTiter-Glo luminescent assay kit (Promega, Madison, WI, USA) according to the manufacturer's instruction. Metabolically active cells produce ATP which reacts with the CellTiter-Glo substrate to induce a luciferase reaction and generates a luminescent signal. Because this signal is dependent on the number of cells, the luminescent signal was normalized to the protein content of the samples.

3.14 XF-96 Extracellular Flux Analyzer^{Tm}

The XF-96 Extracellular Flux Analyzer^{Tm} (Seahorse Bioscience) can be used to measure the oxygen consumption rate (OCR) and extracellular acidification rate (ECAR) in adherent, permeabilized cells. The preloading of reagents and the automatic analysis of the 96-well plate allows a higher throughput than with conventional methods.
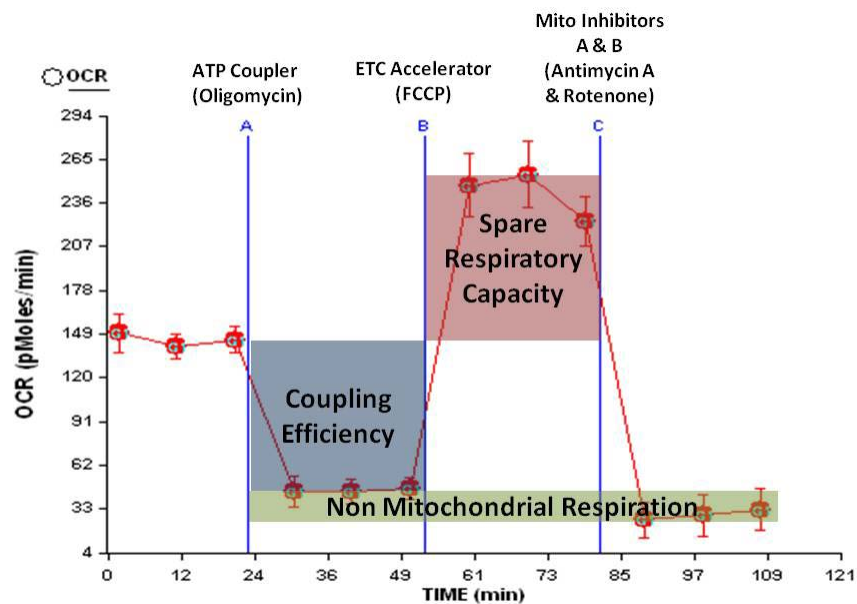
Figure 3.7: **An oxygen sensor measures the OCR..** The OCR rate changes after addition of oligomycin - which inhibits the coupling efficiency, FCCP - an uncoupler, and antimycin A - an electron chain inhibitor [113].

The XF Cell Mito Stress Test Kit^{Tm} was used according to the manufacturer's in-

struction. In brief, $1x10^4$ MPMVECs per well were seeded in the XF Mitoplate and grown overnight. On the following day, the medium was changed to the Seahorse Assay medium and the plate was incubated at $37\,°C$ in a CO_2 free incubator for 1h. Different reagents were preloaded into the reagent delivery chamber and injected pneumatically into the media. An oxygen sensor which is coupled to a fiber-optic waveguide (Seahorse Bioscience XF96 Flux Analyzer^{Tm}) recorded the OCR emission at an excitation wavelength of 532nm [149]. Data was analyzed by the Wave Software. Basal mitochondrial respiration is dominated by proton flow through the ATP synthase and proton leakage before addition of any reagents. The first injection, oligomycin ($1\,µM$), inhibits the ATP synthase (Complex V). The remaining non-mitochondrial oxygen consumption is due to the proton leak across the inner mitochondrial membrane. The second injection, FCCP ($1\,µM$), uncouples respiration from oxidative phosphorylation and therefore allows H^+ to diffuse back to the matrix without passing the ATP synthase. As a result, any substrate available in the medium is oxidized and contributes to the maximal respiration rate. At last, the electron transport chain inhibitors rotenone, a complex I inhibitor and antimycin A, a complex III inhibitor (both $1\,µM$) are added. The residual respiration after blocking the electron chain is non-mitochondrial (see figure 3.7) [113].

Similar to analyzing the OCR with an oxygen sensor, ECAR can be analyzed using a pH sensor at an excitation wavelength of 470nm. Pyruvate is converted to lactic acid during anaerobic glycolysis. When lactic acid is released, it acidifies the extracellular space and can be measured as an increase in ECAR [113] [10]. Basal glycolytic flux is measured in glucose-free media. The first injection, glucose at saturating concentration (10mM), is generates glycolysis and thereby produces ATP and protons. The protons are released into the media and can be measured as an increase in ECAR. The second injection, oligomycin ($1\,µM$), inhibits mitochondrial ATP production and therefore shifts metabolically the energy production to glycolysis (maximal glycolytic capacity). The final injection, 2-DG (2-deoxy-D-glucose), a glucose analog, inhibits the first enzyme during glycolysis glucose hexakinase. The residual ECAR after blocking glycolysis is non-glycolytic [113].

3.15 Clark electrode

The Clark electrode can be used to measure mitochondrial respiration in intact or permeabilized cells or isolated mitochondria. It is composed of a platinum cathode and a silver anode which are linked by an electrolyte solution. When a small voltage is applied, the platinum electrode adopts the externally applied potential. This negative potential induces that oxygen is reduced at the platinum surface to hydrogen peroxide. Consequently, a current flows towards the silver electrode and silver is oxidized to silver chloride which is deposited at the anode. The current is correlated to the oxygen consumed at the platinum cathode [141].

$3x10^5$ MPMVECs were resuspended in intracellular medium composed of 120 mM KCl, 10mM NaCl, 1mM KH_2PO_4, 20mM Hepes-tris (pH 7.2). 40 μg/ml digitonin, to permeabilize membranes, and 10 μM thapsigargin, to block the SERCA pump, were added. The cell suspension was transferred immediately to the MT200A Mito-Cell chamber of a MT200A MitoCell Clark-type electrode (Strathkelvin Instruments, Motherwell, United Kingdom) and stirred constantly at 37 °C. After baseline recording, mitochondrial substrates were added in 30 seconds intervals via a Hamilton syringe. 1 mM pyruvate and 1 mM malate were added first. Pyruvate oxidation in the tricarboxylic acid cycle (TCA) cycle generates electrons from NADH which feed complex I. Malate supports the TCA cycle. Electrons from complex I are passed down the respiratory electron chain and enhance complex III and IV activity. Then, succinate (1mM) was added which provides electrons for complex II and bypasses complex I. Next, 0.5 mM TMPD (tetramethylphenylendiamin), an artificial electron donor, and 1mM ascorbate as antioxidants keeping TMPD in its reduced state was added. At last, excessive natriumazide was added to block complex IV and the OCR decreases to the calibrated instrument baseline [153]. The rate of oxygen consumption was measured and displayed as nmol O^2/min.

3.16   Statistical analysis

Data from multiple experiments were quantified and illustrated as means $\pm$ SD if not indicated otherwise. Differences between groups were analyzed by an unpaired t-test, one-way ANOVA or rank sum test. $P < 0.05$ was considered significant. Data were analyzed with ZEN2 2010 software, ImageJ or FlowJo and plotted with either GraphPad Prism version 5.0 or SigmaPlot 11.0 software.

Chapter 4

Results

4.1 Roles of STIM1/2/Orai proteins and TRPC channels in receptor and store-operated Ca^{2+} entry (ROCE/SOCE)

4.1.1 Analysis of heterozygous STIM1$^{+/-}$/Orai1$^{+/-}$ mice

Homozygous STIM and Orai knockout mice die perinatally of unknown reason. Thus, we have established a heterozygous STIM1$^{+/-}$/Orai1$^{+/-}$ C57BL/6 mouse strain by mating two independent STIM1$^{+/-}$ and Orai1$^{+/-}$ mouse strains generated by the gene-trapping method (see figure 3.1 of methods section). We designed specific primers and established the genotyping of the double heterozygous mice. One of the primers binds to the β-geo cassette (encoding β-galactosidase-neomycin fusion protein)
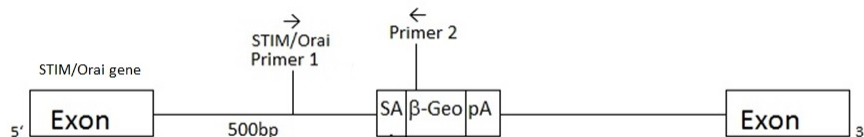
Figure 4.1: **Location of primer for genotyping of double heterozygous STIM1$^{+/-}$/Orai1$^{+/-}$ C57BL/6 mice.** Primers bind to the β-geo cassette (encoding β-galactosidase-neomycin fusion protein) and in the adjacent genomic intron DNA. SA: splicing acceptor site, pA: polyA tail

the other in the adjacent genomic intron DNA (see figure 4.1). Figure 4.2 shows resulting DNA fragments from a typical PCR-genotyping of DNAs from mouse tails of heterozygous STIM1$^{+/-}$ and Orai1$^{+/-}$ mice.
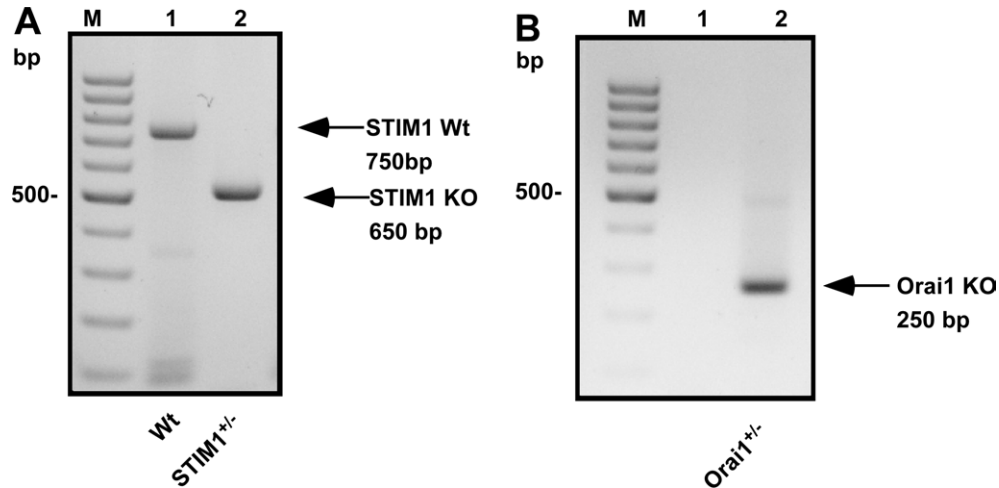
Figure 4.2: **Agarose gel electrophoresis of genomic DNA fragments from a typical PCR-genotyping of DNAs from mouse tails of heterozygous Stim1$^{+/-}$ and Orai1$^{+/-}$ mice.** A) Wt-PCR PCR-fragments amplified from the Wt (lane 1) and the mutated STIM1 gene locus (lane 2) B) PCR- fragments amplified from the mutated Orai1 gene locus (lane 2). M: 100bp DNA marker
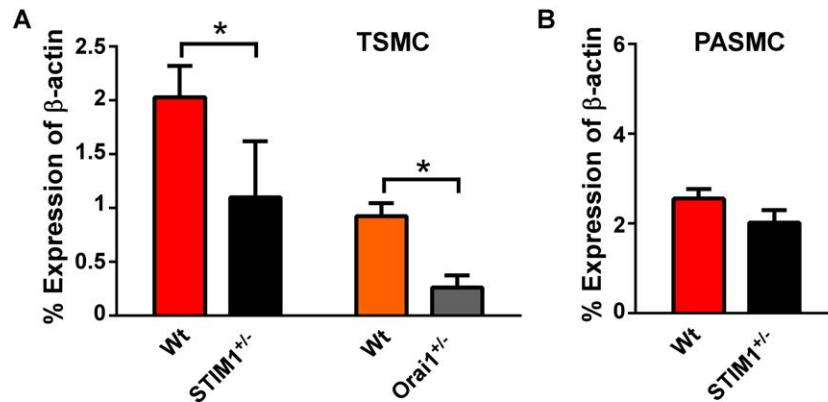
Figure 4.3: **STIM1 and Orai1 mRNA expression in TSMCs and PPASMCs isolated from STIM1$^{+/-}$/Orai1$^{+/-}$ mice.** A) Wt-mRNA expression from the STIM1 and Orai1 genes in TSMCs of STIM1$^{+/-}$/Orai1$^{+/-}$ mice, passage 2 B) Wt-mRNA expression from the STIM1 gene in PPASMCs of STIM1$^{+/-}$ mice, passage 0, 3-4 mice per group, P values were determined by unpaired t-test; * P<0.05

M-RNA-transcription from the Wt STIM1 and Orai1 allele was quantified in STIM1$^{+/-}$/Orai1$^{+/-}$ and Wt mice. Figure 4.3 shows that STIM1 and Orai Wt mRNA

was significantly reduced in STIM1$^{+/-}$/Orai1$^{+/-}$ tracheal smooth muscle cells (TSMC). In contrast to these results, STIM1 Wt mRNA expression in PPASMC from STIM1$^{+/-}$ mice was not significantly different compared to PPASMC from wildtype mice. STIM1 protein is downregulated significantly in MPMVECs from STIM1$^{+/-}$/Orai1$^{+/-}$ mice compared to MPMVECs from Wt mice by 11% (see figure 4.4). This reduction however is less than expected and makes it difficult to interpret the results obtained with this mouse line.
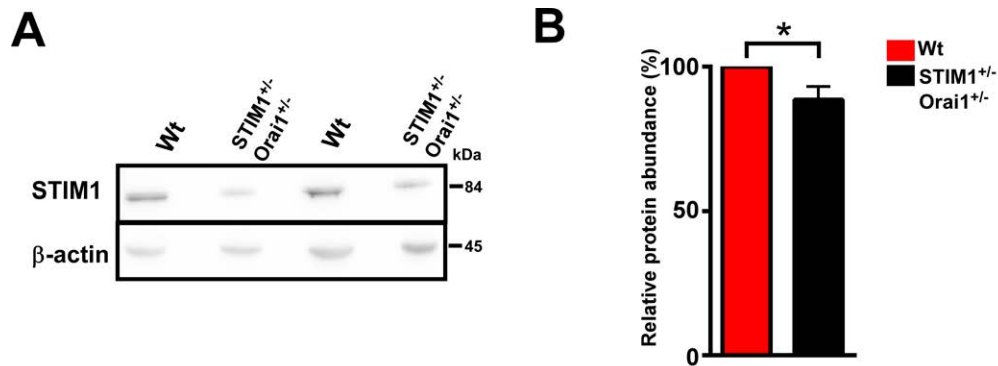
Figure 4.4: **STIM1 protein expression in STIM1$^{+/-}$/Orai1$^{+/-}$ and Wt MP-MVECs.** A) Representative blot B) Quantification of STIM1 protein on n=3 blots, P values were determined by unpaired t-test; * P<0.05
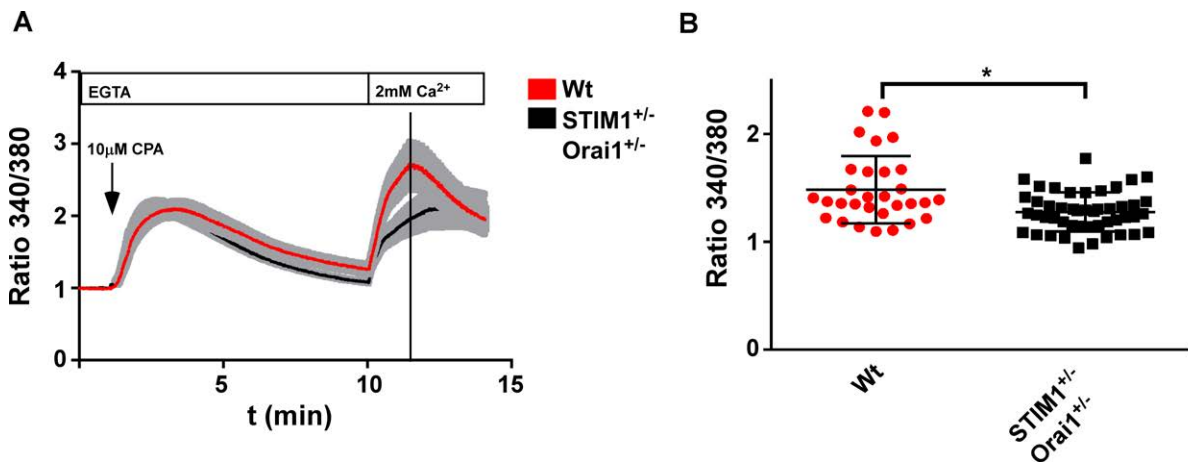
Figure 4.5: **CPA-induced SOCE in STIM1$^{+/-}$/Orai1$^{+/-}$ PPASMCs.** A) CPA-induced ER depletion and restoration of external Ca^{2+} to 2mM results in SOCE B) Quantification of maximum Ca^{2+} influx during CPA-induced SOCE at the indicated time point. Graphs show the result of 33-43 cells, isolated from three mice per group ± SEM, unpaired t-test; * P<0.05, CPA: cyclopiazonic acid

Next, we analyzed if reduced STIM1$^{+/-}$/Orai1$^{+/-}$ levels resulted into a functional

SOCE defect. PPASMCs were grown on glass cover slips and loaded with the Ca^{2+} indicator Fura2-AM. After depletion of internal Ca^{2+} stores by $10\,\mu M$ CPA in Ca^{2+}-free HEPES solution containing 2mM EGTA, extracellular Ca^{2+} solution was added to quantify the store-operated calcium influx. The maximum Ca^{2+} influx after store depletion was quantified (see figure 4.5).

After emptying internal stores by $10\,\mu M$ CPA, external Ca^{2+} was restored to 2mM which resulted into SOCE. We observed a significantly reduced SOCE in PPASMCs isolated from $STIM1^{+/-}/Orai1^{+/-}$ mice (see figure 4.5). Nevertheless, this reduction was much smaller than expected and makes it difficult to draw conclusions from the planned experiments.
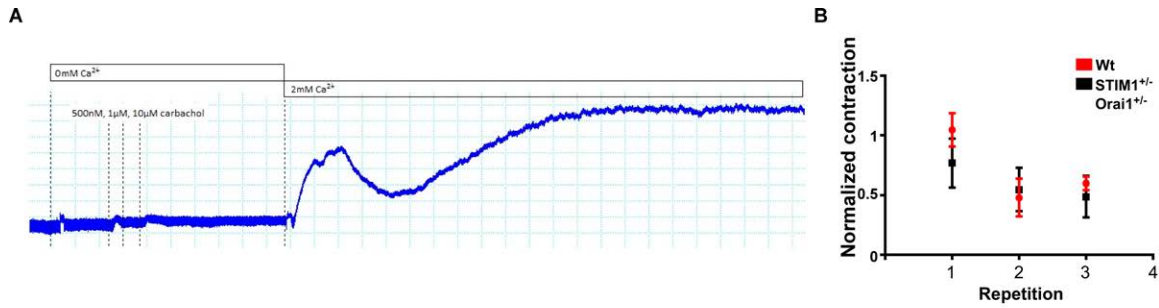
Figure 4.6: **Repetitive contraction of tracheal rings from primary bronchi of $STIM1^{+/-}/Orai1^{+/-}$ and Wt mice.** A) Contraction of tracheal rings following carbachol-induced ($10\,\mu M$) ER depletion in (Ca^{2+}-free buffer) and restoration of external Ca^{2+} to 2mM B) Four repetitive contractions of of the same bronchus were quantified and normalized to the first contraction of the same bronchus, n=3-5 mice, unpaired t-test; * P<0.05,

To test if the small but significant STIM1 and Orai1 downregulation is sufficient to detect differences in repetitive contraction of tracheal rings from primary bronchi we used a myograph system. Isolated primary bronchial rings were mounted in a myograph and incubated with Ca^{2+}-free Krebs-Henseleit-Buffer. Intracellular stores were depleted by carbachol (CCH, 500nM, $1\,\mu M$, $10\,\mu M$) which induced only a weak bronchoconstriction. When extracellular Ca^{2+} was restored to 2mM, tracheal rings contracted again (see figure 4.6). The contraction protocol was repeated at least four times on the same tracheal ring to investigate if primary bronchi of $STIM1^{+/-}/Orai1^{+/-}$ mice exhaust faster than primary bronchi of Wt mice. The contraction response was

normalized to the first contraction of the same bronchus. As shown in figure 4.6 we were not able to detect any differences between STIM1$^{+/-}$/Orai1$^{+/-}$ and Wt bronchi. Quality control of mounted tracheal or aortic rings is only possible by the response to other stimuli, such as the response of potassium chloride (KCl) on membrane depolarisation and the following activation of voltage-dependent Ca^{2+} channels which results in contraction. Some bronchi or aortae display a good KCl response but are not able to hold the contraction over a longer period or start oscillating. This results into variations in contraction or dilatation between the samples which makes it difficult to analyze the results. Therefore, we tried to establish a contraction model using precision cut lung slices (PCLS) as an alternative to the myograph. 200 μM thick PCLS which have been cultivated for several days were examined for intact smooth muscle layers and ciliary activity. Only intact PCLS were treated with cumulative concentrations of carbachol (500nM-2,3mM) which resulted into a bronchoconstriction after 40min (see figure 4.7).
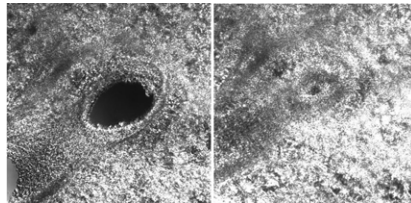
Figure 4.7: **Carbachol-induced bronchoconstriction in precision cut lung slices.** Contraction of a bronchus before and after application of carbachol in precision cut lung slices (PCLS). Slices were treated repeatingly with additive concentrations of carbachol (500nM-2,3mM) over a period of 40min, representative bronchus

Even though we were able to record a strong bronchoconstriction of some bronchi, many bronchi responded weak or not all all. Fig 4.7 shows a representative bronchus which constricted almost completely after 40min. Moreover, the analyzed bronchus was not focused any more after changing buffers which is essential to establish a SOCE protocol. Therefore, we decided not to proceed with this method.

4.1.2 Analysis of a tamoxifen-induced smooth muscle cell-specific STIM1/2 knockout in STIM1/2(Myh11-Cre/ERT2) mice

Mice with an overall STIM1 knockout die 1-4 weeks after birth of unknown reason, but smooth muscle cell specific STIM1 knockout mice have been shown to be viable [83]. We therefore generated STIM1/2flox(Myh11-Cre/ERT2) mice to induce a smooth muscle cell specific knockout of STIM1 and STIM2 proteins after tamoxifen injection by mating a STIM1/2 floxed mouse line with Mhy11-Cre/ERT2 mice. Myh11-Cre/ERT2 mice express the Cre-recombinase under the control of the smooth muscle cell specific promotor Mhy11. Therefore, the Cre-recombinase only deletes the STIM1/2 exons in smooth muscle cells. ERT2-Cre-recombinase is only expressed after tamoxifen injection of the mouse because the Cre-recombinase is fused to the ligand binding domain of the human estrogen receptor.
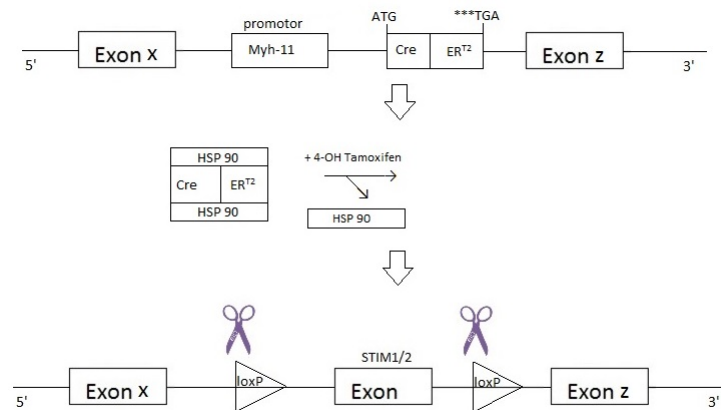
Figure 4.8: **Inducible smooth muscle cell specific knockout of STIM1 and STIM2 alleles using tamoxifen.** The Cre-recombinase is expressed under the control of the promotor Mhy11 only in smooth muscle cells. Upon tamoxifen application, the Cre-recombinase is activated and deletes the floxed STIM1/2 exons. HSP90: heatshock protein90, Cre: Cre-recombinase, ERT2: estrogen receptor2, see text for more details

Moreover, three point mutations in the ligand binding domain prevent the binding with its natural ligand estradiol. In the absence of tamoxifen, Cre-ERT2 is bound to the heatshock protein 90 which inhibits the Cre-recombinase activity. Upon tamoxifen application, the heatshock protein is dissociated and the Cre-recombinase is now

activated and deletes the floxed exons from the STIM1 and STIM2 genes resulting in a STIM1/2 knockout only in smooth muscle cells (see figure 4.8).
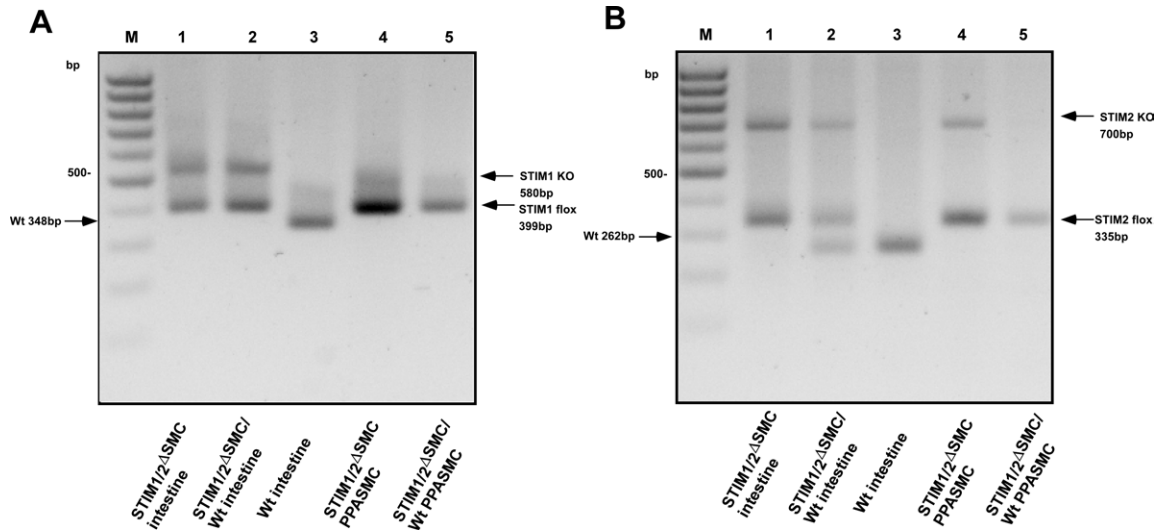
Figure 4.9: **Agarose gel electrophoresis of DNA fragments from PCR-genotyping of genomic DNAs from intestine cells and PPASMCs isolated from STIM1/2 flox (Myh11 Cre/ERT2) mice after injection of tamoxifen.** Genomic DNA from the intestine or PPASMC were isolated for PCR A)Separation of PCR products from the floxed (STIM1 flox) and the deleted (STIM1 KO) STIM1 allele. B) Separation of PCR products from the floxed (STIM2 flox) and the deleted (STIM2 KO) STIM2 allele. M: 100bp DNA marker

However, intraperitoneal injections of tamoxifen induced only a partial knockout of PPASMC (see figure 4.9). First we assumed, that the tamoxifen injection protocol was not optimal. But neither an increase of the tamoxifen dosage nor of the injection frequency improved the efficiency. Therefore, we decided to induce the deletion of STIM1 and STIM2 exons in PPASMCs directly.

4.1.3 Analysis of SOCE and ROCE in STIM1/2, TRPC1/3/6 and quintuple knockout PPASMC.

Therefore, we treated the isolated cells with a lentivirus encoding for the Cre-recombinase to obtain a STIM1/2 knockout in the STIM1/2 floxed but Mhy11-Cre negative cells from STIM1/2 floxed mice. The lentivirus was produced as described in the methods sections. The mCherry-tagged Cre-recombinase plasmid was obtained from addgene

and used to produce recombinant lentiviruses expressing Cre-recombinase and the mCherry fluorescent protein in the infected cell. During Ca^{2+} imaging we were therefore able to select cells with red fluorescence as STIM1/2 knockout and cells without fluorescence as control cells (see figure 4.10B).
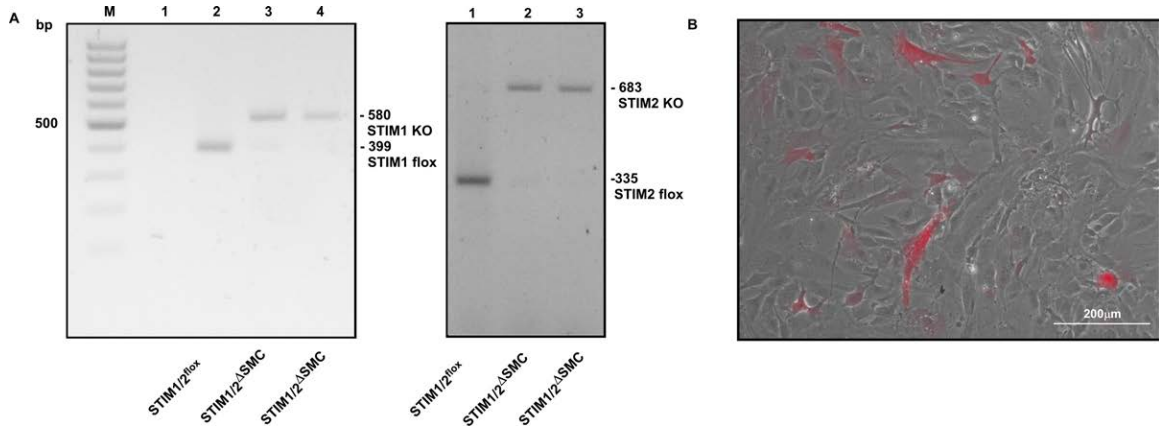
Figure 4.10: **Characterization of lentiviral transfected cells by PCR and fluorescence imaging.** A) Agarose gel electrophoresis of DNA fragments from PCR-genotyping of genomic DNAs from PPASMCs infected (STIM1/2$^{\Delta SMC}$) or not infected (STIM1/2^{flox}SMC) with lentiviruses expressing Cre recombinase. Left panel: products from a STIM1 genotyping PCR (lane 2 nontransfected, lane 3 and 4 transfected cells). Right panel: products from a STIM2 genotyping PCR (lane 1 nontransfected, lane 2 and 3 transfected cells). B) Transfection efficiency of mCherry tagged Cre-recombinase lentivirus 4 days after transfection of PPASMC. Transfected cells can be identified by their red fluorescence.

Unfortunately, we faced a very low transfection efficiency of approximately 5% with the mCherry-tagged Cre-recombinase virus. Accordingly, we were only able to measure a few cells per coverslip (see figure 4.10). When we had used Cre-recombinase adenoviruses for other experiments, we observed a similar low transfection efficiency in the GFP-tagged ad-Cre virus and a nearly complete transfection of cells with lentiviruses coding for the untagged Cre-recombinase.

Therefore, we assumed that loxP-mediated deletion with untagged Cre-recombinase lentivirus would be similarly complete as with an untagged Cre-recombinase adenovirus. As expected, the transfection with untagged Cre-recombinase lentiviruses resulted into an almost complete deletion of STIM1/2 exons (see figure 4.11) in PPASMC isolated from STIM1/2$^{flox/flox}$ mice.
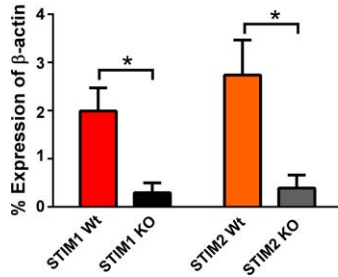
Figure 4.11: **Wt-STIM1- and STIM2-mRNA quantification after lentiviral expression of Cre-recombinase 4 days after infection (STIM1/2 KO) compared to uninfected PPASMC (STIM1/2 Wt) isolated from STIM1/2$^{\text{flox/flox}}$ mice.** n=3-5 mice, P values were determined by t test; * P<0.05

4.1.4 Contribution of TRPC1/3/6 in receptor- and store-operated Ca^{2+} entry (ROCE and SOCE)

We isolated PPASMC from STIM1/2$^{\text{flox/flox}}$ and STIM1/2$^{\text{flox/flox}}$/TRPC1/3/6 $^{-/-}$ mice, cultivated them until passage two and transfected the cells with untagged or mCherry-tagged Cre-recombinase lentivirus. Four days after transfection, loxP-induced deletion by Cre recombinase was complete as determined by quantitative, reverse, transcription (RT)-PCR. These cells were used as STIM1/2$^{\Delta\text{SMC}}$ (PPASMCs with deleted STIM1 and 2 genes) and STIM1/2$^{\Delta\text{SMC}}$/TRPC1/3/6 $^{-/-}$ PPASMC (PPASMC with deleted STIM1/2 and TRPC1/3/6 genes) for calcium imaging experiments. A G5A control virus was used to transfect wildtype PPASMCs. One day before the analysis, cells were split and seeded on glass cover slips. PPASMCs were loaded with the Ca^{2+} indicator Fura2-AM.

To quantify ROCE, infected cells with different genotypes were loaded with the Ca^{2+} indicator Fura2-AM and stimulated with 1 µM endothelin in HEPES solution containing 2mM Ca^{2+}. As expected, ROCE was unchanged in STIM1/2$^{\Delta\text{SMC}}$ compared to Wt cells when comparing the maximal ROCE at the indicated time point or quantifying enothelin1-induced ROCE areas under the curves (AUC). However, when STIM1/2$^{\Delta\text{SMC}}$ ROCE was compared to Wt cells at time points 4 or 4.5 min, a significant difference was observed in comparison to STIM1/2 flox cells. Therefore, STIM1/2 proteins by mediating Ca^{2+} influx through Orai channels may be important

for the long lasting ROCE.
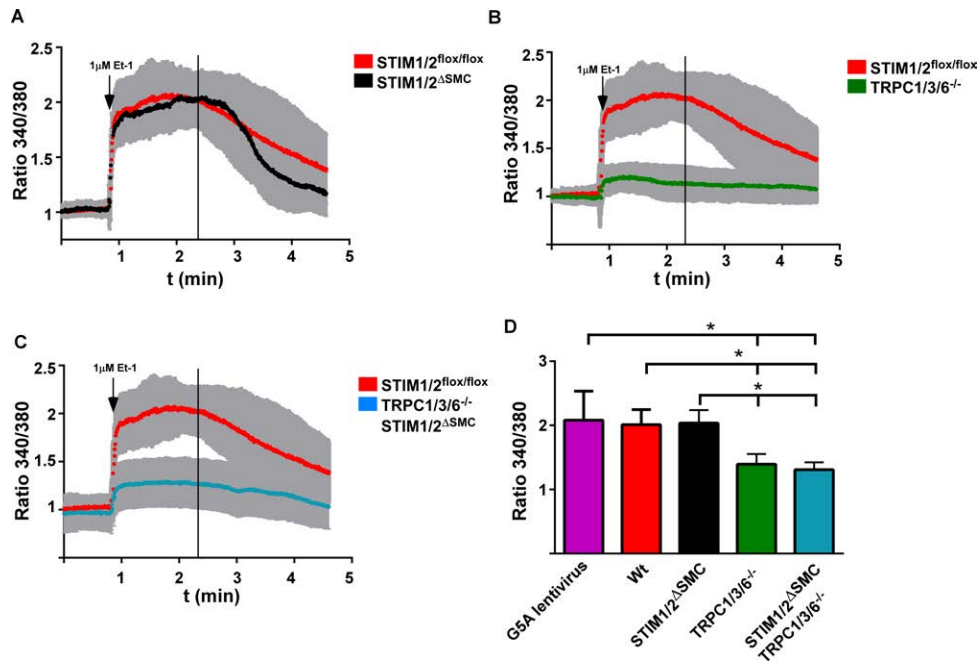
Figure 4.12: **Endothelin-1 induced ROCE in STIM1/2$^{\Delta\text{SMC}}$, TRPC1/3/6$^{-/-}$ and STIM1/2$^{\Delta\text{SMC}}$/TRPC1/3/6$^{-/-}$ PPASMC.** A) Endothelin-1 induced ROCE in STIM1/2$^{\Delta\text{SMC}}$ transfected with lentiviral Cre-recombinase compared to STIM1/2$^{\text{flox/flox}}$ PPASMC B) Endothelin-1 induced ROCE in TRPC1/3/6$^{-/-}$ PPASMC compared to STIM1/2$^{\text{flox/flox}}$ PPASMC C) Endothelin-1 induced ROCE in STIM1/2$^{\Delta\text{SMC}}$/TRPC1/3/6$^{-/-}$ transfected with lentiviral Cre-recombinase compared to STIM1/2$^{\text{flox/flox}}$ PPASMC D) Quantification of endothelin-1 induced ROCE of PPASMCs, 28-32cells from n=3-5mice, all cells were in passage 3 (G5A GFP-tagged control lentiviruses n=1, 8 cells) Kruks-Wallis test, Dunn's multiple comparison test * P<0.05

TRPC1/3/6$^{-/-}$ PPASMCs reduced significantly ROCE compared to Wt cells. STIM1/2$^{\Delta\text{SMC}}$/TRPC1/3/6$^{-/-}$ did not further reduce ROCE compared to TRPC1/3/6$^{-/-}$ PPASMCs. This result was obtained when quantifying both the maximum ROCE at the indicated time point (2.37 min) and the AUC of ROCE. The clearly reduced ROCE in TRPC1/3/6$^{-/-}$ KO PPASMCs matches our hypothesis that TRPCs are mainly receptor-operated (see figure 4.12).

After depletion of internal Ca^{2+} stores by $1\,\mu M$ thapsigargin in Ca^{2+}-free HEPES solution containing 2mM EGTA, extracellular Ca^{2+} solution was added to quantify the store-operated calcium influx. First of all, SOCE induced by adding thapsigargin (Tg) and recalcification was similar in wildtype cells transfected with G5A lentiviruses
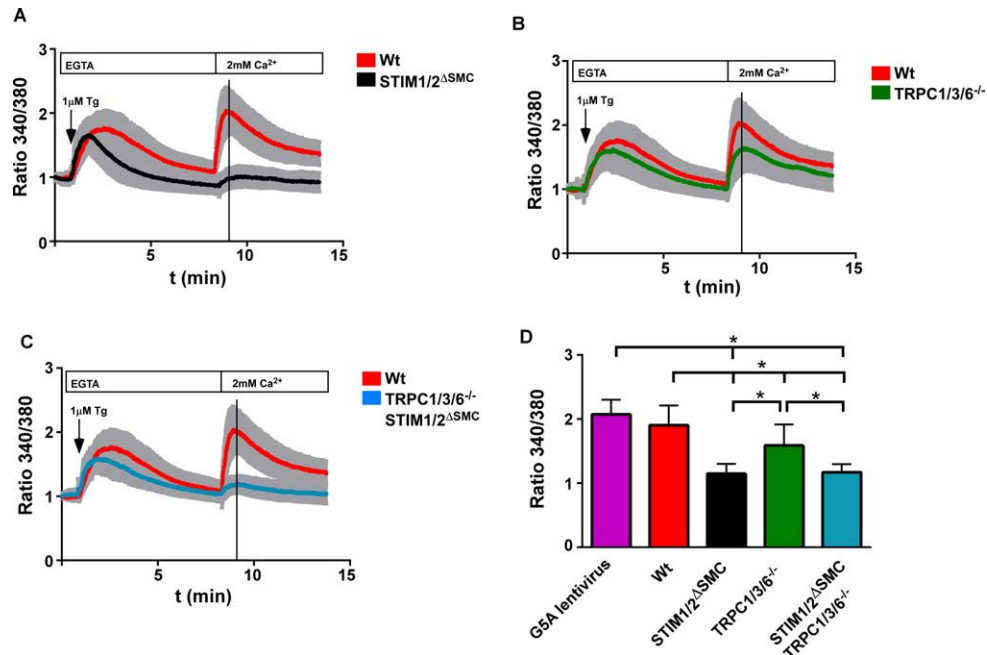
Figure 4.13: **Thapsigargin-induced store-operated Ca^{2+} entry (SOCE) in STIM1/2$^{\Delta SMC}$, TRPC1/3/6$^{-/-}$ and STIM1/2$^{\Delta SMC}$/TRPC1/3/6$^{-/-}$ PPASMC.** A) Thapsigargin-induced SOCE in STIM1/2$^{\Delta SMC}$ transfected with lentiviruses coding for Cre-recombinase compared to Wt non-transfected PPASMCs B) Thapsigargin-induced SOCE in TRPC1/3/6$^{-/-}$ PPASMC compared to Wt PPASMC C) Thapsigargin-induced SOCE in STIM1/2$^{\Delta SMC}$/TRPC1/3/6$^{-/-}$ transfected with lentiviruses coding for Cre-recombinase compared to Wt PPASMC D) Quantification of thapsigargin induced SOCE, mean of 29-48 cells from n=4-7 mice, all cells were in passage 3 (except for G5A GFP-tagged control lentiviruses transfected PPASMCs: 8 cells from 1 Wt mouse), Kruks-Wallis test, Dunn's multiple comparison test * P<0.05

and non-transfected wildtype cells indicating that lentiviral transfection itself does not have an impact on SOCE. As expected, SOCE was almost completely inhibited in STIM1/2$^{\Delta SMC}$ when the maximal SOCE was compared to wildtype SOCE at the time point indicated by a line (see figure 4.13). Quantification of the areas under the curves (AUC) of SOCE confirmed these results (see figure 4.14).

Moreover, we observed a small but significantly different reduction of SOCE in TRPC1/3/6$^{-/-}$ cells compared to wildtype PPASMC indicating a contribution of TRPC1/3/6 channels to SOCE. There was no significant different reduction in quintuple (STIM1/2$^{\Delta SMC}$/TRPC1/3/6$^{-/-}$) PPASMC identified as compared to STIM1/2$^{\Delta SMC}$ cells.
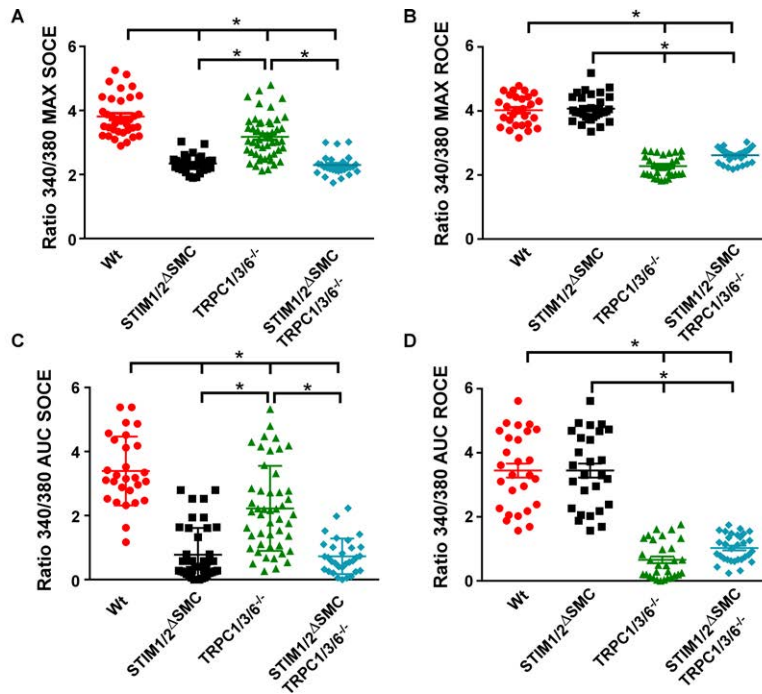
Figure 4.14: **Quantification of maxima and area under the curves for store-operated Ca^{2+} entry (SOCE) and receptor-operated Ca^{2+} entry (ROCE).**
A) Quantification of SOCE maxima displayed as scatter blot B) Quantification of ROCE maxima displayed as scatter blot C) Quantification of areas under the curves (AUC) for SOCE D) Quantification of areas under the curves (AUC) for ROCE, mean ± SEM of 28-48cells from 3-7mice, Kruks-Wallis test, Dunn's multiple comparison test P<0.05

4.2 Analysis of SOCE in endothelial cells and its contribution to vasodilatation, edema formation, proliferation and migration

4.2.1 Isolation and identification of Wt and STIM1/2/Orai1-deficient murine pulmonary microvascular endothelial cells (MPMVECs)

MPMVECs were isolated using CD-144 (VE-Cadherin5) antibody labeled magnetic dynabeads. The identity of endothelial cells was confirmed by Dil-Ac-LDL staining in passage 3 (see figure 4.15). Dil-Ac-LDL only stains endothelial cells and macrophages, but macrophages do not adhere to the culture dishes. There were still dynabeads attached to some MPMVECs at this passage which usually get lost during the following passages.
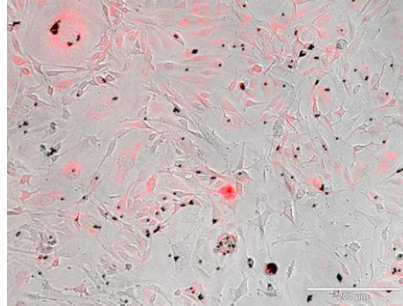
Figure 4.15: **Dil-Ac-LDL staining of MPMVECs.** Representative image of MP-MVECs isolated from Wt mice (passage 3) and stained with Dil-Ac-LDL

MPMVECs deficient of STIM1/2 and Orai proteins were isolated from STIM1/2$^{\Delta EC}$ and Orai1$^{\Delta EC}$ mice. For generation of the endothelial cell-specific knockout mice (ΔEC mice), floxed STIM1/2 and floxed Orai1 mice were bred with a mouse line carrying the Cre-recombinase gene under the control of the endothelium-specific cadherin 5 promoter. The knockout was confirmed by immunoblotting of protein lysates from MPMVECs. STIM1, STIM2 and Orai1 was markedly reduced in STIM1/2$^{\Delta EC}$ and Orai1$^{\Delta EC}$ MPMVEC (see figure 4.16).
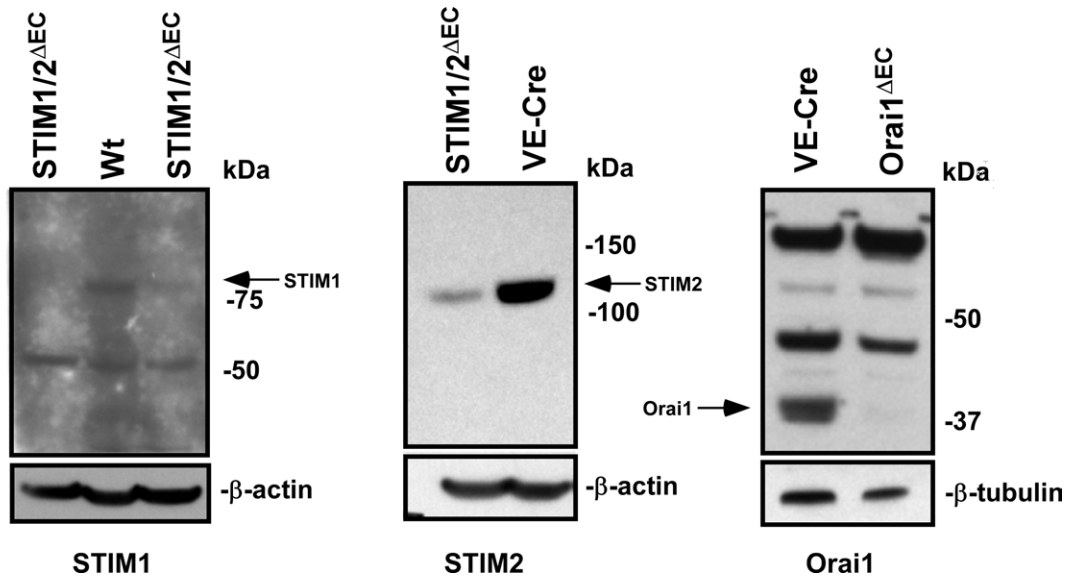
Figure 4.16: **Expression of STIM1, STIM2 and Orai1 in STIM1/2$^{\Delta EC}$ and Orai1$^{\Delta EC}$.** A) Representative Western Blots of protein lysates from STIM1/2$^{\Delta EC}$, Orai1$^{\Delta EC}$ and VE-Cre MPMVEC.
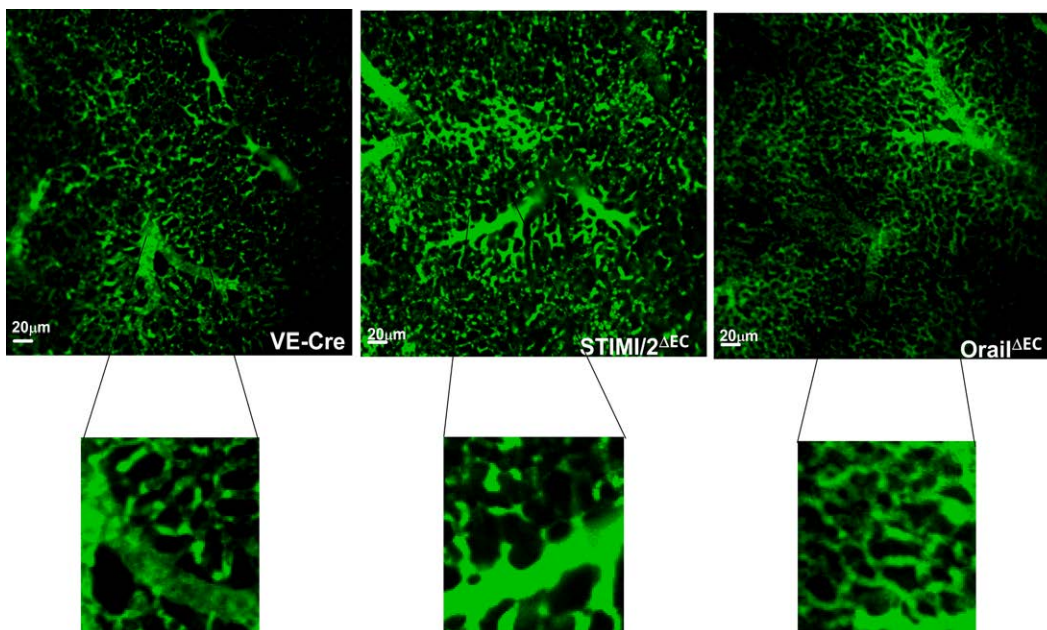
Figure 4.17: **Lungs of STIM1/2$^{\Delta EC}$ and Orai1$^{\Delta EC}$ mice injected with FITC-dextran.** Representative images of mice injected intraocularly with FITC-dextran. The fluorescent dye distributes in the vasculature and visualizes the pulmonary vessels in the ex-vivo lung.

Furthermore, the STIM1/2$^{\Delta EC}$ and Orai1$^{\Delta EC}$ knockout did not affect the pulmonary vascular distribution (see figure 4.17). STIM1/2$^{\Delta EC}$ and Orai1$^{\Delta EC}$ knockout mice

94

were injected intraocularly with 5% FITC-dextran. The fluorescent dye distributes in the vasculature and visualizes the pulmonary vessels in the ex-vivo lung when imaged at 488nm excitation with a Zeiss 710 META NLO 2-photon microscope. Lungs from STIM1/2$^{\Delta EC}$ and Orai1$^{\Delta EC}$ mice did not show any morphological differences compared to lungs from VE-Cre mice (see figure 4.17).

4.2.2 Contribution of SOCE to endothelium-induced vasodilatation

We used thoraic aortic rings as a model for vasoconstriction and -dilatation. Previous authors have already shown that aortic rings isolated from STIM1$^{\Delta EC}$ mice treated with acetylcholine dilatated significantly less than heterozygous STIM1$^{\Delta EC}$ and wild-type aortic rings [61]. Consequently, we hypothesized that an endothelial STIM1/2 double knockout would result even in a stronger impaired vasodilatation than a single endothelial STIM1 knockout.
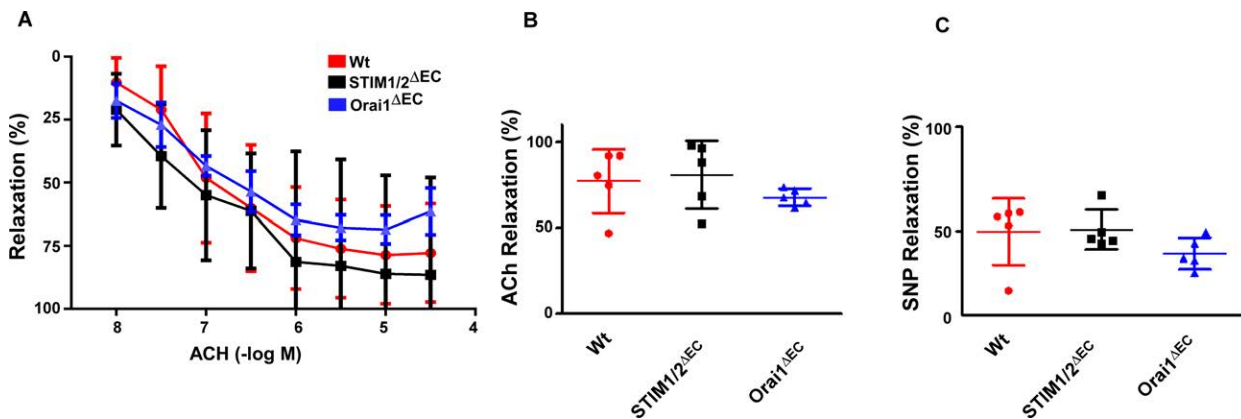
Figure 4.18: **Relaxation of STIM1/2$^{\Delta EC}$ and Orai1$^{\Delta EC}$ aortic rings.** A) Aortic rings were treated with 1 µM phenylephrine. At steady maximal contraction increasing concentrations of ACh (0.01 µM-30 µM) were added B) Quantification of ACh-induced (1 µM) relaxation C) Quantification SNP-induced (3 µM) relaxation, ACh: acetylcholine, SNP: sodium nitroprusside, n=5 mice, P values were determined by unpaired t-test

Accordingly, we mounted aortic rings of STIM1/2$^{\Delta EC}$ and Orai1$^{\Delta EC}$ mice in a wire myograph and treated them with cumulative concentrations of acetylcholine (ACh)

and sodium nitroprusside (SNP). The resulting vasodilatation however, was not different from Wt mice after ACh or SNP addition (see figure 4.18).

4.2.3   SOCE in endothelial migration and proliferation

Migrating endothelial cells have been shown to have lower intracellular Ca^{2+} levels. Bovine aortic endothelial cells treated with SERCA-inhibitors have been reported to migrate less and removal of cyclopiazonic acid 6hs after scratch formation rescued migration measured after 24hs [15].

Consequently, we hypothesized that the migration of STIM1/2$^{\Delta EC}$ and Orai1$^{\Delta EC}$ would be reduced compared to VE-Cre MPMVECs. According to our expectations, the wound healing was significantly reduced in STIM1/2$^{\Delta EC}$ and Orai1$^{\Delta EC}$ 24hs and 48hs after gap formation (see figure 4.19).

Superoxide is produced during oxygen reduction by NOX proteins [5] and NOX-mediated superoxide production stimulates migration in vascular endothelial cells [136]. Gandhirajan et al. has demonstrated that cytosolic superoxide production and NOX levels were unaltered in STIM1$^{\Delta EC}$ but Szewczyk et al. showed that a dysfunctional eNOS, which is affected by Ca^{2+}, produces superoxide instead of NO [127] [38].

Therefore, we speculated that a reduced SOCE would negatively affect NO production and ROS levels. As a result superoxide and eNOS levels would be altered in STIM1/2$^{\Delta EC}$ and Orai1$^{\Delta EC}$. Even though we measured reduced phosphorylated eNOS protein levels in STIM1/2$^{\Delta EC}$ and Orai1$^{\Delta EC}$ lysates in some Western blots, high background did not allow a reliable quantification.

To analyze if superoxide levels were altered in STIM1/2$^{\Delta EC}$ and Orai1$^{\Delta EC}$, we stained MPMVECs with MitoSox red and quantified the intensity of mitochondria. Surprisingly, STIM1/2$^{\Delta EC}$ and Orai1$^{\Delta EC}$ demonstrated significantly elevated superoxide levels compared to mitochondria from VE-Cre mice (see figure 4.20).

We assumed that similar to migration, proliferation of endothelial cells requires SOCE. Therefore, we investigated if the proliferation of endothelial cells was reduced in STIM1/2 and Orai1 deficient MPMVECs isolated from endothelial cell-specific
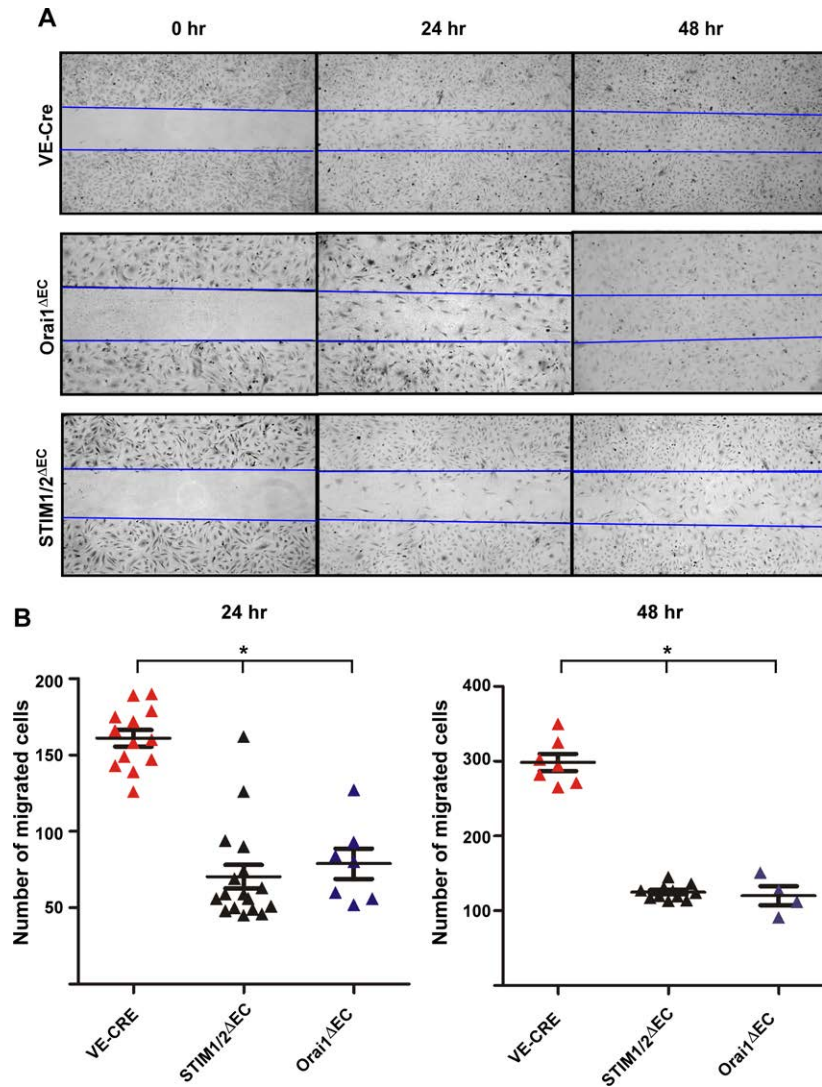
Figure 4.19: **Migration of STIM1/2$^{\Delta\text{EC}}$ and Orai1$^{\Delta\text{EC}}$ after gap formation.**
A) Representative images of VE-Cre (control), STIM1/2$^{\Delta\text{EC}}$ and Orai1$^{\Delta\text{EC}}$ endothelial cells 24hs and 48hs after gap formation B) Quantification of migrated cells, n=3-5 independent experiments, P values were determined by t test; * P<0.05

knockout mice. The proliferation rate was assessed using carboxyfluorescein succinimidyl ester (CFSE), a dye which is incorporated into proteins, passed to the daughter generations and can be quantified by flow cytometry. We identified a reduced proliferation rate in STIM1/2$^{\Delta\text{EC}}$ and unchanged proliferation rate in Orai1$^{\Delta\text{EC}}$ (see figure 4.21).

Figure 4.20: **Mitochondrial superoxide levels in STIM1/2$^{\Delta EC}$ and Orai1$^{\Delta EC}$.**
A) Representative images of MitoSOX red (mitochondrial superoxide indicator)
stained VE-Cre (control), STIM1/2$^{\Delta EC}$ and Orai1$^{\Delta EC}$ MPMVECs B) Quantification of MitoSOX red fluorescence intensity, n=3 independent experiments, n= 62-102
cells, f.a.u.: fluorescence arbitrary units, P values were determined by rank sum test;
* P<0.05.

4.2.4   Contribution of SOCE to edema formation and vascular inflammation

Endothelial cells play an important role during inflammation. Bacterial products like
lipopolysaccharide (LPS) stimulate the endothelium and increase endothelial barrier
permeability. On one hand this cellular reaction helps to combat infection, on the
other hand it can induce a dysfunction of endothelial cells. Dysfunctional endothelial
cells allow fluid to leak into the surrounding tissues which results into lung edema
formation [99] [116]. Vascular permeability of endothelial cells can be investigated
on cellular levels using the coagulation protease thrombin. Under non-stimulated
conditions, the myosin light chain (MLC) phosphatase dephosphorylates the MLC
and consequently prevents opening of the tight junctions. After thrombin stimulation
this preventive mechanism is inhibited [99].

Thrombin stimulation induces stress fiber formation which can be quantified by staining of F-actin with fluorescence labeled phalloidin. We show that the relative phalloidin staining intensity of thrombin-stimulated STIM1$^{+/-}$/Orai1$^{+/-}$ MPMVECs was

Figure 4.21: **Proliferation in STIM1/2$^{\Delta \mathbf{EC}}$ and Orai1$^{\Delta \mathbf{EC}}$.** A) Representative FACS panels of non-proliferated (red) and proliferated (blue) CFSE-stained VE-Cre, STIM1/2$^{\Delta \mathrm{EC}}$ and Orai1$^{\Delta \mathrm{EC}}$ B) Relative proliferation rates of proliferating endothelial cells to non-proliferating cells of the same genotype, CFSE = carboxyfluorescein succinimidyl ester, n=3 independent experiments, P values were determined by one-way ANOVA; * P<0.05.

reduced compared to thrombin-stimulated wildtype MPMVECs (see figure 4.22). Gandhirajan et al. have shown that STIM1 is essential for the NFATc3-mediated transcription of proinflammatory mediators. STIM1$^{\Delta \mathrm{EC}}$ transfected with adenovirus encoding NFATc3-GFP displayed a significantly reduced number of NFATc3-GFP translocated cells compared to wildtype MPMVECs. This was further confirmed by the significantly reduced luciferase activity in STIM1$^{\mathrm{KD}}$ MPMVECs compared to wildtype MPMVECs [39]. Based on these findings the question arose if only STIM1 or both STIM isoforms, STIM1 and STIM2, or Orai attenuate the NFAT nuclear translocation. Thus, MPMVECs were transfected with adenovirus encoding NFATc3-GFP for 36 hours, followed by LPS treatment for additional 16hs as described in [39]. According to our expectations, the number of NFATc3-GFP translocated cells in LPS-

Figure 4.22: **Thrombin-induced formation of stress fibers.** A) Representative images of phalloidin staining for Wt (left) and STIM1$^{+/-}$/Orai1$^{+/-}$ (right) MPMVECs B) Quantification of phalloidin staining intensity of actin stress fibers after thrombin (5nM) stimulation of STIM1$^{+/-}$/Orai1$^{+/-}$ and Wt MPMVECs in comparison to unstimulated cells of the same genotype, 80-87 cells isolated from 4 different mice, P values were determined by t test; * P<0.05

stimulated VE-Cre MPMVECs compared to unstimulated MPMVECs was increased and this increase was abrogated in LPS-stimulated STIM1/2$^{\Delta EC}$ compared to unstimulated STIM1/2$^{\Delta EC}$ and in LPS-stimulated Orai1$^{\Delta EC}$ compared to unstimulated Orai1$^{\Delta EC}$. The number of NFATc3-GFP translocated cells was moreover significantly reduced in LPS-stimulated STIM1/2$^{\Delta EC}$ compared to LPS-stimulated VE-Cre MPMVECs (see figure 4.23). Comparing our result to Gandhirajan et al. we did not observe a different number of NFATc3-GFP translocated cells in double STIM1/2$^{\Delta EC}$ or Orai1$^{\Delta EC}$ compared to the single STIM1$^{\Delta EC}$ analyzed in [39].
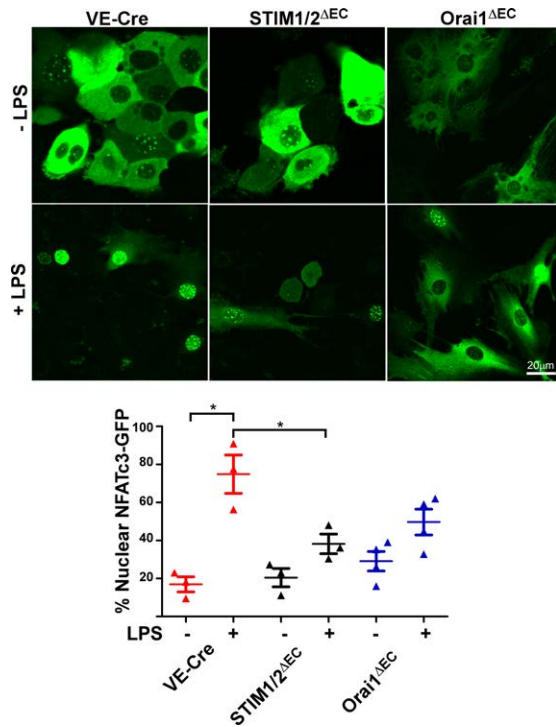
Figure 4.23: **LPS-induced nuclear NFATc3-GFP translocation in STIM1/2$^{\Delta EC}$ and Orai1$^{\Delta EC}$.** A) Representative images of nuclear NFATc3-GFP translocation of VE-Cre, STIM1/2$^{\Delta EC}$ and Orai1$^{\Delta EC}$ MPMVECs with and without pretreatment of LPS B) Quantification of cells with translocated NFATc3 to the nuclei. n=3 independent experiments, P values were determined by t test; * P<0.05

4.3 Contribution of mitochondrial uniporter regulator 1 (MCUR1) to Ca²⁺ uptake in mitochondria

4.3.1 Analysis of mitochondrial Ca²⁺ uptake and $\Delta\Psi_m$ in MCUR1$^{\Delta EC}$ and MCU$^{\Delta EC}$

MCUR1 was identified as a positive regulator of the MCU complex through its interaction with MCU [81]. Our group was recently able to characterize MCUR1 as a MCU complex scaffold factor. MCUR1 and MCU interact via their highly conserved coiled-coil domains. A lack of MCUR1 resulted into the failure of MCU heterooligomeric complex assembly and suppressed the I_{MCU} current in isolated cardiac mitoplasts [132]. The functional role of MCUR1 during mitochondrial Ca²⁺ entry, its impact on the $\Delta\Psi_m$ and on the mitochondrial bioenergetics however has not been investigated yet in primary cells.

Figure 4.24: **Deletion of MCUR1 and MCU in MPMVEC.** A) MCU and B) MCUR1 Wt-mRNA (left panels) and protein levels (Western Blots and right panels) in MPMVECs isolated from VE-Cre, MCUR1$^{\Delta EC}$ and MCU$^{\Delta EC}$ mice, n=3, P values were determined by t test; * P<0.05

To investigate the functional role of MCUR1, our group recently created MCUR1$^{\Delta EC}$ mice. Even though these mice did not have any morphological phenotype, they had a higher heat production at rest than MCUR1 floxed mice. The knockout of MCU and MCUR1 in MPMVECs isolated from MCU$^{\Delta EC}$ and MCUR1$^{\Delta EC}$ mice was confirmed by mRNA and protein analysis (see figure 4.24).

Figure 4.25: **Mitochondrial membrane potential** ($\Delta\Psi_m$) **in MCUR1**$^{\Delta EC}$**, VE-Cre MPMVECs, MCUR1**$^{\Delta MLF}$ **or MCU**$^{\Delta MLF}$**.** Murine lung fibroblasts (MLF) were isolated from MCUR1$^{\Delta EC}$ or MCU$^{\Delta EC}$ mice and transfected with adenoviruses encoding Cre-recombinase-GFP (MCUR1$^{\Delta MLF}$ and MCU$^{\Delta MLF}$). Cells were loaded with tetramethylrhodamine methyl ester (TMRM) (50 nM) to assess the $\Delta\Psi_m$. Representative confocal images (A) and quantification of $\Delta\Psi_m$ (B)

Mitochondrial Ca^{2+} influx is driven by the electrochemical potential gradient. The potential is maintained by the process of mitochondrial respiration and the Na^+-Ca^{2+} exchanger [31]. Because the mitochondrial Ca^{2+} uptake is dependent on the $\Delta\Psi_m$, we investigated if the $\Delta\Psi_m$ was physiological in MCU$^{\Delta EC}$ and MCUR1$^{\Delta EC}$.
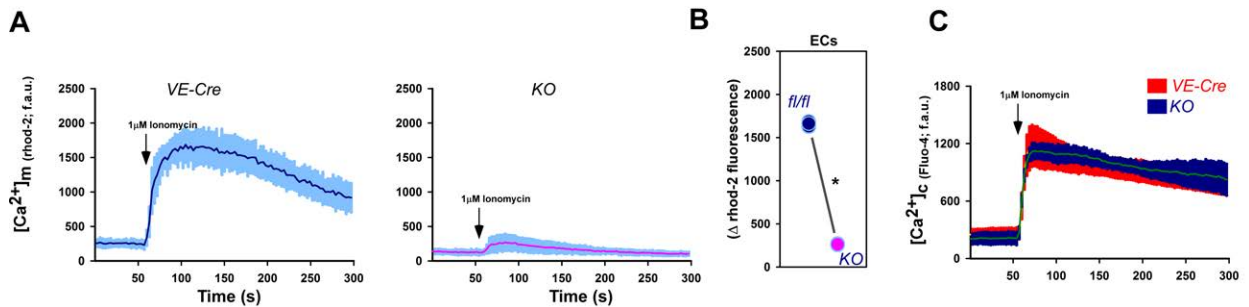
Figure 4.26: **MCU-dependent mitochondrial** Ca^{2+} **(**$[Ca^{2+}]_m$**) entry in MCUR1**$^{\Delta EC}$**.** A) Ionomycin-induced (1 μM) $[Ca^{2+}]_m$-entry in VE-Cre MPMVECs (left) and MCUR1$^{\Delta EC}$ (right) loaded with the mitochondrial Ca^{2+} indicator Rho2/AM B) Quantification of $[Ca^{2+}]_m$-entry C) Cytosolic Ca^{2+} ($[Ca^{2+}]_c$) entry in VE-Cre MPMVECs (red) and MCUR1$^{\Delta EC}$ (blue) loaded with the cytosolic Ca^{2+} indicator Fluo-4/AM, n=3 independent experiments, P values were determined by one-way ANOVA, *P < 0.05.

Neither in MLFs nor in MPMVECs isolated from MCU$^{\Delta EC}$ and MCUR1$^{\Delta EC}$ mice the $\Delta\Psi_m$ was altered compared to cells from floxed or VE-Cre mice. MPMVECs or adeno-Cre-GFP viruses transfected MLFs were stained with tetramethylrhodamine methyl

ester (TMRM) and fluorescence intensities of the mitochondrial $\Delta\Psi_m$ indicator was quantified (see figure 4.25).
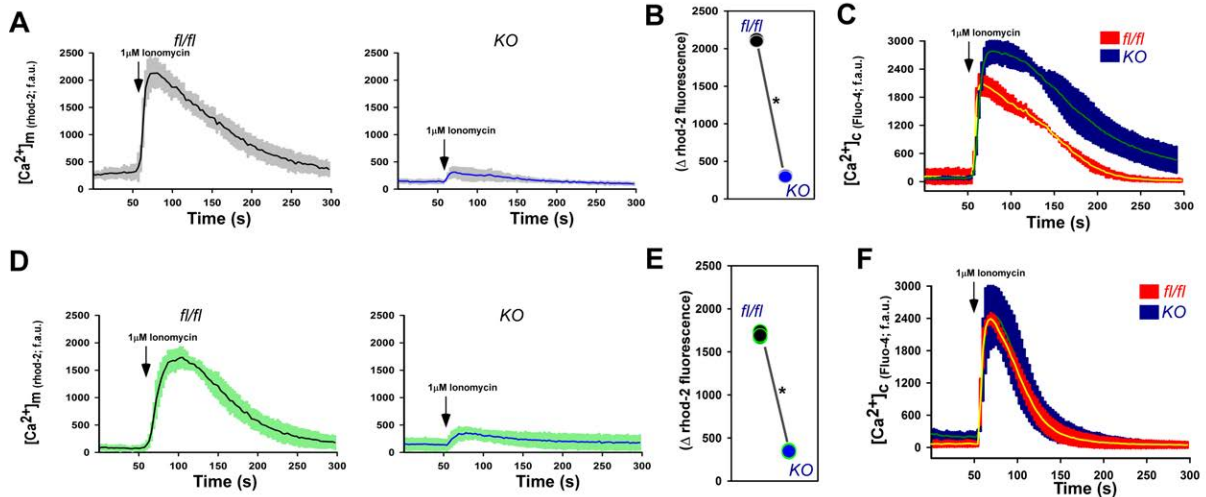
Figure 4.27: **MCU-dependent mitochondrial Ca²⁺ ($[Ca^{2+}]_m$) entry in MCUR1$^{\Delta MLF}$ and MCU$^{\Delta MLF}$.** A/D) Ionomycin-induced (1 µM) $[Ca^{2+}]_m$-entry in murine lung fibroblasts (MLF) isolated from MCUR1$^{\Delta EC}$ or MCU$^{\Delta EC}$ mice and transfected with adenoviruses encoding Cre-recombinase (A:MCUR1$^{\Delta MLF}$ and D:MCU$^{\Delta MLF}$ right panel, non-transfected MLFs left panel) were loaded with Rho2/AM. B/E) Quantification of $[Ca^{2+}]_m$-entry. Cytosolic Ca²⁺ ($[Ca^{2+}]_c$) entry in MCUR1$^{\Delta MLF}$ (C) and MCU$^{\Delta MLF}$ (F) loaded with Fluo-4/AM, n=3 independent experiments, The P values were determined by one-way ANOVA, *P < 0.05.

After having confirmed that the $\Delta\Psi_m$ was unaltered in MCU$^{\Delta EC}$ and MCUR1$^{\Delta EC}$, we next analyzed if the knockout resulted into a functional Ca²⁺ entry defect. MPMVECs or MLFs transfected with adenoviruses encoding Cre-recombinase (MCUR1$^{\Delta MLF}$ and MCU$^{\Delta MLF}$) were grown on glass cover slips and loaded with the cytosolic Ca²⁺ indicator Fluo-4AM and the mitochondrial Ca²⁺ indicator Rhod-2AM. The Ca²⁺ entry was observed after ionomycin stimulation under a Zeiss LSM510 META microscope. As expected, only a nominal mitochondrial Ca²⁺ uptake was observed in MCUR1$^{\Delta EC}$, MCUR1$^{\Delta MLF}$ and MCU$^{\Delta MLF}$. The extracellular Ca²⁺ entry into the cytosol was unchanged from VE-Cre MPMVECs or floxed MLFs (see figure 4.26 and 4.27). Imaging techniques allow the analysis of only a small population of selected cells per coverslip. Furthermore, a simultaneous recording of time-dependent Ca²⁺ uptake and $\Delta\Psi_m$ is not possible. Consequently, we used a multiwavelength excitation,

dual-wavelength emission fluorimeter for further analysis. This fluorimeter allows the analysis of 10^6 cells per sample compared to 10 cells per coverslip with imaging techniques. The cell membrane MPMVECs was permeabilized with digitonin. Thapsigargin, to block the SERCA pump, the mitochondrial substrate succinate and the intracellular Ca^{2+} indicator Fura-2FF were added. After baseline recording, the $\Delta\Psi_m$ indicator JC-1 was applied. Simultaneously, the excitation ratio of Fura-2FF and JC-1 were measured quantifying the intracellular Ca^{2+} concentration and the $\Delta\Psi_m$. The mitochondrial Ca^{2+} uptake is indicated indirectly by a decrease of the intracellular Ca^{2+} concentration. Because $\Delta\Psi_m$ affects the mitochondrial Ca^{2+} uptake, Ca^{2+} can be added to the cells until the $\Delta\Psi_m$ is disrupted.
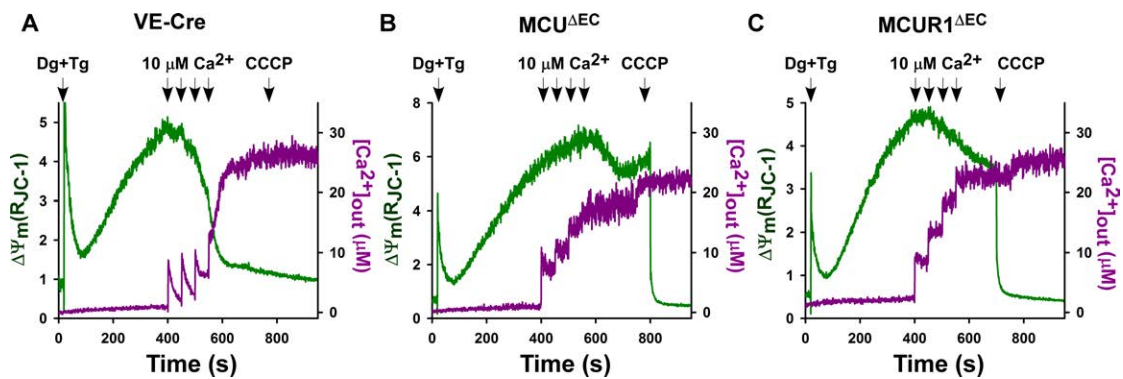
Figure 4.28: **Simultaneous measurement of MCU-mediated $[Ca^{2+}]_m$ uptake and $\Delta\Psi_m$ in VE-Cre, MCU$^{\Delta EC}$ and MCUR1$^{\Delta EC}$ MPMVECs.** After reaching steady state $\Delta\Psi_m$, permeabilized VE-Cre, MCU$^{\Delta EC}$ and MCUR1$^{\Delta EC}$ MPMVECs were treated in intracellular like media (containing $2\,\mu M$ thapsigargin and $1\,\mu M$ bath Ca^{2+} indicator Fura2FF) with series of extramitochondrial Ca^{2+} ($10\,\mu M$) pulses before the addition of mitochondrial uncoupler CCCP ($2\,\mu M$), purple: $[Ca^{2+}]_{out}$ indicated by Fura2FF, green: $\Delta\Psi_m(R_{JC-1})$ indicated by JC-1, CCCP: carbonyl cyanide m-chorophenylhydrazone, representative traces

Mitochondrial Ca^{2+} uptake capacity was evaluated in MCU$^{\Delta EC}$, MCUR1$^{\Delta EC}$ and VE-Cre MPMVECs by adding $10\,\mu M$ Ca^{2+} pulses. The simultaneous recording of $[Ca^{2+}]_m$ uptake and $\Delta\Psi_m$ discovered that both MCU$^{\Delta EC}$ and MCUR1$^{\Delta EC}$ failed to take up Ca^{2+} (see figure 4.29 and 4.28). Upon exposure to excessive Ca^{2+}, the VE-Cre cells exhibited a rapid mitochondrial membrane potential collapse due to mitochondrial Ca^{2+} entry, which was not observed in MCU$^{\Delta EC}$ and MCUR1$^{\Delta EC}$ MPMVECs (see figure 4.29).

105
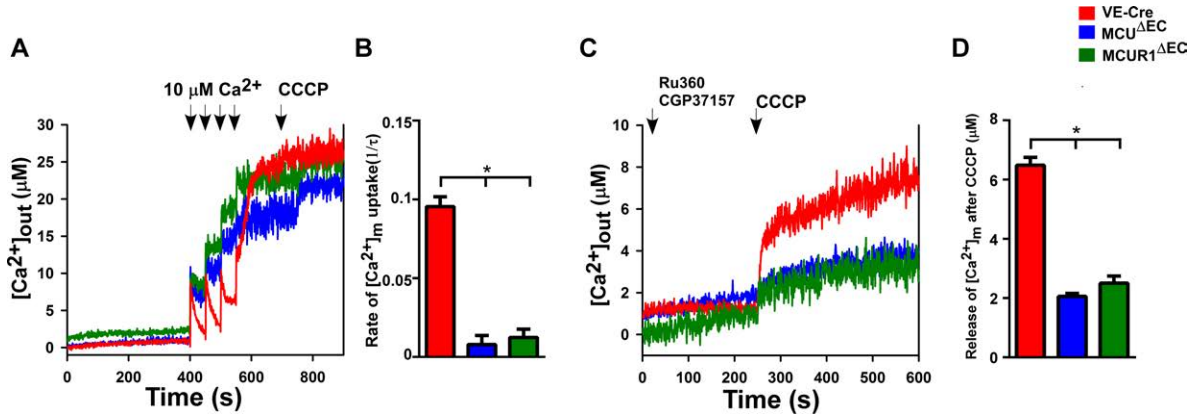
Figure 4.29: **MCU-mediated mitochondrial Ca^{2+} ([Ca^{2+}]$_m$) uptake in MCU$^{\Delta EC}$ and MCUR1$^{\Delta EC}$ MPMVECs.** A) Comparison of representative traces of extramitochondrial Ca^{2+} ([Ca^{2+}]$_{out}$) of VE-Cre MPMVECs, MCU$^{\Delta EC}$ and MCUR1$^{\Delta EC}$ MPMVECs. B) Quantification of rate of mitochondrial Ca^{2+} uptake ([Ca^{2+}]$_m$) before addition of mitochondrial uncoupler CCCP (2 µM) C) Representative traces of [Ca^{2+}]$_{out}$ of MPMVECs in the presence of SERCA inhibitor thapsigargin (2 µM), Na$^+$/Ca^{2+} exchanger inhibitor (CGP-37157, 1 µM) and MCU inhibitor (Ru360, 1 µM). After addition of CCCP, free [Ca^{2+}]$_m$ was released from the mitochondrial matrix and quantified (D). CCCP: carbonyl cyanide m-chorophenylhydrazone, n=3 independent experiments, The P values were determined by one-way ANOVA, *P < 0.05.

To examine baseline [Ca^{2+}]$_m$ content, permeabilized MPMVECs were loaded with Fura-2FF, SERCA inhibitor thapsigargin (2 µM), Na$^+$/Ca^{2+} exchanger inhibitor (CGP-37157, 1 µM) and MCU inhibitor (Ru360, 1 µM) to block all Ca^{2+} flux. CCCP was injected to dissipate $\Delta\Psi_m$ and free [Ca^{2+}]$_m$ was released from the mitochondrial matrix and quantified. Quantification demonstrated a reduced [Ca^{2+}]$_m$ release after addition of CCCP in MCU$^{\Delta EC}$ and MCUR1$^{\Delta EC}$ (see figure 4.28).

4.3.2 Contribution of MCU and MCUR1 to the mitochondrial respiratory chain and ATP production

Mitochondrial Ca^{2+} regulates metabolic functions, such as ATP production by oxidative phosphorylation. ATP production is either stimulated directly by Ca^{2+} or indirectly by NADH, activation of the pyruvate dehydrogenase, enhanced respiratory chain complex activity or Ψ_m [106] [130] [146]. A perturbed [Ca^{2+}]$_m$ uptake may lead to cellular bioenergetic crisis [85] [120].
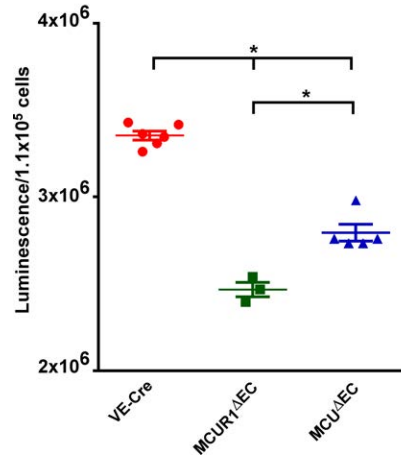
Figure 4.30: **ATP levels in MCUR1$^{\Delta \textbf{EC}}$, MCU$^{\Delta \textbf{EC}}$**. Normalized ATP luminescence of MCUR1$^{\Delta EC}$, MCU$^{\Delta EC}$ and VE-Cre MPMVECs, n=3-6, P values were determined by one-way ANOVA; *P<0.05.

To determine if the reduced mitochondrial Ca^{2+} uptake decreases ATP production, we measured ATP levels of MPMVECs derived from MCUR1$^{\Delta EC}$ and MCU$^{\Delta EC}$ mice. As expected basal ATP levels were significantly reduced in MCUR1$^{\Delta EC}$ and MCU$^{\Delta EC}$ endothelial cells (see figure 4.30). ATP levels were reduced significantly more in MCUR1$^{\Delta EC}$ compared to MCU$^{\Delta EC}$ MPMVECs (see figure 4.30).

We next analyzed if reduced ATP levels are the result of decreased mitochondrial Ca^{2+} levels or of an impaired function of respiratory chain complexes. The activity of the respiratory chain complexes was investigated by measuring the oxygen consumption rate (OCR). The reduction of oxygen to water by complex IV consumes electrons which are transferred by complex I, II and III. Addition of substrates of individual complexes, enhances specific complex activity, electron flow increases and therefore the oxygen consumption rate of the final electron acceptor complex IV increases. The current measured by the Clark electrode is correlated to the oxygen consumed [141] [153]. Ca^{2+} enhances the activity of the mitochondrial complexes I, III and IV and the pyruvate dehydrogenase activity which provides NADH from the TCA cycle to oxidative phosphorylation, is Ca^{2+} dependent [106] [130] [146] [93]. Therefore, we proposed that the OCR might be reduced in MCUR1$^{\Delta EC}$ and MCU$^{\Delta EC}$ MPMVECs. In contrast to MCU$^{\Delta EC}$, MCUR1$^{\Delta EC}$ did not result in a significant increase of the oxygen consumption rate levels after addition of complex 1 and 2 substrates. After
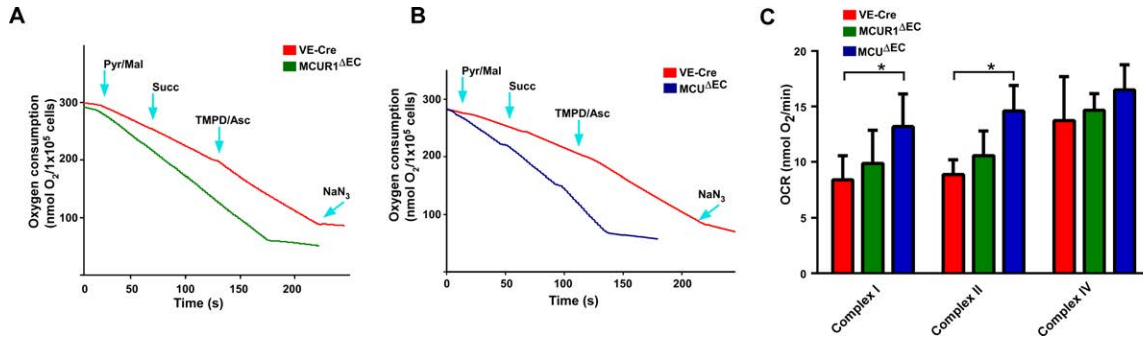
Figure 4.31: **Complex I, II and IV activity in MCUR1$^{\Delta \mathbf{EC}}$ and MCU$^{\Delta \mathbf{EC}}$ analyzed by Clark electrode.** Oxygen consumption rate (OCR) in digitonin-permeabilized MCUR1$^{\Delta EC}$, MCU$^{\Delta EC}$ and VE-Cre MPMVECs after addition of pyruvate, maleate, succinate, TMPD (tetramethylphenylendiamine), ascorbate and sodium azide. A/B) representative traces of MCUR1$^{\Delta EC}$ (A) and MCU$^{\Delta EC}$ (B) C) Quantification of OCR, n= 3, Mann-Whitney test; *P<0.05

application of complex IV substrates, TMPD and ascorbate, the OCR levels between VE-Cre, MCU$^{\Delta EC}$ and MCUR1$^{\Delta EC}$ remained the same (see figure 4.31). This result indicates that the function of complex I, II and IV is not impaired in MCU$^{\Delta EC}$ and MCUR1$^{\Delta EC}$. The observed enhanced complex I and II activity in MCU$^{\Delta EC}$ needs further investigation. Protein levels of the mitochondrial oxidative phosphorylation components indicates that all components were equally expressed in MCUR1$^{\Delta EC}$, MCU$^{\Delta EC}$ and VE-Cre MPMVECs (see figure 4.32).

To further investigate the function of the respiratory chain in MCU$^{\Delta EC}$ and MCUR1$^{\Delta EC}$, we analyzed MPMVECs with the XF-96 Extracellular Flux Analyzer^{Tm} quantifying oxygen consumption rates (OCR) and extracellular acidification rate (ECAR) in adherent, permeabilized cells before and after adding drugs which inhibit or accelerate oxidative phosphorylation or glycolysis. The basal OCR values were similar in MCU$^{\Delta EC}$, MCUR1$^{\Delta EC}$ and VE-Cre MPMVECs. Similarly, we observed that oxygen consumption of MCUR1$^{\Delta EC}$ mice were not different from control mice under a normal chow diet at 8 weeks [132].

After addition of oligomycin blocking ATP-synthase, the remaining OCR is due to proton leakage and therefore caused by uncoupling. Because oligomycin blocks the ATP synthesis during oxidative phosphorylation, the cell shifts its ATP production to glycolysis [113] [10]. After addition of oligomycin we did not observe any difference in
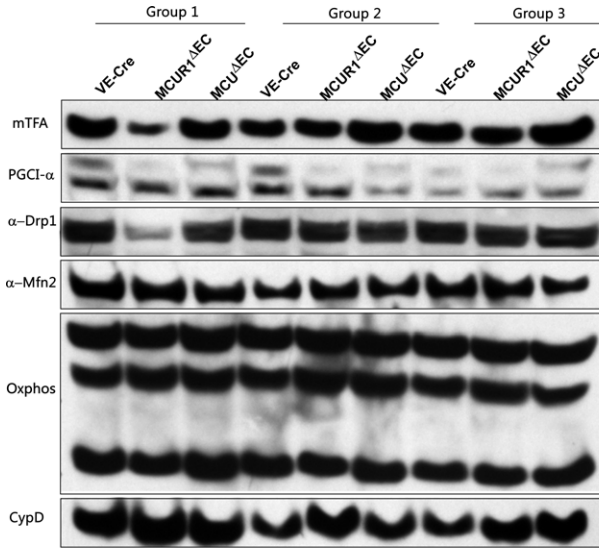
Figure 4.32: **Expression of mitochondrial oxidative phosphorylation complex components in MCUR1$^{\Delta \text{EC}}$ and MCU$^{\Delta \text{EC}}$.** Western Blot analysis of cell lysates from MCUR1$^{\Delta \text{EC}}$, MCU$^{\Delta \text{EC}}$ and VE-Cre MPMVECs probed for anti-mTFA (Mitochondrial Transcription Factor A), PGC1 (Peroxisome proliferator-activated receptor gamma coactivator), Drp1 (Dynamin-related protein), Mfn2 (Mitofusin-2), OXPHOS (antibody cocktail showing complex II-30kDa, complex IV subunit I and complex V α subunit) and CypD (Cyclophilin D), lysates of cells isolated from 3 different mice

the OCR values in MCU$^{\Delta \text{EC}}$, MCUR1$^{\Delta \text{EC}}$ compared to VE-Cre MPMVECs (see figure 4.33) indicating that protons are pumped during electron transport which results in oxygen consumption but not ATP production in MCU$^{\Delta \text{EC}}$ and MCUR1$^{\Delta \text{EC}}$. The unaltered ATP-linked OCR values in MCU$^{\Delta \text{EC}}$ and MCUR1$^{\Delta \text{EC}}$ further illustrates that ATP demand and substrate availability is intact in MCU$^{\Delta \text{EC}}$ and MCUR1$^{\Delta \text{EC}}$. FCCP (carbonyl cyanide-4-(trifluoromethoxy)phenylhydrazone) uncouples respiration from oxidative phosphorylation and therefore allows H$^+$ to diffuse back to the matrix without passing the ATP synthase which induces a collapse of $\Delta \Psi_m$. In an attempt to rescue the $\Delta \Psi_m$ OCR rises and the cell switches its metabolism from oxidative phosphorylation to glycolysis. As a result, any substrate available in the medium is oxidized and contributes to the maximal respiration rate [113] [10]. The values for the 'maximal respiration rate' were increased in MCUR1$^{\Delta \text{EC}}$ and MCU$^{\Delta \text{EC}}$ compared to VE-Cre MPMVEC (see figure 4.33) and were significantly higher in MCUR1$^{\Delta \text{EC}}$

Figure 4.33: **Oxygen consumption rate in MCUR1$^{\Delta\mathbf{EC}}$ and MCU$^{\Delta\mathbf{EC}}$ using the XF-96 Extracellular Flux Analyzer$^{\mathbf{Tm}}$.** A) Representative traces for oxygen consumption rate (OCR) after addition of oligomycin, FCCP, rotenone and antimycin in MCUR1$^{\Delta\mathrm{EC}}$, MCU$^{\Delta\mathrm{EC}}$ and VE-Cre MPMVECs B) Basal OCR values before addition of oligomycin subtracted of non-mitochondrial respiration values C) 'Maximal respiration values' after addition of FCCP subtracted of non-mitochondrial respiration values, FCCP: carbonyl cyanide-4-(trifluoromethoxy)phenylhydrazone, representative experiment from n=3, one-way ANOVA, *P<0.05

compared to MCU$^{\Delta\mathrm{EC}}$.

Addition of the complex inhibitors I and III, rotenone and antimycin A completely blocked the electron transfer of the respiratory chain. This resulted into decreased OCR values to maintain energy homeostasis [113] [10]. Rotenone and antimycin A decreased the OCR values in all genotypes in a similar way (see figure 4.33) indicating that the non-mitochondrial respiration is intact in MCUR1$^{\Delta\mathrm{EC}}$ and MCU$^{\Delta\mathrm{EC}}$.

Pyruvate is converted to lactic acid during anaerobic glycolysis. When lactic acid is released, it acidifies the extracellular space and can be measured as an increase in ECAR [113] [10]. Values for the basal extracellular acidification rate (ECAR) in glucose-free media were similar in MCU$^{\Delta\mathrm{EC}}$, MCUR1$^{\Delta\mathrm{EC}}$ and VE-Cre MPMVECs (see figure 4.34) and addition of glucose generates glycolysis and thereby produces ATP and protons. The protons are released and acidify the media which results in an increase in ECAR values [113]. We did not observe any differences in ECAR glycolysis between MCUR1$^{\Delta\mathrm{EC}}$, MCU$^{\Delta\mathrm{EC}}$ and VE-Cre MPMVECs after addition of glucose (see figure 4.34).

Figure 4.34: **Extracellular acidification rate (ECAR) in MCUR1$^{\Delta EC}$ and MCU$^{\Delta EC}$.** A) Representative traces of ECAR after addition of glucose, oligomycin and 2-DG (2-deoxy-D-glucose)in MCUR1$^{\Delta EC}$, MCU$^{\Delta EC}$ and VE-Cre MPMVECs B) Glycolysis rate after addition of glucose minus non-glycolytic ECAR C) Glycolytic capacity after addition of oligomycin minus non-glycolytic ECAR, representative experiment from n=3, one-way ANOVA, *P<0.05

The second injection of oligomycin (1 µM), inhibits mitochondrial ATP production and therefore shifts metabolically the energy production to glycolysis (maximal glycolytic capacity) [113]. Values for the 'maximum glycolytic capacity' were enhanced in MCUR1$^{\Delta EC}$ and MCU$^{\Delta EC}$ compared to VE-Cre MPMVEC (see figure 4.34). Interestingly, the serum glucose levels of MCUR1$^{\Delta EC}$ mice were not different from control mice under a normal chow diet of 8 weeks [132].

The final injection of 2-DG (2-deoxy-D-glucose), a glucose analog, inhibits the first enzyme during glycolysis, glucose hexakinase. The residual ECAR values after blocking glycolysis are non-glycolytic [113]. MCUR1$^{\Delta EC}$, MCU$^{\Delta EC}$ and VE-Cre MPMVECs showed similar non-glycolytic ECAR values after 2-DG injection.

Enhanced maximal OCR and ECAR values in MCUR1$^{\Delta EC}$ and MCU$^{\Delta EC}$ could be due to the stimulation of compensatory substrate utilization pathways. If the stimulating effect of Ca^{2+} on mitochondrial complex activity, pyruvate dehydrogenase, proton gradient and $\Delta\Psi_m$ is abrogated, MCUR1$^{\Delta EC}$ and MCU$^{\Delta EC}$ might express compensatory proteins to rescue the energy supply of the cell. Along these lines, we investigated if expression of UCP2, the main isoform in endothelial cells [127], was changed in MCUR1$^{\Delta EC}$ and MCU$^{\Delta EC}$. UCP2 has been shown to be involved

in the mitochondrial uptake of intracellular Ca^{2+} [140] [22] [7] but does not interact directly with MCU [110]. In contrast to UCP1, it seems unlikely that UCP2 acts as an uncoupler [119]. Instead, UCP2 is assumed to play a role in the reprogramming of metabolic pathways [139].

Western Blot analysis of cell lysates from $MCUR1^{\Delta EC}$, $MCU^{\Delta EC}$ and VE-Cre MP-MVECs revealed that UCP2 protein levels were significantly increased in $MCUR1^{\Delta EC}$ compared to VE-Cre MPMVECs (see figure 4.35). High UCP2 levels have been reported to limit the contribution of glucose to OCR and to promote the oxidation of substitute substrates such as glutamine and fatty acids. Moreover, high UCP2 levels are assumed to promote the conversion of pyruvate to lactate [139]. We therefore assume, that the upregulation of UCP2 protein levels allows a better energy supply which might explain the enhanced OCR values after addition of substrates which fuel complex I (pyruvate and maleate) or complex II substrate (succinate) (see figure 4.31) as well as the enhanced glycolytic capacity after uncoupling (see figure 4.33 and 4.34).
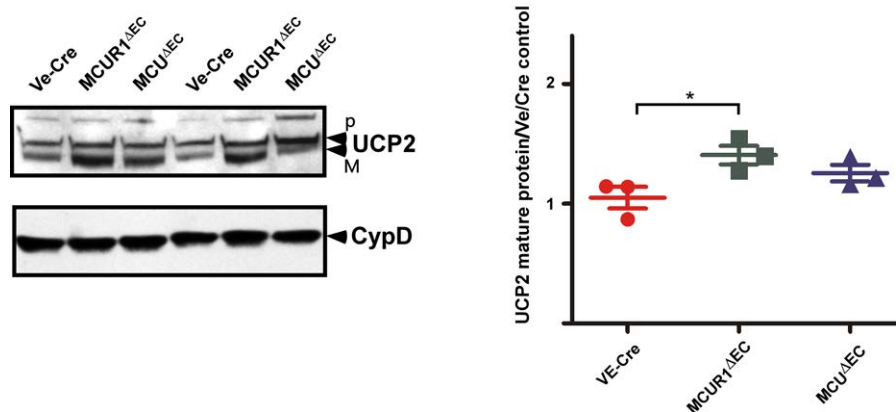
Figure 4.35: **UCP2 expression in $MCUR1^{\Delta EC}$ and $MCU^{\Delta EC}$.** Western Blot analysis of cell lysates from $MCUR1^{\Delta EC}$, $MCU^{\Delta EC}$ and VE-Cre MPMVECs probed for anti-UCP2 antibody A) Representative Western Blot, P:precursor (non-glutathioylated), M:mature protein (glutathioylated) B) Quantification of the mature normalized UCP2 protein levels, n=3 independent experiments, P values were determined by the Mann-Whitney test; *P<0.05.

4.3.3 Contribution of MCUR1 and MCU to proliferation, migration and autophagy

ROS is produced in mitochondria by premature utilization of oxygen which can occur at complex I, II and III of the electron transport chain. Oxygen can accept an additional electron to form superoxide. If antioxidant scavenging enzymes are expressed sufficiently they can detoxify superoxide. Otherwise superoxide can react with other components and damage irreversibly proteins of the electron transport chain [47] [20]. UCPs and ANTs limit ROS production by lowering the $\Delta\Psi_m$ [63].

MCUR1$^{\Delta EC}$ and MCU$^{\Delta EC}$ display an intact function of the respiratory chain (see figure 4.31) but a decreased ATP production (see figure 4.30). Based on the influence of mitochondrial calcium uptake 1 (MICU1), SLC25A23 and UCP2 on superoxide formation, we hypothesized that superoxide levels would be reduced in MCUR1$^{\Delta EC}$ and MCU$^{\Delta EC}$. MPMVECs were stained with the superoxide indicator MitoSOX Red and the intensity of mitochondrial superoxide levels was quantified. MCUR1$^{\Delta EC}$ and MCU$^{\Delta EC}$ showed significantly reduced superoxide levels compared to VE-Cre MPMVECs (see figure 4.36).

Moderate levels of ROS are proposed to be essential for cell proliferation and migra-
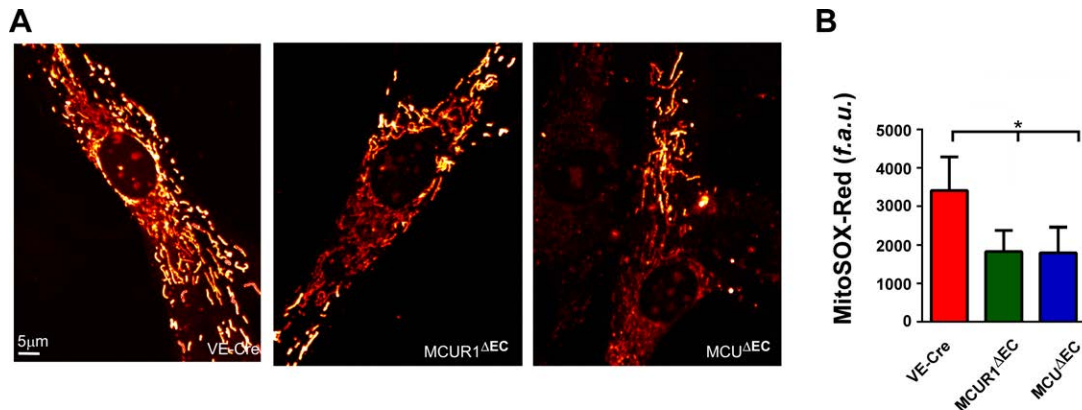
Figure 4.36: **Superoxide levels in MCUR1$^{\Delta EC}$ and MCU$^{\Delta EC}$.** MCUR1$^{\Delta EC}$, MCU$^{\Delta EC}$ and VE-Cre MPMVECs were stained with MitoSOX Red A) Representative confocal images B) Quantification of fluorescence intensities, f.a.u.: fluorescence arbitrary units, n=3 independent experiments, P values were determined by the Mann-Whitney test, *P<0.05.

tion [47] and mitochondrial Ca^{2+} handling could affect endothelial proliferation and migration which are important during wound healing [20]. Therefore, we investigated whether the lack of MCU or MCUR1 affects proliferation and migration by assessing $MCU^{\Delta EC}$ and $MCUR1^{\Delta EC}$ by flow cytometry and scratch assay.
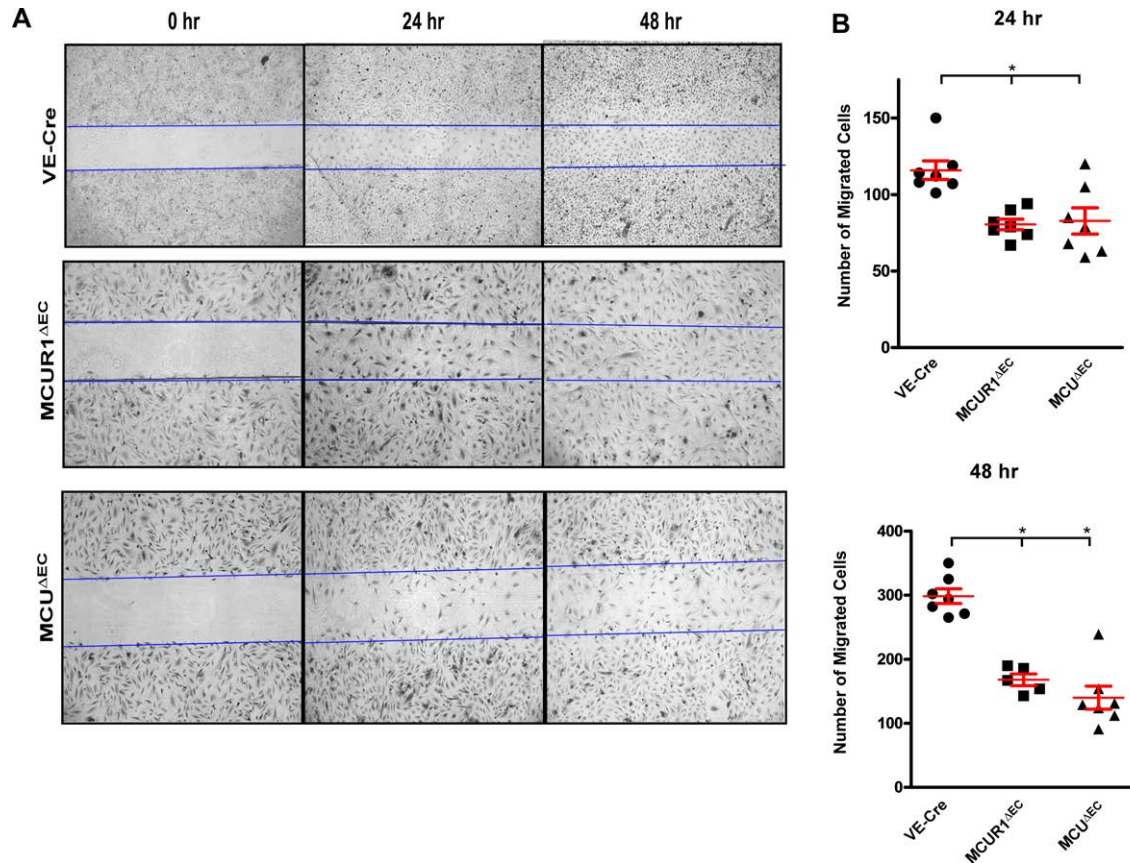
Figure 4.37: **Migration behavior of MCUR1$^{\Delta EC}$ and MCU$^{\Delta EC}$ MPMVECs.** A) Representative images of VE-Cre, MCUR1$^{\Delta EC}$ and MCU$^{\Delta EC}$ MPMVECs which have migrated 24hs and 48hs after gap formation B) Scatter Blots summarizing values of migrated cells 24 and 48h after gap formation, n=3-4 independent experiments, P values were determined by one-way ANOVA; * P<0.05

The scratch assay showed a significantly reduced migration rate for $MCU^{\Delta EC}$ and $MCUR1^{\Delta EC}$ compared to VE-Cre endothelial cells 24hs and 48hs after gap formation (see figure 4.37). These results suggest that Ca^{2+} influx between cytosol and mitochondria was perturbed. Proliferation rates were assessed by using carboxyfluorescein succinimidyl ester (CFSE), a dye which is incorporated in proteins, passed to the daughter generations and quantified by flow cytometry. $MCU^{\Delta EC}$ and $MCUR1^{\Delta EC}$

MPMVECs showed a significantly attenuated proliferation (see figure 4.38).
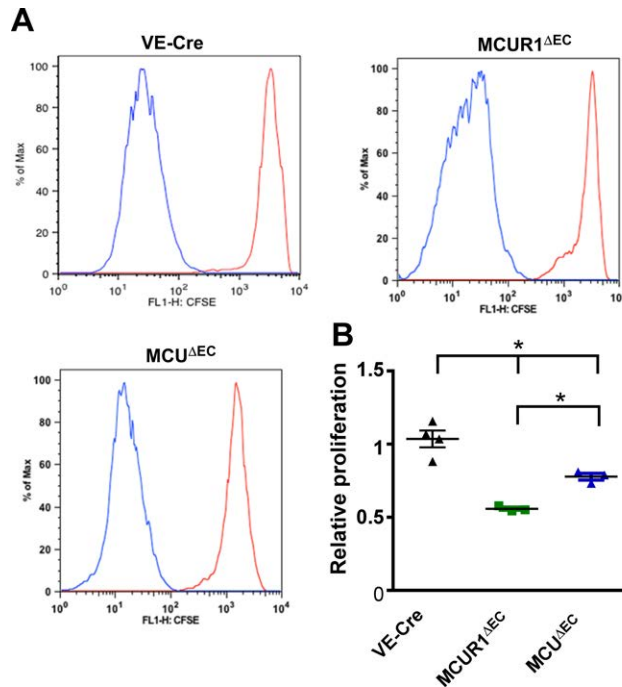
Figure 4.38: **Proliferation in VE-Cre, MCU$^{\Delta EC}$ and MCUR1$^{\Delta EC}$.** A) Representative FACS panels of non-proliferated (red) and proliferated (blue) CFSE-stained VE-Cre, MCUR1$^{\Delta EC}$, MCU$^{\Delta EC}$ MPMVECs B) Relative proliferation rates of proliferating endothelial cells to non-proliferating cells of the same genotype, CFSE: carboxyfluorescein succinimidyl ester, n=3 independent experiments, P values were determined by one-way ANOVA; * P<0.05.

Having demonstrated that MCUR1-deficiency in MPMVECs results in low cellular ATP levels, we propose that alternative modes of cell survival might be upregulated. One mode of cell survival which might be induced is autophagy. Autophagy rescues the cell from energy deprivation by activation of the AMP-activated protein kinase (AMPK). The AMPK phosphorylates substrates to limit anabolic pathways, that consume ATP and activates catabolic pathways to generate substrates supporting oxidative phosphorylation [12] [48]. We hypothesized that the low ATP levels in MCUR1$^{\Delta EC}$ and MCU$^{\Delta EC}$ would result into enhanced autophagic activity.

To investigate the role of MCUR1 and MCU in autophagy MPMVEC protein lysates of MCUR1$^{\Delta EC}$, MCU$^{\Delta EC}$ and VE-Cre mice were analyzed by Western Blotting. According to our expectation, the phosphorylated AMPK and LC3 protein expression was significantly enhanced in MCUR1$^{\Delta EC}$ and MCU$^{\Delta EC}$. To answer the question if

autophagy was terminated by rescue of MCU or MCUR1, MCUR1$^{\Delta EC}$ and MCU$^{\Delta EC}$ were transfected with adenoviral MCUR1 and MCU. As expected, the rescue terminated the autophagy in MCUR1$^{\Delta EC}$ and MCU$^{\Delta EC}$ indicated by the significantly lower microtubule-associated protein light chain 3 (LC3) and phosphorylated AMPK protein levels (see figure 4.39).

Figure 4.39: **Microtubule-associated protein light chain3 (LC3) and phosphorylated AMP-activated protein kinase (p-AMPK) expression in MCUR1$^{\Delta EC}$ and MCU$^{\Delta EC}$.** A) Western Blot analysis of cell lysates from MCUR1$^{\Delta EC}$, MCU$^{\Delta EC}$ and VE-Cre MPMVECs probed with anti-LC3, anti p-AMPK and anti-AMPK antibody B) Quantification of normalized LC3 and p-AMPK protein levels, n=3 independent blots, mean $\pm$ SEM, *P< 0.05, This result was kindly provided by Zhiwei Dong with the MPMVECs isolated by me.

Chapter 5

Discussion

5.1 STIM1/2 proteins are not involved in receptor-operated Ca^{2+} entry (ROCE), but TRPC1, TRPC3 and TRPC6 channels may be activated by store-operated Ca^{2+} entry (SOCE)

TRPCs, the first cloned mammalian transient receptor potential channels, were originally described as store-operated Ca^{2+} (SOC) channels . After cloning STIM proteins and Orai channels and their identification as molecular correlates of SOCE (summarized in [11]), regulation and activation of TRPCs were questioned and extensively discussed. Some research groups reported interaction of TRPC channels with Orai and STIM proteins in vitro in cell lines ([73], [69] summarized in [14]), while others postulated a receptor-operated activation of TRPC channels independent of Orai and STIM ([23]). The scientific community agrees that it is essential to dissect molecular components of SOCE in native cells or whole organs from appropriate gene-deficient 'knock-out' mice. However, STIM/Orai-deficient mice are embryonic lethal and double heterozygous STIM1$^{+/-}$/Orai1$^{+/-}$ mice show only insufficient down-regulation of these proteins (see figure 4.4). Therefore, we decided to use lentiviral mediated Cre-recombinase expression in STIM1/2 floxed cells to delete both proteins in precapillary

pulmonary arterial smooth muscle cells (PPASMCs).

TRPC6 and TRPC3 have been shown to be upregulated in smooth muscle cells of IPAH patients and in a rat model of pulmonary hypertension [25] and several reports identified TRPC1 as the most important TRPC channel involved in SOCE ([25]). Thus, we compared $TRPC1/3/6^{-/-}$ triple deficient with STIM1/2 double deficient and Wt control PPASMC in ROCE and SOCE experiments.

When investigating the function of TRPC as SOCE, one has to deal with several challenges: The main challenge is definitely to distinguish SOCE from other Ca^{2+} entry. TRPCs can be activated by DAG which might mask the STIM-dependent activation. Mutation of TRPCs which electrolytically interact with STIM are an important tool to distinguish between the Orai and and TRPC-mediated SOCE but only in easily to transfect cell lines.

We have shown that TRPC1/3/6 channels are clearly receptor operated in PPASMC. $TRPC1/3/6^{-/-}$ PPASMCs showed an almost completely abolished endothelin-1-induced ROCE in comparison to Wt and STIM1/2 double deficient cells (see figure 4.12). A quintuple STIM1/2/TRPC1/3/6 knock-out did not further reduce ROCE in PPASMCs (see figure 4.12). Next we analyzed different postulated SOCE pathways (1-4) by STIM/Orai and TRPC channels in PPASMC (see figure 5.1).

The research group of Lutz Birnbaumer claims that TRPCs and Orai form heteromers which could be involved in both ROCE and SOCE based on co-immunoprecipitation and functional Ca^{2+} entry experiments of Orai1, TRPC3 and TRPC6 [71][73] next to the identified STIM/Orai pathway (see 2 and 1 in figure 5.1). We can not exclude such a pathway, because we did not down-regulate Orai1/2/3 channels in PPASMC. But a vast almost complete reduction of SOCE in STIM1/2 deficient PPASMCs, does not favor a prominent role of this pathway (2) in SOCE.

According to the research group of Shmuel Muallem, the SOAR region of STIM interacts separately with the coiled coil domains of either TRPCs or Orai. This interaction allows STIM to interact electrostatically with TRPC1 and therefore gates TRPC-mediated SOCE [152] [68]. The use of Orai mutants which allow interaction with STIM but do not mediate Orai-induced SOCE would be an approach to distin-
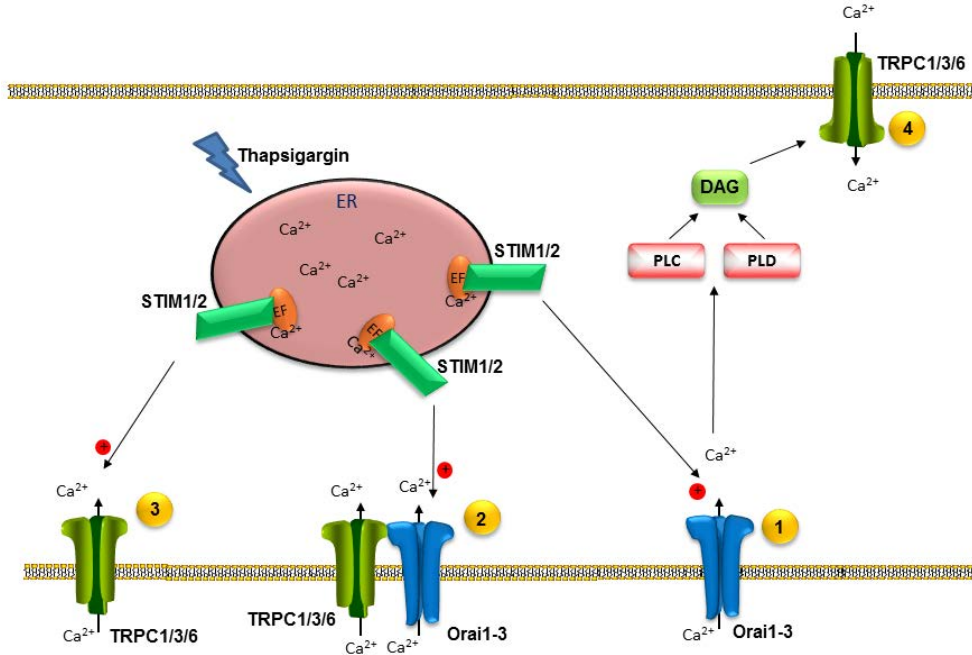
Figure 5.1: **Four postulated SOCE signaling pathways.** 1)STIM/Orai interaction 2) Proposed TRPC-Orai interaction by Lutz Birnbaumer's research group [71][73] 3) Proposed TRPC-STIM interaction by Shmuel Muallem's research group [152] [68] 4) Indirect activation of TRPC channels by SOCE proposed by Attila Braun's research group in platelets [13]

guish between TRPC and Orai-mediated SOCE. However, primary cells are difficult to transfect and an overexpression of these proteins does not represent the in-vivo situation. The generation of so called 'knock-in' mice expressing the Orai-mutants is highly desirable but a technical difficult and time consuming approach. Therefore, we used our experimental set-up to challenge their hypothesis. SOCE experiments with PPASMCs after siRNA mediated down-regulation of Orai1/2/3 or with Orai1/2/3 deficient PPASMCs in comparison to STIM1/2-deficient PPASMCs would be essential to further investigate their hypothesis.

Thapsigargin-induced SOCE was slightly but significantly reduced in TRPC1/3/6 $^{-/-}$ PPASMCs compared to wildtype cells (see figure 4.13 and pathway 4 in figure 5.1). The knockout of both TRPC1/3/6 and STIM1/2 reduced SOCE not significantly further than STIM1/2$^{\Delta SMC}$ (see figure 4.13). These results exclude any prominent role of pathway 2,3 and 4 in SOCE.

However, we did not investigate in our experimental setup if the Orai expression was

affected by the TRPC1/3/6 knockout. Cheng et al. has reported that the TRPC1 expression was affected by Orai1 knockdown [14]. Therefore, TRPC1/3/6 knockout mice might express reduced levels of Orai1/2/3 and consequently show decreased SOCE. Future experiments with siRNA directed against Orai1/2/3 or Orai1/2/3$^{\Delta SMC}$ PPASMC in comparison to TRPC1/3/6 $^{-/-}$ PPASMC and STIM1/2$^{\Delta SMC}$ will clarify functionally if reduced SOCE in TRPC1/3/6 $^{-/-}$ PPASMC is due to altered expression of Orai channels.

Our collaboration partner in Würzburg, Attila Braun, collected data for a fourth signaling pathway in platelets. They demonstrated that thapsigargin-induced Orai mediated SOCE activates phospholipase C (PLC) and phospholipase D (PLD). PLC and PLD can in turn activate Ca^{2+} entry via heteromeric channels of TRPC1 with TRPC3 and TRPC6 by the production of diacylglycerol (DAG) [13]. According to them, PLC and PLD activity would be enhanced during thapsigargin-induced SOCE in Wt but not in Orai-deficient platelets but could not result into TRPC 3 and 6 mediated Ca^{2+} entry because of the TRPC1/3/6 knockout in PPASMCs. Experiments with siRNA directed against PLC and PLD in wildtype cells will demonstrate if knockdown of these phospholipases reduces SOCE compared to wildtype cells.

Different from these research groups, we didn't focus on the molecular setup and the functional interaction of the TRPC/STIM/Orai but on Ca^{2+} entry in primary cells of TRPC1/3/6 $^{-/-}$, STIM1/2$^{\Delta SMC}$ and STIM1/2$^{\Delta SMC}$/TRPC1/3/6 $^{-/-}$ mice and Wt control mice. We are the first who are able to study TRPC-dependent SOCE in PPASMCs from different gene-deficient mice. Previous authors implemented experiments using transfected cell lines or TRPC inhibitors of unknown specificity. The use of these gene-deficient mice is an important tool to further analyze the role of TRPC1/3/6 channels and STIM1/2 proteins for ROCE and SOCE in lung cells.

5.2 Role of SOCE in vasoconstriction, migration, proliferation and lung edema formation

5.2.1 SOCE and NO-induced vasorelaxation and vasoconstriction

We bred STIM1/2$^{\Delta EC}$ and Orai1$^{\Delta EC}$ mice as outlined in the methods section. Ex-vivo lungs showed no morphological significant differences in size and distribution of arterial vessels (see figure 4.17) in comparison to control mice. To analyze SOCE in endothelial function, we isolated and identified endothelial cells from these mice and control mice.

NO-mediated vasodilatation is initiated by the Ca^{2+}-sensitive endothelial NO-synthase [45]. Because SOCE is an important Ca^{2+} entry pathway in endothe-lial cells [102] [94], we investigated how STIM1/2 and Orai1-deficiency contributes to endothelium-induced vasodilatation. We have shown that endothelial-dependent acetylcholine-induced vasodilatation did not differ in STIM1/2$^{\Delta EC}$ and Orai1$^{\Delta EC}$ mice compared to Wt mice (see figure 4.18). Our results contrast Kassan et al. demon-strating that STIM1$^{\Delta EC}$ aortic rings after application of acetylcholine dilatated sig-nificantly less than heterozygous STIM1$^{\Delta EC}$ and wildtype aortic rings [61]. If an endothelial STIM1 knockout results into less vasodilatation, we would have expected an even stronger impaired dilatation in endothelial STIM1/2 double knockout. This discrepancy may be due to much higher variation of our data compared to Kassan et al. which detected significant differences between data points with very low variation. The reason for high variations in vasorelaxation of up to 25% is not known, but might be due to different sample preparation and handling. Existing differences in vasore-laxation of gene-deficient aortic rings compared to control rings might be masked by these variations. Using a SOCE protocol where internal stores where depleted by phenylephrine and thapsigargin, the research group of Donald Gill concluded that aortic rings from STIM1$^{\Delta SMC}$ showed a reduced SOCE-mediated contraction [83]. Even though thapsigargin and cyclopiazonic acid, which empty internal Ca^{2+} stores,

are cell permeable, it is not clear which concentration finally reaches the cytosol of smooth muscle cells after passing the endothelial layer of the aorta and the contraction after Ca^{2+} addition must not necessarily be due to SOCE. Due to these challenges, we decided not to proceed and canceled experiments on the role of SOCE in vasoconstriction by pulmonary arterial smooth muscle cells. The same was true for bronchial rings analyzed in double heterozygous STIM/Orai and control mice (see figure 4.6). To investigate boncho- or vasoconstriction with a myograph intact bronchial or vascular rings are a prerequisite. However, quality control from the tissue is difficult and can only be carried out by KCl-mediated contraction and visual observation. Therefore, we tried to quantify bronchoconstriction in an alternative precision cut lung slices (PCLS) model (see figure 4.7). Even though first experiments were promising, we faced several other difficulties. After seeking advice from PCLS experts, we realized that the different response of bronchi resulted from the dichotomous branching of the lung and only the main bronchus can be quantified. A further challenge was the time of quantification because of constant oscillations of the bronchus. Because we were originally interested in implementing a SOCE-induced constriction protocol, it was necessary to exchange extracellular Ca^{2+} containing and Ca^{2+}-free buffer. However this was not possible without loosing the position of the bronchus of interest.

Furthermore, it is noteworthy that we used heterozygous mice for initial experiments in which the STIM1 and Orai1 levels are downregulated only slightly similar to a STIM1 protein reduction of 11,44%±2,652 in MPMVECs (see figure 4.16). Consequently, we would have been able to detect only huge differences in constriction with these heterozygous mice. Because only STIM1 but not STIM2 is downregulated in these mice, STIM2 could also substitute the defect STIM1 protein. The exact role of STIM2 is still debated [78].

5.2.2 Reduced proliferation and migration in STIM1/2$^{\Delta EC}$ and Orai1$^{\Delta EC}$

Bovine aortic endothelial cells treated with SERCA-inhibitors have been reported to migrate less. Removal of cyclopiazonic acid 6hs after scratch formation rescued migration measured after 24hs [15]. These results suggest that SOCE plays an important role during endothelial migration. In line with this hypothesis, we demonstrated that STIM1/2$^{\Delta EC}$ and Orai1$^{\Delta EC}$ showed a significantly reduced migration compared to VE-Cre endothelial cells 24hs and 48hs after gap formation (see figure 4.19).

Our result differs from that of Gandhirajan et al. showing that gap closure of STIM1$^{\Delta EC}$ was unaltered after 24h [39]. Futher investigation is needed to distinguish if the reduced migration is a direct effect of reduced SOC-mediated Ca^{2+} entry or lower internal Ca^{2+} store levels resulting from the SOCE defect. Ca^{2+} which triggers migration could also originate from the mitochondrium. Santhanam et al. have recently shown that lack of STIM1 or Orai1 reduced MCU-mediated mitochondrial Ca^{2+}-uptake in DT40 lymphocytes [120]. Treatment of STIM1/2$^{\Delta EC}$ and Orai1$^{\Delta EC}$ with the MCU inhibitor ruthenium red, a Na$^+$/Ca^{2+} exchanger inhibitor and a SERCA inhibitor in a scratch assay could show if Ca^{2+} originating from the internal stores or from the extracellular space is responsible for the endothelial migration.

We assumed that similar to migration, proliferation of endothelial cells requires intracellular Ca^{2+}. Therefore, we investigated if proliferation of endothelial cells was reduced in STIM1/2 and Orai1 deficient MPMVECs isolated from STIM1/2$^{\Delta EC}$ and Orai1$^{\Delta EC}$ mice. The proliferation rate was assessed after 72h using carboxyfluorescein succinimidyl ester (CFSE), a dye which after incorporation in proteins, is passed to the daughter generations and can be quantified by flow cytometry. STIM1/2$^{\Delta EC}$ displayed a reduced proliferation rate while proliferation rates of Orai1$^{\Delta EC}$ were unchanged (see figure 4.21). Our results for STIM1/2$^{\Delta EC}$ are in line with Abdullaev et al. but are in contrast to Orai1$^{\Delta EC}$. Abdullaev et al. transfected human umbilical vein endothelial cells (HUVECs) with siRNA for 72 hrs and stained with trypan blue. According to his results HUVECs transfected with siRNA specific for STIM 1/2 and

Orai1 showed a reduced proliferation rate compared to control cells. Moreover, HU-VECs transfected with siRNA specific for Orai proliferated even less than STIM 1/2 siRNA transfected cells. Different from our experiment for which we used murine lung microvascular endothelial cells isolated from gene-deficient mice, Abdullaev et al. used siRNA transfected primary human umbilical vein endothelial cells in which the protein of interest is downregulated according to the efficiency of the siRNA but not deleted completely.

Abdullaev et al. also employed a trypan blue exclusion assay. Trypan blue cannot pass the cell membrane of intact, but of dead cells. An aliquot of the resuspended cells has to be counted either manually or with a cell counter. In both cases only a relatively small number of cells is counted and extrapolated to the entire population. To be precise, trypan blue exclusion assay indicates the viability of cells and one of the characteristics of viable cells are that they proliferate. In comparison to trypan blue exclusion, the FACS measurement of CFSE is a more elegant method. During cell division CFSE is passed from the mother to the daughter cell and thereby the intensity of CFSE reduces. Subsequently, the intensity of CFSE is a direct marker of proliferation and not an indirect marker such as trypan blue. Therefore we were able to analyze 15 000 cells per sample. However as a result of the gene-deficiency during early development other genes may compensate the lack of the proteins. Further studies are need to exclude any compensation by up-regulation of related proteins.

Cytosolic Ca^{2+} is not only essential for migration but also for NO synthesis. In accordance with the lower intracellular Ca^{2+} levels in STIM1/2 deficient endothelial cells, the NO-synthase activity may be reduced. A dysfunctional eNOS produces superoxide instead of NO. ROS has been shown to trigger SOCE [39] which could stimulate endothelial migration. Even though Gandhirajan et al. had demonstrated that the cytosolic superoxide production and NOX levels were unaltered in STIM1$^{\Delta EC}$, we observed enhanced mitochondrial superoxide levels in STIM1/2$^{\Delta EC}$ and Orai1$^{\Delta EC}$ (see figure 4.20). Further studies are needed to evaluate if SOCE protects from mitochondrial superoxide production and if antioxidant scavenging enzymes are upregulated in STIM1/2$^{\Delta EC}$ and Orai1$^{\Delta EC}$.

5.2.3 Reduced nuclear NFAT translocation in endothelial STIM1/2 or Orai1 KO mice and challenges to reproduce endothelial permeability models

Dysfunctional endothelial cells, induced by bacterial LPS, allow fluid to leak into the surrounding tissues which results into lung edema formation [99] [116]. Under non-stimulated conditions, MLC phosphatase dephosphorylates the MLC and consequently prevents opening of the tight junctions. After thrombin stimulation this preventive mechanism is inhibited [99].

Thrombin stimulation induces stress fiber formation which can be quantified by staining of F-actin with fluorescence labeled phalloidin. We showed that phalloidin staining intensities of thrombin-stimulated STIM1$^{+/-}$/Orai1$^{+/-}$ MPMVECs were reduced compared to thrombin-stimulated wildtype MPMVECs (see figure 4.22).

The research group of Mohammed Trebak has previously shown that immortalized HUVECs transfected transiently with siRNA specific for STIM1 were protected from disruption of the endothelial barrier after stimulation with 100nM thrombin analyzed by electrical cellular impedance sensing (ECIS). Transfection of HUVECs with Orai-specfic siRNAs did not show any difference compared to control cells [121]. However, we failed to establish an ECIS or permeability transwell assay which could have shown if a SOCE defect in primary MPMVECs protects from endothelial barrier disruption. The reason for this was the failure of primary MPMVECs to grow completely confluent and to form tight junctions.

Gandhirajan et al. have shown that STIM1 is essential for NFAT-mediated transcription of proinflammatory mediators. NFATc3-GFP transfected STIM1$^{\Delta EC}$ translocated significant lower amounts of NFATc3-GFP to the nucleus compared to control MPMVECs expressing NFATc3-GFP. This was further confirmed by significantly reduced luciferase activity in STIM1^{KD} MPMVECs compared to wildtype MPMVECs [39]. Based on these findings the question arose if only STIM1 or both STIM isoforms, STIM1 and STIM2, or Orai attenuate the NFATc3 nuclear translocation. Thus, MPMVECs were transfected with adenovirus encoding NFATc3-GFP for 36 hours,

followed by LPS treatment for additional 16h [39]. According to our expectations, the number of VE-Cre MPMVECs with nuclear translocation of NFATc3-GFP after LPS stimulation was increased compared to unstimulated MPMVECs was increased and this increase after LPS stimulation was abrogated in LPS-stimulated STIM1/2$^{\Delta EC}$ compared to unstimulated STIM1/2$^{\Delta EC}$ and in LPS-stimulated Orai1$^{\Delta EC}$ compared to unstimulated Orai1$^{\Delta EC}$. The number of cells with NFATc3-GFP translocated to nuclei was also significantly reduced in LPS-stimulated STIM1/2$^{\Delta EC}$ compared to LPS-stimulated Ve-Cre MPMVECs (see figure 4.23). Comparing our result to Gandhirajan et al., we did not observe a different number of NFATc3-GFP translocated to nuclei in double STIM1/2$^{\Delta EC}$ or Orai1$^{\Delta EC}$ compared to the single STIM 1 ΔEC analyzed [39].

5.3 The influence of mitochondrial Ca^{2+} uniporter (MCU) and mitochondrial Ca^{2+} uniporter regulator 1 (MCUR1) in endothelial cells on mitochondrial bioenergetics

MCUR1 was identified as a positive regulator of the MCU complex through its interaction with MCU [81]. We investigated the functional role of MCUR1 during mitochondrial Ca^{2+} entry demonstrating that only a nominal mitochondrial Ca^{2+} uptake was observed in MCUR1$^{\Delta EC}$, MCUR1$^{\Delta MLF}$ and MCU$^{\Delta MLF}$ (see figure 4.26 and 4.27) while the $\Delta\Psi_m$ was similar compared to cells from floxed or VE-Cre mice (see figure 4.25). These results support our previous data demonstrating that both MCU and MCUR1 are essential for the MCU-mediated Ca^{2+} uptake in a HeLa cell line stably overexpressing MCUR1 [81]. Overexpressing MCUR1 HeLa cells showed an enhanced histamine-stimulated mitochondrial Ca^{2+} uptake and this uptake was abrogated after knockdown of MCU in the MCUR1 overexpressing cells. Vise versa, overexpression of MCU elevated mitochondrial Ca^{2+} uptake in wildtype but not after

down-regulation of MCUR1 [81].

Simultaneous recording of $[Ca^{2+}]_m$ uptake and $\Delta\Psi_m$ discovered that both $MCU^{\Delta EC}$ and $MCUR1^{\Delta EC}$ failed to take up Ca^{2+} (see figure 4.29 and 4.28). Upon exposure to excessive Ca^{2+}, the VE-Cre cells exhibited a rapid $\Delta\Psi_m$ collapse due to mitochondrial Ca^{2+} entry, which was not observed in $MCU^{\Delta EC}$ and $MCUR1^{\Delta EC}$ MPMVECs (see figure 4.29). Basal $[Ca^{2+}]_m$ was reduced in in $MCU^{\Delta EC}$ and $MCUR1^{\Delta EC}$ compared to VE-Cre MPMVECs (see figure 4.28).

These results confirm our previous data showing that permeabilized $MCUR1^{KD}$ HeLa or HEK293T cells display a reduced Ru360 (MCU blocker)- and CCCP (uncoupler)-sensitive mitochondrial Ca^{2+} uptake after 10 µM Ca^{2+} pulses. Overexpression of MCUR1 in HeLa cells rescued the mitochondrial Ca^{2+} uptake. Basal mitochondrial Ca^{2+} was reduced in HEK293T cells expressing downregulated levels of MCUR1 ($MCUR1^{KD}$) indicated by the mitochondrial Ca^{2+} release after the addition of carbonyl cyanide 3-chlorophenylhydrazone (CCCP). Basal mitochondrial Ca^{2+} levels were enhanced after rescue of MCUR1. Overexpression of MCUR1 in MCU knockdown cells and vise versa demonstrated a requirement of both MCU and MCUR1 for the mitochondrial Ca^{2+} uptake [81]. Luongo et al. reported that murine embryonic fibroblasts isolated from floxed MCU mice, infected with adenoviral Cre-recombinase ($MCU^{\Delta MLF}$), showed nearly a complete loss of mitochondrial Ca^{2+} uptake after 5 µM Ca^{2+} pulses [76].

Moreover, our group was able to characterize MCUR1 as MCU complex scaffold factor. MCUR1 and MCU interact via their highly conserved coiled-coil domains. A lack of MCUR1 resulted into defective MCU heterooligomeric complex assembly and suppressed the I_{MCU} current in isolated cardiac mitoplasts [132].

The impact of MCUR1 and MCU on the mitochondrial bioenergetics has not been investigated yet in primary cells. Based on the finding that perturbed $[Ca^{2+}]_m$ uptake may lead to a cellular bioenergetic crisis [85] [120], we investigated ATP levels of $MCU^{\Delta EC}$ and $MCUR1^{\Delta EC}$. ATP levels were reduced in both, but significant smaller in $MCUR1^{\Delta EC}$ than in $MCU^{\Delta EC}$ (see figure 4.30). These data confirm previous results showing an enhanced AMP/ATP ratio, and therefore a reduced ATP production, in

HeLa cells with downregulated expression levels of MCUR1 [81]. Our group further examined whether agonist-induced $[Ca^{2+}]_m$ uptake affects ATP levels in MCUR1$^{\Delta EC}$ and MCU$^{\Delta EC}$. VE-Cre MPMVECs stimulated with the GPCR agonist thrombin (500mU/ml) showed increased ATP levels compared to MCUR1$^{\Delta EC}$ [132].

We next analyzed if reduced ATP levels resulted directly from decreased mitochondrial Ca^{2+} levels or from an impaired function of the respiratory chain complexes. Oxygen consumption rate (OCR) measurements with the Clark electrode and the XF-96 Extracellular Flux Analyzer^{Tm} revealed an elevated complex I and II activity in MCU$^{\Delta EC}$ (see figure 4.31) and an enhanced maximal respiration rate after addition of the uncoupler FCCP in MCU$^{\Delta EC}$ and MCUR1$^{\Delta EC}$ (see figure 4.33). But theses results are in contrast to previous data showing that the basal OCR was reduced in MCUR1^{KD} HeLa but the maximal OCR after addition of FCCP was not significantly different from control cells. The rescue of MCUR1 resulted into comparable maximal OCR levels compared to control cells [81]. However, the previous results were obtained in a human cancer cell line while we used murine primary endothelial cells now. Therefore, it has to be taken into account that different cellular properties may influence the results.

The research group of T. Finkel showed that murine embryonic fibroblasts isolated from MCU KO mice had a similar maximal OCR as wildtype fibroblasts after addition of FCCP [93] and that hepatic mitochondria isolated from MCU KO mice treated with complex I substrates glutamate and malate displayed similar levels of respiration as wildtype mitochondria. The basal oxygen consumption of the MCU KO mice was not altered. Serum lactate levels were elevated but not other TCA intermetabolites such as succinate, malate, fumarate and citrate [93]. Proteins of mitochondrial oxidative phosphorylation components were equally expressed in MCUR1$^{\Delta EC}$, MCU$^{\Delta EC}$ and VE-Cre MPMVECs (see figure 4.32). Consequently, we conclude from our results, that OCR is intact in MCU$^{\Delta EC}$ and MCUR1$^{\Delta EC}$.

The enhanced maximal respiration rate in MCUR1$^{\Delta EC}$ and MCU$^{\Delta EC}$ could indicate an utilization of the proton gradient that prevents $\Delta\Psi_m$ hyperpolarization. An unchanged $\Delta\Psi_m$ in MCUR1$^{\Delta EC}$, MCU$^{\Delta EC}$ would support this hypothesis. Similar to

us, Mallilankaraman et al. had shown that HeLa cells with down-regulated MCUR1 did not show an altered $\Delta\Psi_m$ compared to wildtype cells [81].

Dissipation of the proton gradient without involvement of the ATP-synthase is facilitated by uncoupling proteins (UCPs) or adenine nucleotide transporters (ANTs). H^+ enters the matrix and consequently decreases $\Delta\Psi_m$ [63]. The proton gradient which is not used for ATP production, would be used for heat generation by UCP proteins instead. Therefore, UCP, especially its main isoform expressed in endothelial cells UCP2 [127], could be responsible for the higher heat dissipation of MCUR1$^{\Delta EC}$ mice. According to our hypothesis, UCP2 protein levels were upregulated (see figure 4.35) in MCUR1$^{\Delta EC}$. We therefore concluded that upregulation of UCP2 is a compensatory mechanism to MCUR1 deficiency and UCP2 fluxes protons to prevent $\Delta\Psi_m$ hyperpolarization.

However, other groups have presented data which argues against the role of UCP2 in uncoupling [66][119]. They suggest that UCP2 promotes a metabolic switch which limits the contribution of glucose to OCR and promotes the oxidation of substitute substrates such as glutamine and fatty acids [139]. We observed an elevated extracellular acidification rate (ECAR) in in MCU$^{\Delta EC}$ and MCUR1$^{\Delta EC}$ after addition of oligomycin (see figure 4.34). Oligomycin inhibits mitochondrial ATP production and therefore shifts metabolically the energy production to glycolysis [113]. From this result we could speculate that MCUR1$^{\Delta EC}$ MPMVECs, in which UCP2 is upregulated, depend more on glycolysis than MPMVECs with normal level of UCP2. Endothelial cells mainly use glucose, fatty acids and glutamine as substrates and glucose for glycolysis but not for oxidative phosphorylation even when oxygen is present [100]. Because of this substrate demand, MPMVECs were grown in our experiments in high glucose medium containing $4.5\,\mathrm{g\,ml^{-1}}$ glucose and 4mM glutamine. As an alternative to this hypothesis MCUR1$^{\Delta EC}$ MPMVECs, in which UCP2 is upregulated, might utilize substrates which fuel complex I, pyruvate and maleate, or complex II substrate succinate better as indicated by the enhanced OCR (see figure 4.31). We further observed an AMP-kinase (AMPK) activation in MCU$^{\Delta EC}$ and MCUR1$^{\Delta EC}$ which was abrogated by a rescue of MCU and MCUR1(see figure 4.39). AMPK is activated dur-

ing energy deprivation indicated by low ATP levels and induces catabolic pathways [48].

A third approach, postulated by the Graier group, claims that UCP2 is involved in $[Ca^{2+}]_m$ uptake [140] [22] [7]. In a Nature cell biology paper, the Graier group has demonstrated that UCP2 overexpression in the human endothelial cell line EA.hy926 significantly enhanced $[Ca^{2+}]_m$ stimulation by histamine. SiRNA-mediated knockdown of UCP2 reduced $[Ca^{2+}]_m$ levels to levels in control cells [134]. However, their results were controversially discussed by Matthijnssens et al. They criticized that the observed higher $[Ca^{2+}]_m$ levels were not due to mitochondrial Ca^{2+} uptake or efflux mechanisms but rather due to a defective UCP2 protein expressed in abnormal high levels. Alternatively, they suggest that UCP2 could mediate the Na^+/Ca^{2+} or H^+/Ca^{2+} exchangers [84]. In 2013, Sancak et al. demonstrated the absence of a direct interaction between UCP2 and MCU in a proteomic assay [110].

Recent studies on cardiac mitochondria isolated from UCP2$^{-/-}$ mice showed that the Ru360 sensitive $[Ca^{2+}]_m$ was significantly reduced. Measuring the Ru360 sensitive current in cardiac mitoplast from UCP2$^{-/-}$ mice revealed a reduced channel activity compared to control mitoplasts [88]. In 2015, the Graier group presented results that overexpression of UCP2 enhanced the open probability of extralarge mitoplast Ca^{2+} currents but did not result in an additional mitoplast Ca^{2+} current indicating that UCP2 does not form a new Ca^{2+} channel itself. SiRNA-mediated knockdown of UCP2 HeLa cells reduced the open probability of extralarge mitoplast Ca^{2+} currents [7].

According to this hypothesis, UCP2 is upregulated in MCUR1$^{\Delta EC}$ as a compensatory mechanism to rescue $[Ca^{2+}]_m$-uptake. However, in our experiments, MCUR1$^{\Delta EC}$ showed only a nominal $[Ca^{2+}]_m$ uptake after stimulation with ionomycin. Only experiments with double knockout cells for MCUR1 and UCP2 will reveal if $[Ca^{2+}]_m$ uptake is abolished completely after stimulation by agonists.

Superoxide is mainly produced if oxygen is used prematurely during the electron transport chain [47] [20]. It has been proposed that ROS promotes autophagy and apoptosis [60]. Our group has previously demonstrated that loss of the negative MCU

regulator MICU1 induces basal mitochondrial Ca^{2+} accumulation and increased mitochondrial ROS production [82]. Intact OCR levels in MCUR1$^{\Delta EC}$ and MCU$^{\Delta EC}$ suggest that electron leakage does not occur more often than in control cells and superoxide levels are expected to be unchanged. But also downregulation of several proteins involved in the MCU-mediated mitochondrial Ca^{2+} uptake have demonstrated to influence superoxide production [49] [82]. According to our expectation, superoxide levels were not elevated in MCUR1$^{\Delta EC}$ and MCU$^{\Delta EC}$ (see figure 4.36). Presumably, due to reduced mitochondrial Ca^{2+} levels, basal superoxide formation was even reduced in MCUR1$^{\Delta EC}$ and MCU$^{\Delta EC}$ (see figure 4.36).

If UCP2 acts as an uncoupler, the UCP2 upregulation in MCUR1$^{\Delta EC}$ may explain the observed reduced ROS production. This hypothesis would be supported by Szewczyk et al.[127] who has reported that high UCP2 levels protect from ROS overproduction. Teshima et al. reported that high UCP2 levels prevented from oxidative-stress induced cell death. They added H_2O_2 to cardiomyocytes which increased the fluorescence of the cellular oxidative stress marker DCF (2',7'-dichlorofluorescein). Cardiomyocytes stably overexpressing adenoviral UCP2 showed significantly reduced DCF fluorescence levels after H_2O_2 stimulation [131].

Alternatively, MCUR1 and MCU deficiency might affect adenine nucleotide transporters (ANT) expression. Besides UCP, ANT also dissipates the proton gradient without involvement of the ATP-synthase [63]. Thus, it would be of interest if ANT levels are upregulated in MCUR1$^{\Delta EC}$ and MCU$^{\Delta EC}$. Furthermore, silencing of UCP2 and ANT in MCUR1$^{\Delta EC}$ and MCU$^{\Delta EC}$ may show if UCP2 and ANT or the lack of Ca^{2+} is responsible for the low levels of superoxide production. Investigation of antioxidant enzymes could highlight if ROS is produced but scavenged or if less ROS is produced in MCUR1$^{\Delta EC}$ and MCU$^{\Delta EC}$. If Ca^{2+} is required for ANT activity is not known.

Moderate levels of ROS have been proposed to be essential for cell proliferation and migration [47]. In accordance with lower superoxide production and mitochondrial Ca^{2+} uptake, we observed a reduced proliferation and migration in MCUR1$^{\Delta EC}$ and MCU$^{\Delta EC}$ (see figure 4.21 and 4.37). If upregulation of UCP2 has an effect on pro-

liferation and migration in endothelial cells is not clear but UCP2 has been reported to play a role in the Warburg effect describing the capability of fast-proliferating cancer cells to switch their metabolism from oxidative phosphorylation to anaerobic glycolysis [139]. Further investigation is needed on MCU1- and MCUR1-deficient endothelial cells overexpressing UCP2 to reveal if they have an altered migration and proliferation.

Low mitochondrial Ca^{2+} uptake and low cellular ATP levels in $MCUR1^{\Delta EC}$ and $MCU^{\Delta EC}$ activated AMPK and turned on autophagy, as indicated by enhanced microtubule-associated protein light chain 3 (LC3) expression (see figure 4.39). The elevated levels of phosphorylated AMPK and LC3 was abrogated after rescue of MCUR1 and MCU (see figure 4.39). Our data obtained with murine primary endothelial cells confirmed our previous results demonstrating enhanced phosphorylated AMPK and LC3-II protein levels which were again normal after rescue of MCUR1 expression in the human MCUR1 KD HeLa cell line. This clearly demonstrates that MCU and MCUR1 have an essential function during autophagy. However, we do not know if autophagy is induced by the lack of Ca^{2+} uptake or the lack of MCUR1 and MCU itself.

MacVicar et al. have already investigated the role of intracellular Ca^{2+} and MCU in a Parkin-induced mitophagy model [77]. Parkin is an ubiquitin E3 ligase which is recruited to depolarized mitochondria and induces mitochondrial autophagy, called mitophagy. To deplete the cytosol from Ca^{2+}, MacVicar et al. treated YFP-Parkin expressing RPE1 cells with $10\,\mu M$ BAPTA-AM (a cell-permeant chelator, which is a highly selective for Ca^{2+} over Mg^{2+}) to buffer cytosolic Ca^{2+}. BAPTA-AM blocked CCCP-induced mitophagy dose dependently. Transient MCU or IP_3R knockdown of YFP-Parkin expressing RPE1 cells treated with $10\,\mu M$ CCCP for 24hs showed reduced mitophagy [77]. They conclude that an intact MCU-mediated Ca^{2+}-uptake would predispose cells to mitophagy and that reduced mitochondrial Ca^{2+} levels could have an inhibitory effect on Parkin-mediated mitophagy.

These data clearly contrasts our result showing that a lack of MCU makes endothelial cells more vulnerable to autophagy. However, one has to keep in mind that the

CCCP they used for their experiments induces a collapse of the $\Delta\Psi_m$ and a reduced mitochondrial Ca^{2+} uptake. Different from our autophagy model in murine primary endothelial cells, they used a Parkin-induced mitophagy model in the human retinal pigment epithelial cell line RPE1. Therefore, only a detailed further analysis will reveal the role of Ca^{2+} and its downstream targets in autophagy pathways.

Chapter 6

Appendix

6.1 Acronyms

$\Delta\Psi_m$ mitochondrial membrane potential.

acetyl-CoA acetyl coenzyme A.

AMPK AMP-activated protein kinase.

ANT adenine nucleotide transporters.

BH$_4$ tetrahydrobiopterin.

CaMKK calmodulin-dependent protein kinase kinases.

CFSE 5-(and-6)-carboxyfluorescein diacetate succinimidyl ester.

cGMP cyclic guanosine monophosphate.

CPA cyclopiazonic acid.

CRAC Ca^{2+} release-activated Ca^{2+} current.

DAG diacylglycerol.

ECAR extracellular acidification rate.

ECIS Electrical Cell-Substrate Impedance Sensing.

ECM extracellular medium.

eNOS endothelial NOS.

ER endoplasmatic reticulum.

ES embryonic stem.

FAD flavin adenine dinucleotide.

FMN flavin mononucleotide.

G$_q$PCR G$_q$ protein coupled receptor.

HDMECs human dermal microvascular endothelial cells.

HUVECs human umbilical vein endothelial cells.

ICAM1 intercellular adhesion molecule 1.

IMM inner mitochondrial membrane.

IP$_3$ inositoltriphosphate.

IPAH idiopathic pulmonary arterial hypertension.

LC microtubule-associated protein light chain.

LPS lipopolysaccharide.

MCU mitochondrial Ca^{2+} uniporter.

MCUR1 mitochondrial Ca^{2+} uniporter regulator1.

MICU1 mitochondrial calcium uptake 1.

MLC myosin light chain.

MLCK myosin light chain kinase.

MLF murine lung fibroblasts.

MPMVEC mouse pulmonary microvascular endothelial cells.

Myh11 myosin heavy chain 11.

NADH nicotinamide adenine dinucleotide.

NADPH nicotinamide adenine dinucleotide phosphate.

NFAT nuclear factor of activated T-cells.

NOS nitrite oxide synthase.

NOX NADPH oxidase.

OCR oxygen consumption rate.

PA phosphatidic acid.

PAH pulmonary arterial hypertension.

PAP phosphatidic acid phosphohydrolase.

PCLS precision cut lung slices.

PIP$_2$ phosphatidylinositol 4,5-bisphosphate.

PLC phospholipase C.

PLD phospholipase D.

PPASMC precapillary pulmonary arterial smooth muscle cells.

PTP permeability transition pore.

Rho–GEF guanine nucleotide exchange factor.

ROC receptor operated Ca^{2+}.

ROS reactive oxygen species.

SCID severe combined immunodeficiency.

Ser serine.

SERCA sarcoplasmic/endoplasmic reticulum ATPase.

SOAR STIM-Orai activating region.

SOC store-operated Ca^{2+}.

STIM stromal interaction molecule.

tBH$_3$ trihydrobiopterin.

TCA tricarboxylic acid cycle.

TLR4 Toll-like receptor4.

TMRM tetramethyl rhodamine methyl ester.

TRP transient receptor potential.

TRPC classical transient receptor potential.

TSMC tracheal smooth muscle cells.

UCP uncoupling proteins.

VCAM1 vascular cell-adhesion molecule 1.

VEGF vascular endothelial growth factor.

Bibliography

[1] Abdullaev I.F., Bisaillon J.M., Potier M., Gonzalez J.C., Motiani R.K. and Trebak M. STIM1 and Orai1 mediate CRAC currents and store-operated Calcium entry important for endothelial cell proliferation. *Circulation Research*, 103(11):1289–1299 (2008).

[2] Addgne. Lentivirus. http://www.addgene.org/viral-vectors/lentivirus/ (2016).

[3] Balaban R.S., Nemoto S. and Finkel T. Mitochondria, Oxidants, and Aging. *Cell*, 120(4):483–495 (2005).

[4] Baughman J.M., Perocchi F., Girgis H.S., Plovanich M., Belcher-Timme C.a., Sancak Y., Bao X.R., Strittmatter L., Goldberger O., Bogorad R.L., Koteliansky V. and Mootha V.K. Integrative genomics identifies MCU as an essential component of the mitochondrial calcium uniporter. *Nature*, 476(7360):341–345 (2011).

[5] Bedard K. and Krause K.H. The NOX family of ROS-generating NADPH oxidases: physiology and pathophysiology. *Physiological reviews*, 87(1):245–313 (2007).

[6] Bisaillon J.M., Motiani R.K., Gonzalez-Cobos J.C., Potier M., Halligan K.E., Alzawahra W.F., Barroso M., Singer H.a., Jourd'heuil D. and Trebak M. Essential role for STIM1/Orai1-mediated calcium influx in PDGF-induced smooth muscle migration. *American Journal of Physiology - Cell Physiology*, 298(5):C993–1005 (2010).

[7] Bondarenko A.I., Parichatikanond W., Madreiter C.T., Rost R., Waldeck-Weiermair M., Malli R. and Graier W.F. UCP2 modulates single-channel properties of a MCU-dependent Ca^{2+} inward current in mitochondria. *Pflügers Archiv - European Journal of Physiology*, 467:2509–2518 (2015).

[8] Boulay G., Zhu X., Peyton M., Jiang M., Hurst R., Stefani E. and Birnbaumer L. Cloning and expression of a novel mammalian homolog of Drosophila Transient receptor potential (Trp) involved in calcium entry secondary to activation of receptors coupled by the G_q class of G protein. *Journal of Biological Chemistry*, 272(47):29672–29680 (1997).

[9] Brand M.D. Keilin Memorial Lecture: The efficiency and plasticity of mitochondrial energy transduction. *Biochemical Society - Biochemical Society Transactions*, 33(Pt 5):897–904 (2005).

[10] Brand M.D. and Nicholls D.G. Assessing mitochondrial dysfunction in cells. *The Biochemical Journal*, 435(2):297–312 (2011).

[11] Cahalan M.D. STIMulating store-operated Ca^{2+} entry. *Nature Cell Biology*, 11(6):669–677 (2009).

[12] Cárdenas C., Miller R.A., Smith I., Bui T., Molgó J., Müller M., Vais H., Cheung K.H., Yang J., Parker I., Thompson C.B., Birnbaum M.J., Hallows K.R. and Foskett J.K. Essential Regulation of Cell Bioenergetics by Constitutive InsP3 Receptor Ca^{2+} Transfer to Mitochondria. *Cell*, 142(2):270–283 (2010).

[13] Chen W., Thielmann I., Gupta S., Subramanian H., Stegner D., Van Kruchten R., Dietrich A., Gambaryan S., Heemskerk J.W.M., Hermanns H.M., Nieswandt B. and Braun A. Orai1-induced store-operated Ca^{2+} entry enhances phospholipase activity and modulates canonical transient receptor potential channel 6 function in murine platelets. *Journal of Thrombosis and Haemostasis*, 12(4):528–39 (2014).

[14] Cheng K., Ong H. and Ambudkar I. Contribution and Regulation of TRPC Channels in Store-Operated Calcium Entry. *Current Topics in Membranes*, 71:149–79 (2013).

[15] Chiwaka K., Oike M. and Koyama T. Alterations of Calcium moblilizing properties in migrating endothelial cells. *American Journal of Heart Circulatory Physiology*, 281:H745–H754 (2001).

[16] Clapham D.E., Julius D., Montell C. and Schultz G. Nomenclature and structure-function relationships of transient receptor potential channels. *Pharmacological reviews*, 57(4):427–450 (2005).

[17] Cooper G. and Sunderland M. *The Cell: A Molecular Approach. 6th edition.* Sinauer Associates, Boston (2013).

[18] Cosens A. and Manning A. Abnormal electroretinogram from a Drosophila mutant. *Nature*, 224(5216):285–7 (1969).

[19] Csordás G., Golenár T., Seifert E.L., Kamer K.J., Sancak Y., Perocchi F., Moffat C., Weaver D., De la Fuente Perez S., Bogorad R.L., Koteliansky V., Adijanto J., Mootha V.K. and Hajnóczky G. MICU1 controls both the threshold and cooperative activation of the mitochondrial Ca^{2+} uniporter. *Cell Metabolism*, 18(9):1199–1216 (2013).

[20] Davidson S.M. and Duchen M.R. Endothelial Mitochondria: Contributing to Vascular Function and Disease. *Circulation Research*, 100(8):1128–1141 (2007).

[21] De Stefani D., Raffaello A., Teardo E., Szabò I. and Rizzuto R. A forty-kilodalton protein of the inner membrane is the mitochondrial calcium uniporter. *Nature*, 476(7360):336–340 (2011).

[22] Deak A.T., Blass S., Khan M.J., Groschner L.N., Graier W.F., Malli R. and Physiology C. IP3-mediated STIM1 oligomerization requires intact mitochondrial Ca^{2+} uptake. *Journal of Cell Science*, 127:2944–55 (2014).

[23] DeHaven W.I., Jones B.F., Petranka J.G., Smyth J.T., Tomita T., Bird G.S. and Putney J.W. TRPC channels function independently of STIM1 and Orai1. *The Journal of Physiology*, 587(Pt 10):2275–98 (2009).

[24] D'Esposito M., Strazzullo M., Cuccurese M., Spalluto C., Rocchi M., D'Urso M. and Ciccodicola A. Identification and assignment of the human transient receptor potential channel 6 gene TRPC6 to chromosome 11q21 until q22. *Cytogenetic Genome Research*, 83(1-2):46–47 (1998).

[25] Dietrich A. and Gudermann T. *Mammalian Transient Receptor Potential (TRP) Cation Channels*, volume 222 of *Handbook of Experimental Pharmacology*. Springer Berlin Heidelberg, Berlin, Heidelberg (2014).

[26] Dietrich A., Kalwa H. and Gudermann T. TRPC channels in vascular cell function. *Thrombosis and Haemostasis*, 103(2):262–70 (2010).

[27] Dietrich A., Kalwa H., Storch U., Mederos y Schnitzler M., Salanova B., Pinkenburg O., Dubrovska G., Essin K., Gollasch M., Birnbaumer L. and Gudermann T. Pressure-induced and store-operated cation influx in vascular smooth muscle cells is independent of TRPC1. *Pflügers Archiv - European Journal of Physiology*, 455(3):465–77 (2007).

[28] Dietrich A., Mederos Y Schnitzler M., Emmel J., Kalwa H., Hofmann T. and Gudermann T. N-Linked Protein Glycosylation Is a Major Determinant for Basal TRPC3 and TRPC6 Channel Activity. *Journal of Biological Chemistry*, 278(48):47842–47852 (2003).

[29] Dietrich A., Mederos y Schnitzler M., Gollasch M., Gross V., Storch U., Dubrovska G., Obst M., Yildirim E., Salanova B., Kalwa H. and Others. Increased vascular smooth muscle contractility in TRPC6-/-mice. *Molecular and Cellular Biology*, 25(16):6980 (2005).

[30] Doonan P.J., Chandramoorthy H.C., Hoffman N.E., Zhang X., Cárdenas C., Shanmughapriya S., Rajan S., Vallem S., Chen X., Foskett J.K., Cheung J.Y., Houser S.R. and Madesh M. LETM1-dependent mitochondrial Ca^{2+} flux modulates cellular bioenergetics and proliferation. *Federation of American Societies for Experimental Biology*, 28(11):4936–49 (2014).

[31] Duchen M.R. Mitochondria and calcium: from cell signalling to cell death. *The Journal of Physiology*, 529(1):57–68 (2000).

[32] Earley S. and Brayden J.E. Transient receptor potential channels in the vasculature. *Physiological reviews*, 95(2):645–90 (2015).

[33] Eddahibi S. and Adnot S. Endothelins and pulmonary hypertension, what directions for the near future? *European Respiratory Journal*, 18(1):1–4 (2001).

[34] Eddahibi S., Morrell N., D'Ortho M.P., Naeije R. and Adnot S. Pathobiology of pulmonary arterial hypertension. *European Respiratory Journal*, 20(6):1559–1572 (2002).

[35] Feske S. CRAC channelopathies. *European Journal of Physiology*, 460(2):417–35 (2010).

[36] Feske S., Giltnane J., Dolmetsch R., Staudt L.M. and Rao A. Gene regulation mediated by calcium signals in T lymphocytes. *Nature Immunology*, 2(4):316–24 (2001).

[37] Feske S., Gwack Y., Prakriya M., Srikanth S., Puppel S.H., Tanasa B., Hogan P.G., Lewis R.S., Daly M. and Rao A. A mutation in Orai1 causes immune deficiency by abrogating CRAC channel function. *Nature*, 441(7090):179–85 (2006).

[38] Förstermann U. and Sessa W.C. Nitric oxide synthases: Regulation and function. *European Heart Journal*, 33(7):829–837 (2012).

[39] Gandhirajan R., Meng S., Chandramoorthy H., Mallilankaraman K., Mancarella S., Gao H., Razmpour R., Yang X., Houser S., Chen J., Koch W., Wang H., Soboloff J., Gill D. and Madesh M. Blockade of NOX2 and STIM1 signaling limits lipopolysaccharide-induced vascular inflammation. *The Journal of Clinical Investigation*, 123(14):887–902 (2013).

[40] Genetrap. Gene Trap. http://www.genetrap.org/tutorials/overview.html (2016).

[41] Glancy B. and Balaban R.S. Role of mitochondrial Ca^{2+} in the regulation of cellular energetics. *Biochemistry*, 51(14):2959–73 (2012).

[42] Gudermann T. and Steinritz D. STIMulating Stress Fibers in Endothelial Cells. *Science Signaling*, 6(267):pe8 (2013).

[43] Gunter T.E. and Pfeiffer D.R. Mechanisms by which mitochondria transport calcium. *The American Journal of Physiology*, 258(5 Pt 1):C755–C786 (1990).

[44] Guo R.W., Wang H., Gao P., Li M.Q., Zeng C.Y., Yu Y., Chen J.F., Song M.B., Shi Y.K. and Huang L. An essential role for stromal interaction molecule 1 in neointima formation following arterial injury. *Cardiovascular research*, 81(4):660–8 (2009).

[45] Haga T. Molecular properties of muscarinic acetylcholine receptors. *Proceedings of the Japan Academy - Series B, Physical and Biological Sciences*, 89(6):226–56 (2013).

[46] Hagensen M.K., Raarup M.K., Mortensen M.B., Thim T., Nyengaard J.R., Falk E. and Bentzon J.F. Circulating endothelial progenitor cells do not contribute to regeneration of endothelium after murine arterial injury. *Cardiovascular Research*, 93(2):223–231 (2012).

[47] Hamanaka R. and Chandel N. Mitochondiral reactive oxygen species regulate cellular signaling and dictate biological outcomes. *Trends in Biochemical Science*, 35(9):505–513 (2011).

[48] Hardie D.G. AMP-activated/SNF1 protein kinases: conserved guardians of cellular energy. *Nature reviews. Molecular Cell Biology*, 8(10):774–785 (2007).

[49] Hoffman N.E., Chandramoorthy H.C., Shamugapriya S., Zhang X., Rajan S., Mallilankaraman K., Gandhirajan R.K., Vagnozzi R.J., Ferrer L.M., Sreekrishnanilayam K., Natarajaseenivasan K., Vallem S., Force T., Choi E.T., Cheung J.Y. and Madesh M. MICU1 Motifs Define Mitochondrial Calcium Uniporter Binding and Activity. *Cell Reports*, 5(6):1576–1588 (2013).

[50] Hoffman N.E., Chandramoorthy H.C., Shanmughapriya S., Zhang X.Q., Vallem S., Doonan P.J., Malliankaraman K., Guo S., Rajan S., Elrod J.W., Koch W.J., Cheung J.Y. and Madesh M. SLC25A23 augments mitochondrial Ca^{2+} uptake, interacts with MCU, and induces oxidative stress-mediated cell death. *Molecular Biology of the Cell*, 25(6):936–47 (2014).

[51] Hofmann T., Schaefer M., Schultz G. and Gudermann T. Transient receptor potential channels as molecular substrates of receptor-mediated cation entry. *Journal of Molecular Medicine*, 78(1):14–25 (2000).

[52] Hofmann T., Schaefer M., Schultz G. and Gudermann T. Subunit composition of mammalian transient receptor potential channels in living cells. *Proceedings of the National Academy of Sciences of the United States of America*, 99(11):7461–6 (2002).

[53] Hofmann,Thomas Obukhov,Alexander G. Schaefer M. and Harteneck, Christian Gudermann, Thomas Schultz G. Direct activation of human TRPC6 and TRPC3 channels by diacylglycerol. *Nature*, 397:259–263 (1999).

[54] Holzhauser L. and Zolty R. Endothelin receptor polymorphisms in the cardiovascular system: potential implications for therapy and screening. *Heart Failure reviews*, 19(6):743–758 (2014).

[55] Hong J., Li Q., Kim M., Shin D., Feske S., Birnbaumer L., Cheng K., Ambudkar I. and Muallem S. Polarized but differential localization and recruitment of STIM1, Orai1 and TRPC channels in secretory cells. *Traffic (Copenhagen, Denmark)*, 12(2):232–245 (2012).

[56] Hoth M and PennerR. Depletion of intracellular calcium stores activates a calcium current in mast cells. *Nature*, 355(6358):353–6 (1992).

[57] Hou T., Zhang X., Xu J., Jian C., Huang Z., Ye T., Hu K., Zheng M., Gao F., Wang X. and Cheng H. Synergistic Triggering of Superoxide Flashes by Mitochondrial Ca^{2+} Uniport and Basal Reactive Oxygen Species Elevation. *Journal of Biological Chemistry*, 288(7):4602–4612 (2013).

[58] Humbert M., Lau E.M.T., Montani D., Jais X., Sitbon O. and Simonneau G. Advances in therapeutic interventions for patients with pulmonary arterial hypertension. *Circulation*, 130(24):2189–2208 (2014).

[59] Jardin I., Omez L.J.G., Salido G.M. and Rosado J.A. Dynamic interaction of hTRPC6 with the Orai1 – STIM1 complex or hTRPC3 mediates its role in capacitative or non-capacitative Ca 2 + entry pathways. *The Biochemical Journal*, 276:267–276 (2009).

[60] Kaminsky V.O. and Zhivotovsky B. Free Radicals in Cross Talk Between Autophagy and Apoptosis. *Antioxidants & Redox Signaling*, 21(1):86–102 (2014).

[61] Kassan M., Zhang W., Aissa K.A., Stolwijk J., Trebak M. and Matrougui K. Differential role for stromal interacting molecule 1 in the regulation of vascular function. *Pflügers Archiv - European Journal of Physiology*, 467(6):1195–202 (2015).

[62] Kawasaki T., Nishiwaki T., Sekine A., Nishimura R., Suda R., Urushibara T., Suzuki T., Takayanagi S., Terada J., Sakao S. and Tatsumi K. Vascular Repair by Tissue-Resident Endothelial Progenitor Cells in Endotoxin-Induced Lung Injury. *American Journal of Respiratory Cell and Molecular Biology*, 53(4):500–12 (2015).

[63] Kim E.H., Koh E.H., Park J.Y. and Lee K.U. Adenine nucleotide translocator as a regulator of mitochondrial function: implication in the pathogenesis of metabolic syndrome. *Korean Diabetes Journal*, 34(3):146–53 (2010).

[64] Kirichok Y., Krapivinsky G. and Clapham D.E. The mitochondrial calcium uniporter is a highly selective ion channel. *Nature*, 427:360–364 (2004).

[65] Kuhr F.K., Smith K.a., Song M.Y., Levitan I. and Yuan J.X.J. New mechanisms of pulmonary arterial hypertension: role of Ca^{2+} signaling. *American Journal of Physiology - Heart and Circulatory Physiology*, 302(8):H1546–62 (2012).

[66] Kukat A., Dogan S.A., Edgar D., Mourier A., Jacoby C., Maiti P., Mauer J., Becker C., Senft K., Wibom R., Kudin A.P., Hultenby K., Flögel U., Rosenkranz S., Ricquier D., Kunz W.S. and Trifunovic A. Loss of UCP2 attenuates mitochondrial dysfunction without altering ROS production and uncoupling activity. *PLOS Genetics*, 10(6):e1004385 (2014).

[67] Lamalice L., Le Boeuf F. and Huot J. Endothelial Cell Migration During Angiogenesis. *Circulation Research*, 100(6):782–794 (2007).

[68] Lee K.P., Choi S., Hong J.H., Ahuja M., Graham S., Ma R., So I., Shin D.M., Muallem S. and Yuan J.P. Molecular determinants mediating gating of transient receptor potential canonical (TRPC) channels by stromal interaction molecule 1 (STIM1). *Journal of Biological Chemistry*, 289(10):6372–6382 (2014).

[69] Lee K.P., Yuan J.P., So I., Worley P.F. and Muallem S. STIM1-dependent and STIM1-independent function of Transient Receptor Potential Canonical (TRPC) channels tunes their store-operated mode. *Journal of Biological Chemistry*, 285(49):38666–38673 (2010).

[70] Liao Y., Abramowitz J. and Birnbaumer L. The TRPC family of TRP channels: roles inferred (mostly) from knockout mice and relationship to ORAI proteins. *Handbook of Experimental Pharmacology*, 223:1055–1075 (2014).

[71] Liao Y., Erxleben C., Yildirim E., Abramowitz J., Armstrong D.L. and Birnbaumer L. Orai proteins interact with TRPC channels and confer responsiveness to store depletion. *Proceedings of the National Academy of Sciences of the United States of America*, 104(11):4682–4687 (2007).

[72] Liao Y., Hao Y., Chen H., He Q., Yuan Z. and Cheng J. Mitochondrial calcium uniporter protein MCU is involved in oxidative stress-induced cell death. *Protein & Cell*, 6(6):434–442 (2015).

[73] Liao Y., Plummer N.W., George M.D., Abramowitz J., Zhu M.X. and Birnbaumer L. A role for Orai in TRPC-mediated Ca^{2+} entry suggests that a TRPC:Orai complex may mediate store and receptor operated Ca^{2+} entry. *Proceedings of the National Academy of Sciences of the United States of America*, 106(9):3202–3206 (2009).

[74] Liou J., Kim M.L., Heo W.D., Jones J.T., Myers J.W., James E., Jr F. and Meyer T. STIM is a Ca^{2+} sensor essential for Ca^{2+}-store-depletion-triggered Ca^{2+} influx. *Current Biology*, 15(13):1235–1241 (2011).

[75] Liu X., Cheng K.T., Bandyopadhyay B.C., Pani B., Dietrich A., Paria B.C., Swaim W.D., Beech D., Yildrim E., Singh B.B., Birnbaumer L. and Ambudkar I.S. Attenuation of store-operated Ca^{2+} current impairs salivary gland fluid secretion in TRPC1(-/-) mice. *Proceedings of the National Academy of Sciences of the United States of America*, 104(44):17542–17547 (2007).

[76] Luongo T., Lambert J., Yuan A., Zhang X., Gross P., Song J., Santhanam S., Gao E., Jain M., Houser S., Koch W., Cheung J., Muniswamy M. and Elrod J. The Mitochondrial Calcium Uniporter Matches Energetic Supply with Cardiac Workload during Stress and Modulates Permeability Transition. *Cell Reports*, 12(1):23–34 (2015).

[77] MacVicar T.D.B., Mannack L.V.J.C., Lees R.M. and Lane J.D. Targeted siRNA Screens Identify ER-to-Mitochondrial Calcium Exchange in Autophagy and Mitophagy Responses in RPE1 Cells. *International Journal of Molecular Sciences*, 16(6):13356–80 (2015).

[78] Makino A., Firth A.L. and Yuan J.X.J. Endothelial and smooth muscle cell ion channels in pulmonary vasoconstriction and vascular remodeling. *American Physiological Society - Comprehensive Physiology*, 1(3):1555–602 (2011).

[79] Malczyk M., Veith C., Fuchs B., Hofmann K., Storch U., Schermuly R.T., Witzenrath M., Ahlbrecht K., Fecher-Trost C., Flockerzi V., Ghofrani H.a., Grimminger F., Seeger W., Gudermann T., Dietrich A. and Weissmann N. Classical transient receptor potential channel 1 in hypoxia-induced pulmonary hypertension. *American Journal of Respiratory and Critical Care Medicine*, 188(12):1451–9 (2013).

[80] Malczyk M., Veith C., Schermuly R., Gudermann T., Dietrich A., Sommer N., Weissmann N. and Pak O. NADPH oxidases-do they play a role in TRPC regulation under hypoxia? *Pflügers Archiv - European Journal of Physiology*, 468(1):23–41 (2016).

[81] Mallilankaraman K., Cárdenas C., Doonan P.J., Chandramoorthy H.C., Irrinki K.M., Golenár T., Csordás G., Madireddi P., Yang J., Müller M., Miller R., Kolesar J.E., Molgó J., Kaufman B., Hajnóczky G., Foskett J.K. and Madesh M. MCUR1 is an essential component of mitochondrial Ca^{2+} uptake that regulates cellular metabolism. *Nature Cell Biology*, 14(12):1336–43 (2012).

[82] Mallilankaraman K., Doonan P., Cárdenas C., Harish C., Muller M., Miller R., Hoffman N.E., Molgó J., Birnbaum M.J., Rothberg B., Mak D.o.D., Foskett J.K. and Madesh M. MICU1 is an Essential Gatekeeper for MCU-Mediated Mitochondrial Ca^{2+} Uptake That Regulates Cell Survival. *Cell*, 151(3):630–644 (2012).

[83] Mancarella S., Potireddy S., Wang Y., Gao H., Gandhirajan R.K., Autieri M., Scalia R., Cheng Z., Wang H., Madesh M., Houser S.R. and Gill D.L. Targeted STIM deletion impairs calcium homeostasis, NFAT activation, and growth of smooth muscle. *Federation of American Societies for Experimental Biology*, 27(3):893–906 (2013).

[84] Matthijnssens J., Ciarlet M., Rahman M., Attoui H., Estes M.K., Gentsch J.R., Iturriza-gómara M., Kirkwood C., Mertens P.P.C., Nakagomi O., Patton J.T. and Franco M. UCPs – Unlikely Calcium Porters. *Nature Cell Biology*, 153(8):1621–1629 (2009).

[85] McCormack J. and Denton R.M. Intracellular calcium ions and intramitochondrial Ca^{2+} in the regulation of energy metabolism in mammalian tissues NADH is also Ca^{2+} -dependent and involves the relay of the increases in cytosolic Ca^{2+}

into the mitochondrial matrix . The rise in matrix. *Proceedings of the Nutrition Society*, 57–75 (1990).

[86] McLean MR. Endothelin-1: a mediator of pulmonary hypertension? *Pulmonary Pharmacology and Therapeutics*, 11(2-3):125–32 (1998).

[87] Montell C R.G. Molecular characterization of the Drosophila trp locus: a putative integral membrane protein required for phototransduction. *Neuron*, 2(4):1313–23 (1989).

[88] Motloch L.J., Larbig R., Gebing T., Reda S., Schwaiger A., Leitner J., Wolny M., Eckardt L. and Hoppe U.C. By regulating mitochondrial Ca^{2+}-uptake UCP2 modulates intracellular Ca^{2+}. *PLOS ONE*, 11(2):1–18 (2016).

[89] Nicholls DG and Crompton M. Mitochondrial calcium transport. *Federation of European Biochemical Societies Letters*, 111(2):261–268 (1980).

[90] Nielsen N., Lindemann O. and Schwab a. TRP channels and STIM/ORAI proteins: sensors and effectors of cancer and stroma cell migration. *British Journal of Pharmacology*, 1–17 (2014).

[91] Nilius B. and Grzegorz Owisanik. The transient receptor potential superfamily of ion channels. *Genome Biology*, 15(7):1690–1699 (2011).

[92] Oh-hora M., Yamashita M., Hogan P., Sharma S., Chung W., Prakriya M., Feske S. and Rao A. Dual functions for the endoplasmic reticulum calcium sensors STIM1 and STIM2 in T cell activation and tolerance. *Nature Immunology*, 9(4):432–443 (2009).

[93] Pan X., Liu J., Nguyen T., Liu C., Sun J., Teng Y., Maria M., Rovira I.I., Allen M., Springer D.A., Aponte A.M., Balaban R.S., Murphy E. and Finkel T. The physiological role of mitochondrial calcium revealed by mice lacking the mitochondrial calcium uniporter (MCU). *Nature Cell Biology*, 15(12):1–17 (2014).

[94] Parekh A. and Putney Jr J. Store-operated calcium channels. *Physiological reviews*, 85(2):757–810 (2005).

[95] Parekh A.B. and Penner R. Store depletion and calcium influx. *Physiological reviews*, 77(4):901–30 (1997).

[96] Paupe V., Prudent J., Dassa E.P., Rendon O.Z. and Shoubridge E.a. Short Article CCDC90A (MCUR1) Is a Cytochrome c Oxidase Assembly Factor and Not a Regulator of the Mitochondrial Calcium Uniporter. *Cell Metabolism*, 21(1):109–116 (2015).

[97] Penna A., Demuro A., Yeromin A.V., Zhang S.L., Safrina O., Parker I. and Cahalan M.D. The CRAC channel consists of a tetramer formed by Stim-induced dimerization of Orai dimers. *Nature*, 456(7218):116–120 (2009).

[98] Perocchi F., Gohil V.M., Girgis H.S., Bao X.R., Mccombs J.E., Palmer A.E. and Mootha V.K. MICU1 encodes a mitochondrial EF hand protein required for Ca^{2+} uptake. *Nature*, 467(7313):291–296 (2011).

[99] Pober J.S. and Sessa W.C. Evolving functions of endothelial cells in inflammation. *Nature reviews - Immunology*, 7(10):803–815 (2007).

[100] Polet F. and Feron O. Endothelial cell metabolism and tumour angiogenesis: Glucose and glutamine as essential fuels and lactate as the driving force. *Journal of Internal Medicine*, 273(2):156–165 (2013).

[101] Potier M., Gonzalez J.C., Motiani R.K., Abdullaev I.F., Bisaillon J.M., Singer H.a. and Trebak M. Evidence for STIM1- and Orai1-dependent store-operated calcium influx through ICRAC in vascular smooth muscle cells: role in proliferation and migration. *Federation of American Societies for Experimental Biology*, 23(8):2425–37 (2009).

[102] Putney J.W., Broad L.M., Braun F.J., Lievremont J.P. and Bird G.S. Mechanisms of capacitative calcium entry. *Journal of Cell Science*, 114(Pt 12):2223–2229 (2001).

[103] Putney Jr J. A model for receptor-regulated calcium entry. *Cell Calcium*, 7(1):1–12 (1986).

[104] Rasmussen T.P., Wu Y., Joiner M.L.a., Koval O.M., Wilson N.R., Luczak E.D., Wang Q., Chen B., Gao Z., Zhu Z., Wagner B.a., Soto J., McCormick M.L., Kutschke W., Weiss R.M., Yu L., Boudreau R.L., Abel E.D., Zhan F., Spitz D.R., Buettner G.R., Song L.S., Zingman L.V. and Anderson M.E. Inhibition of MCU forces extramitochondrial adaptations governing physiological and pathological stress responses in heart. *Proceedings of the National Academy of Sciences of the United States of America*, 112(29) (2015).

[105] Rinne A., Banach K. and Blatter L.A. Regulation of Nuclear Factor of Activated T Cells (NFAT) in Vascular Endothelial Cells. *Journal of Molecular and Cellular Cardiology*, 47(3):400–410 (2010).

[106] Rizzuto R., De Stefani D., Raffaello A. and Mammucari C. Mitochondria as sensors and regulators of calcium signalling. *Nature Reviews Molecular Cell Biology*, 13(9):566–578 (2012).

[107] Roos J. STIM1, an essential and conserved component of store-operated Ca^{2+} channel function. *The Journal of Cell Biology*, 169(3):435–445 (2005).

[108] Rosado J.A., Brownlow S.L. and Sage S.O. Endogenously expressed Trp1 is involved in store-mediated Ca^{2+} entry by conformational coupling in human platelets. *Journal of Biological Chemistry*, 277(44):42157–42163 (2002).

[109] Salin K., Auer S.K., Rey B., Selman C. and Metcalfe N.B. Variation in the link between oxygen consumption and ATP production , and its relevance for animal performance. *Proceedings - Biological Sciences*, 282(1812) (2015).

[110] Sancak Y., Markhard A.L., Kitami T., Kovács-Bogdán E., Kamer K.J., Udeshi N.D., Carr S.a., Chaudhuri D., Clapham D.E., Li A.a., Calvo S.E., Goldberger O. and Mootha V.K. EMRE is an essential component of the mitochondrial calcium uniporter complex. *Science*, 342(6164):1379–82 (2013).

[111] Santillo M., Colantuoni A., Mondola P., Guida B. and Damiano S. NOX signaling in molecular cardiovascular mechanisms involved in the blood pressure homeostasis. *Frontiers in Physiology*, 6(July):194 (2015).

[112] Santo-Domingo J. and Demaurex N. Perspectives on: SGP Symposium on Mitochondrial Physiology and Medicine: The renaissance of mitochondrial pH. *The Journal of General Physiology*, 139(6):415–423 (2012).

[113] Seahorse Bioscience Inc. User Manual: XF Cell Mito Stress Test kit. http://cn.agilent.com/cs/library/usermanuals/public/XF_Cell_Mito_ Stress_Test_Kit_User_Guide.pdf (2010).

[114] Seeger W., Adir Y., Barberà J.A., Champion H., Coghlan J.G., Cottin V., De Marco T., Galiè N., Ghio S., Gibbs S., Martinez F.J., Semigran M.J., Simonneau G., Wells A.U. and Vachiéry J.L. Pulmonary hypertension in chronic lung diseases. *Journal of the American College of Cardiology*, 62(25):D109–16 (2013).

[115] Seeger W. and Pullamsetti S.S. Mechanics and mechanisms of pulmonary hypertension-Conference summary and translational perspectives. *Pulmonary Circulation*, 3(1):128–136 (2013).

[116] Seeley E.J., Rosenberg P. and Matthay M.A. Calcium flux and endothelial dysfunction during acute lung injury : a STIMulating target for therapy. *The journal of clinical investigation*, 123(3):1015–1018 (2013).

[117] Seferian A, Chaumais MC, Savale L, Günther S, Tubert-Bitter P, Humbert M M.D. Drugs induced pulmonary arterial hypertension. *Presse médicale*, Sep;42(p Pt 2):e303–10 (2013).

[118] Semenov I., Herlihy J.T. and Brenner R. In vitro measurements of tracheal constriction using mice. *Journal of Visualized Experiments*, 64(1):1–7 (2012).

[119] Shabalina I. and Nedergaard J. Mitochondrial ('mild') uncoupling and ROS production: physiologically relevant or not? *Biochemical Society Transactions*, 39:1305–1309 (2011).

[120] Shanmughapriya S., Rajan S., Hoffman N.E., Zhang X., Guo S., Kolesar J.E., Hines K.J., Ragheb J., Jog N.R., Caricchio R., Baba Y., Zhou Y., Kaufman B.A., Cheung J.Y., Kurosaki T., Gill D.L. and Madesh M. Ca 2 + signals

regulate mitochondrial metabolism by stimulating CREB-mediated expression of the mitochondrial Ca 2 + uniporter gene MCU. *Cell biology*, 8(366):1–14 (2015).

[121] Shinde A., Motiani R., Zhang X., Abdullaev I., Alejandro P., Matrougui K., Vincent P. and Trebak M. STIM1 controls endothelial barrier function independently of Orai1 and Ca^{2+} entry. *Science signaling*, 6(267):ra18 (2013).

[122] Soboloff J., Rothberg B.S., Madesh M. and Gill D.L. STIM proteins : dynamic calcium signal transducers. *Nature Reviews Molecular Cell Biology*, 13(9):549–565 (2012).

[123] Song M.Y., Makino A. and Yuan J.X.J. STIM2 Contributes to Enhanced Store-operated Ca Entry in Pulmonary Artery Smooth Muscle Cells from Patients with Idiopathic Pulmonary Arterial Hypertension. *Pulmonary Circulation*, 1(1):84–94 (2011).

[124] Spinelli A.M., González-Cobos J.C., Zhang X., Motiani R.K., Rowan S., Zhang W., Garrett J., Vincent P.a., Matrougui K., Singer H.a. and Trebak M. Airway smooth muscle STIM1 and Orai1 are upregulated in asthmatic mice and mediate PDGF-activated SOCE, CRAC currents, proliferation, and migration. *Pflügers Archiv - European Journal of Physiology*, 464(5):481–92 (2012).

[125] Storch, Ursula; Forst, Anna-Lena; Maximillian Philipp, Gudermann, T.; Mederos y Schnitzler M. Transient Receptor Potential Channel 1 (TRPC1) Reduces Calcium Permeability in Heteromeric Channel Complexes. *Journal of Biological Chemnistry*, 1(14):1–11 (2011).

[126] Stryke D., Kawamoto M., Huang C., Johns S., King L., Harper C., Meng E., Lee R., Yee A., L'Italien L., Chuang P., Young S., Skarnes W., Babbit P. and Ferrin T. BayGenomics: A resource of insertional mutations in mouse embryonic stem cells. *Nucleic Acids Research*, 31(1):278–281 (2003).

[127] Szewczyk A., Jarmuszkiewicz W., Kozieł A., Sobieraj I., Nobik W., Łukasiak A., Skup A., Bednarczyk P., Drabarek B., Dymkowska D., Wrzosek A. and Zabłocki K. Mitochondrial mechanisms of endothelial dysfunction. *Pharmacological Reports*, 67(4):704–710 (2015).

[128] Takahashi H., Soma S., Muramatsu M., Oka M., Ienaga H. and Fukuchi Y. Discrepant distribution of big endothelin (ET)-1 and ET receptors in the pulmonary artery. *European Respiratory Journal*, 18(1):5–14 (2001).

[129] Tang X., Luo Y.X., Chen H.Z. and Liu D.P. Mitochondria, endothelial cell function, and vascular diseases. *Frontiers in Physiology*, 5(May):175 (2014).

[130] Tarasov A.I., Griffiths E.J. and Rutter G.a. Regulation of ATP production by mitochondrial Ca^{2+}. *Cell Calcium*, 52(1):28–35 (2012).

[131] Teshima Y. and Masaharu Akao, Steven P. Jones E.M. Uncoupling Protein-2 Overexpression Inhibits Mitochondrial Death Pathway in Cardiomyocytes. *Circulation Research*, 93(3):192–200 (2003).

[132] Tomar D., Dong Z., Shanmughapriya S., Koch D., Thomas T., Hoffman N., Timbalia S., Goldman S., Breves S., Corbally D., Nemani N., Fairweather J., Cutri A., Zhang X., Song J., Jana F., Huang J., Barrero C., Rabinowitz J., Luongo T., Schumacher S., Rockman M.E., Dietrich A., Merali S., Caplan J., Stathopulos P., Ahima R.S., Cheung J.Y., Houser S.R., Koch W.J., Patel V., Gohil Vishal M., Elrod John W., Rajan S. and Madesh M. MCUR1 Is a Scaffold Factor for the MCU Complex Function and Promotes Mitochondrial Bioenergetics. *Cell Reports*, 15(8):1673–85 (2016).

[133] Tran P.O., Hinman L.E., Unger G.M. and Sammak P.J. A wound-induced $[Ca^{2+}]_i$ increase and its transcriptional activation of immediate early genes is important in the regulation of motility. *Experimental Cell Research*, 246(2):319–26 (1999).

[134] Trenker M., Malli R., Fertschai I., Levak-Frank S. and Graier W.F. Uncoupling proteins 2 and 3 are fundamental for mitochondrial Ca^{2+} uniport. *Nature Cell Biology*, 9(4):445–452 (2014).

[135] Tronolab. Lentivectors. http://tronolab.epfl.ch/lentivectors (2014).

[136] Ushio-Fukai M. Redox signaling in angiogenesis: Role of NADPH oxidase. *Cardiovascular Research*, 71(2):226–235 (2006).

[137] Varga-Szabo D., Authi K., Braun A., Bender M., Ambily A., Hassock S., Gudermann T., Dietrich A. and Nieswandt B. Store-operated Ca^{2+} entry in platelets occurs independently of transient receptor potential (TRP) C1. *Pflügers Archiv - European Journal of Physiology*, 457:377–387 (2008).

[138] Vig M., Wayne I., Dehaven G., Bird J., Billingsley M., Wang H., Rao P., Hutchings A., Jouvin M., Putney J. and Kinet J. A major defect in mast cell effector functions in CRACM1-/- mice. *Nature Immunology*, 148(4):825–832 (2008).

[139] Vozza A., Parisi G., De Leonardis F., Lasorsa F.M., Castegna A., Amorese D., Marmo R., Calcagnile V.M., Palmieri L., Ricquier D., Paradies E., Scarcia P., Palmieri F., Bouillaud F. and Fiermonte G. UCP2 transports C4 metabolites out of mitochondria, regulating glucose and glutamine oxidation. *Proceedings of the National Academy of Sciences of the United States of America*, 111(3):960–5 (2014).

[140] Waldeck-Weiermair M., Malli R., Naghdi S., Trenker M., Kahn M. and Graier W.F. The contribution of UCP2 and UCP3 to mitochondrial Ca^{2+} uptake is differentially determined by the source of supplied Ca^{2+}. *Cell Calcium* (2010).

[141] Walker, D. Clark electrode. http://www.hansatech-instruments.com/products/introduction-to-oxygen-measurements/general-oxygen-electrode-measurement-principles/ (1987).

[142] Weir K. Mechanisms of Disease: Acute oxygen-sensing mechanisms. *New England Journal of Medicine*, 353(19):2042–2055 (2005).

[143] Weissmann N., Dietrich A., Fuchs B., Kalwa H., Ay M., Dumitrascu R., Olschewski A., Storch U., Mederos y Schnitzler M., Ghofrani H.A., Schermuly R.T., Pinkenburg O., Seeger W., Grimminger F. and Gudermann T. Classical transient receptor potential channel 6 (TRPC6) is essential for hypoxic pulmonary vasoconstriction and alveolar gas exchange. *Proceedings of the National Academy of Sciences of the United States of America*, 103(50):19093–19098 (2006).

[144] Weitzenblum E. Prognostic value of pulmonary artery pressure in chronic obstructive pulmonary disease. *Thorax*, 36:752–758 (1981).

[145] Wes P.D., Chevesich J., Jeromin A., Rosenberg C., Stetten G. and Montell C. TRPC1, a human homolog of a Drosophila store-operated channel. *Proceedings of the National Academy of Sciences of the United States of America*, 92(21):9652–6 (1995).

[146] Williams G.S., Boyman L. and Lederer W.J. Mitochondrial calcium and the regulation of metabolism in the heart. *Journal of Molecular and Cellular Cardiology*, 78:35–45 (2015).

[147] Wirth A., Benyó Z., Lukasova M., Leutgeb B., Wettschureck N., Gorbey S., Orsy P., Horváth B., Maser-Gluth C., Greiner E., Lemmer B., Schütz G., Gutkind J.S. and Offermanns S. G_{12}-G_{13}-LARG-mediated signaling in vascular smooth muscle is required for salt-induced hypertension. *Nature Medicine*, 14(1):64–8 (2008).

[148] Woudenberg-Vrenken, TE., Bindels R.J.M. and Hoenderop J.G.J. The role of transient receptor potential channels in kidney disease. *Nature Reviews Nephrology*, 5(8):441–9 (2009).

[149] Wu M., Neilson A., Swift A., Moran R., Tamagnine J., Parslow D., Armistead S., Lemire K., Orrell J., Teich J., Chomicz S. and Ferrick D. Multiparameter metabolic analysis reveals a close link between attenuated mitochondrial bioenergetic function and enhanced glycolysis dependency in human tumor cells. *American Journal of Physiology - Cell Physiology*, 292(1):C125–36 (2007).

[150] Yu Y., Keller S.H., Remillard C.V., Safrina O., Nicholson A., Zhang S.L., Weihua J., Nivruthi V., Landsberg, Judd W., Wang J.Y., Thistlethwaite P.A., Channick R.N., Robbins I.M., Loyd J.E., Ghofrani, Hossein A. Grimminger F., Schermuly R.T., Cahalan M.D., Rubin L.J. and Yuan J.X.J. A Functional Single-Nucleotide Polymorphism in the TRPC6 Gene Promoter Associated

With Idiopathic Pulmonary Arterial Hypertension. *Circulation*, 4(164):2313–2322 (2009).

[151] Yuan J.P., Zeng W., Huang G.N. and Muallem P.F.W. STIM1 heteromultimerizes TRPC channels to determine their function as store-operated channels. *Nature Cell Biology*, 7(6):636–45 (2007).

[152] Zeng W., Yuan J.P., Kim M.S., Choi Y.J., Huang G.N., Worley P.F. and Muallem S. STIM1 Gates TRPC Channels, but Not Orai1, by Electrostatic Interaction. *Molecular Cell*, 32(3):439–448 (2008).

[153] Zhang J., Nuebel E., Wisidagama D., Setoguchi K. and Hong J. Measuring energy metabolism in cultured cells, including human pluripotent stem cells and differentiated cells. *Nature protocols*, 7(6) (2013).

[154] Zhang M., Rehman J. and Malik A.B. Endothelial Progenitor Cells and Vascular Repair. *Current Opinion in Hematology*, 15(10):1203–1214 (2008).

[155] Zitt C., Zobel A., Obukhov A.G., Harteneck C., Kalkbrenner F., Lückhoff A. and Schultz G. Cloning and functional expression of a human Ca^{2+} permeable cation channel activated by calcium store depletion. *Neuron*, 16:1189 (1996).

6.3 Acknowledgments

Eidesstattliche Versicherung

Ich, Diana Angela Stickel, erkläre hiermit an Eides statt, dass ich die vorliegende Dissertation mit dem Thema

"Cytosolic and mitochondrial Ca^{2+} handling in pulmonary arterial smooth muscle and endothelial cells"

selbstständig verfasst, mich außer der angegebenen keiner weiteren Hilfsmittel bedient und alle Erkenntnisse, die aus dem Schrifttum ganz oder annähernd übernommen sind, als solche kenntlich gemacht und nach ihrer Herkunft unter Bezeichnung der Fundstelle einzeln nachgewiesen habe.

Ich erkläre des Weiteren, dass die hier vorgelegte Dissertation nicht in gleicher oder in ähnlicher Form bei einer anderen Stelle zur Erlangung eines akademischen Grades eingereicht wurde.

_____   _____

Ort, Datum   Unterschrift